

## **ABSTRACT**

HE, TING. A Study of Three Dimensional Warp Knits for Novel Applications as Tissue Engineering Scaffolds. (Under the direction of Dr. Martin W. King, Prof. Nancy B. Powell and Dr. Traci May Lamar).

The success of regenerative medicine requires the design of tissue engineering (TE) scaffolds, which promote cell growth and cellular regeneration of viable tissues and organs by harnessing the body's inherent natural capacity to repair injured tissues. This calls for a 3 dimensional (3D) macrostructure that is highly porous and a microstructure that induces cells to attach, proliferate and regenerate complex tissues. In this study, the latest textile warp knitting technology has been used to create 3D macrostructure scaffolds, which have appropriate mechanical properties and support the adhesion and proliferation of cells for use in a wide range of TE applications. The objectives were to design and produce biocompatible porous spacer fabrics and to evaluate their architecture, mechanical properties, cell viability and functionality. Four 3D spacer fabric prototypes using a multifilament 150 denier polyester yarn were knitted on a Karl Mayer double needle bed warp knitting machine with different gauges (12 and 24 needles per inch) and guide bar numbers (4 and 6) so as to knit scaffolds with diverse structures and properties. Spacer fabrics have a sandwich construction with surface and filling layers providing ideal 3D pores for cell growth. The morphology and architectural geometry were visualized by optical microscopy and scanning electron microscopy (SEM). The dimensional and mechanical properties were studied in terms of total porosity, compression and recovery, thickness, stiffness and bursting strength, and they were found to change depending on the knitting parameters. The results of cell viability and proliferation studies using MTT assays, laser scanning confocal microscopy (LSCM) and SEM confirmed active cell attachment, growth and proliferation throughout the thickness of

the scaffolds. This study has successfully demonstrated for the first time an effective and novel application for knitted porous spacer fabrics as tissue engineering scaffolds. The main advantage of this approach is that the spacer fabric has been shown to promote the attachment and proliferation of cells in three dimensions.

A Study of Three Dimensional Warp Knits for Novel Applications as Tissue Engineering  
Scaffolds

by  
Ting He

A thesis submitted to the Graduate Faculty of  
North Carolina State University  
in partial fulfillment of the  
requirements for the degree of  
Master of Science

Textiles

Raleigh, North Carolina

2011

APPROVED BY:

---

Dr. Martin W. King  
Committee Chair

---

Prof. Nancy B. Powell  
Co-chair of Advisory Committee

---

Dr. Traci May Lamar  
Member of Advisory Committee

## **DEDICATION**

To my beloved Mom and Dad

To Xiaofeng Qin, my love

To Dr. Martin W. King, the Best Mentor

## **BIOGRAPHY**

Ting He was born in Xuzhou, Jiangsu, China, on January 19th, 1987. She is the only daughter of Fujian He and Xin Zhao. She graduated from Xuzhou Senior High, Xuzhou, Jiangsu, China in May 2005. Following high school graduation, she entered the Donghua University College of Textiles, Shanghai, China. While at Donghua University, she was the Chairman of Society for Textile Technology and Engineering from 2005 to 2006 and a member of Society for the Advancement of Material and Process Engineering. Ting graduated with a Bachelor of Science in Textile Engineering with a major in Knitting and Apparel Engineering in May, 2010.

In the third year of her undergraduate degree, she entered the Global Training Initiative at North Carolina University, and earned a US Culture and Education-CTU Certificate in December 2009. Following her BS completion from Donghua University, she was admitted to the accelerated non-thesis master program Master of Textiles in College of Textile, and then transferred to a Master of Science in Textiles program in August, 2010. She was awarded a graduate research assistantship by National Textile Center (NTC). She was a student member of American Association of Textile Chemists and Colorist (AATCC). She was nominated by the MS in Textiles Program for the 2011 Graduated Student Research Symposium and awarded Outstanding Student Researcher. She was invited to give poster presentations about her graduate research on international conferences including FiberMed11 at Tampere, Finland, August 2011, the Society for Biomaterials 2011 Annual Meeting & Exposition, Orlando, FL, the Tissue Engineering and Regenerative Medicine International

Society (TERMIS) 2010 Meeting, Orlando, FL and National Textile Center 2010 Forum, Greenville, SC.

Ting experts to complete her MS degree in August 2011. She looks forward to the next adventure in her life.

## ACKNOWLEDGMENTS

I would like to sincerely thank Dr. Martin W. King for his constant support, guidance and mentorship throughout my years at NC State. It is he who opened the door of biomedical textiles in front of me and led all the way to the goals I never thought possible. His vast knowledge, experience, enthusiasm, and unwavering dedication to his career, to the university and industry inspire all his students.

I would also like to express my appreciation to the other members of my advisory committee, Prof. Nancy B. Powell and Dr. Traci May Lamar for their encouragement and guidance. My special thanks go to Al Inman and Dr. Nancy Monteiro-Riviere from the College of Veterinary Medicine, NCSU for a wonderful collaboration. Many thanks go to Dr. Russell Gorga and Dr. Bhupender Gupta for their valuable support and for the generous use of their laboratory facilities to generate my research results. My special thanks go to Charlie King from Unifi Inc. and Bill Christmann from Gehring Textiles Inc. for providing us with valuable materials.

My appreciation also goes to my best friend and coworker Katharina Sippel who always stands with me and supports me through difficulties in our life and research. I would also thank the lab member of Biomedical Textiles Group: Sangwon Chung, Leslie Eadie, Jin Di and Nisarg. I would like to thank all my fellow researchers, graduate students and support staff who have helped and provided me with their great support: Brian Davis, Tim Pleasants, James Watson, Matthew Laney and Hai M Bui. My special thanks also go to Dr. Susan Bernaki, Chuck Mooney, Michael Dykstra, Dr. Eva Johannes, Birgit Andersen and Judy Elson.

I would like to express my gratitude to my father Fujian He and mother Xin Zhao as well as my relatives for their love, support and encouragement through my life. And last but not the least, I would sincerely express my thanks to my beloved Xiaofeng Qin, who accompanies me and takes care of me through the whole journey through the United States of America.

## TABLE OF CONTENTS

<b>LIST OF TABLES</b>	<b>x</b>
<b>LIST OF FIGURES</b>	<b>xi</b>
<b>CHAPTER 1 INTRODUCTION</b>	<b>1</b>
<b>1.1 Aims and Objectives</b>	<b>3</b>
<b>1.2 Outline of Thesis</b>	<b>6</b>
<b>CHAPTER 2 REVIEW OF LITERATURE</b>	<b>7</b>
<b>2.1 Tissue Engineering</b>	<b>7</b>
2.1.1 Overview	7
2.1.2 Characteristics and Demand of Scaffold Design	8
2.1.2.1 Materials	8
2.1.2.2 Architecture	11
2.1.2.3 Mechanical properties	12
2.1.2.4 Biological properties	13
<b>2.2 Fabrication Methodologies</b>	<b>14</b>
2.2.1 Overview	14
2.2.2 Textile technologies used in medical applications	17
2.2.3 Spacer fabric current design and application	19
2.2.4 Warp knit spacer fabric technology	20
2.2.5 Biomedical application of spacer fabric	24
<b>CHAPTER 3 EXPERIMENTAL</b>	<b>27</b>
<b>3.1 Experimental Design</b>	<b>27</b>
3.1.1 Material	28
3.1.2 Spacer Fabric Design and Production	29
<b>3.2 Evaluation of Constructional Characteristics</b>	<b>35</b>
3.2.1 Fabric Structure and Surface Morphology by Optical Image Analysis	35

3.2.2	Fabric Count, Thickness, and Density _____	35
3.2.3	Total Porosity _____	37
3.2.4	Pore size Characterization _____	38
<b>3.3</b>	<b>Mechanical Tests _____</b>	<b>40</b>
3.3.1	Compression and Recovery _____	40
3.3.2	Flexural Rigidity (Stiffness) _____	41
3.3.3	Bursting Strength _____	42
3.3.4	Tensile strength _____	44
<b>3.4</b>	<b><i>In Vitro</i> Cell Culture Study _____</b>	<b>46</b>
3.4.1	Preparation of Sample _____	46
3.4.2	Cell Viability (MTT Assay) _____	47
3.4.3	Scanning Electron Microscopy (SEM) _____	48
3.4.4	Laser Scanning Confocal Microscopy (LSCM) _____	48
<b>3.5</b>	<b>Statistics _____</b>	<b>49</b>
<b>CHAPTER 4 RESULTS AND DISCUSSION _____</b>		<b>51</b>
<b>4.1</b>	<b>Effect of Knitting Parameters on Constructional Characteristics _____</b>	<b>51</b>
<b>4.2</b>	<b>Pore Size Characterization by Image Analysis _____</b>	<b>54</b>
<b>4.3</b>	<b>Mechanical Properties _____</b>	<b>61</b>
4.3.1	Compression and Recovery _____	61
4.3.2	Flexural Rigidity (Stiffness) _____	64
4.3.3	Bursting Properties _____	66
4.3.4	Tensile Properties _____	67
<b>4.4</b>	<b>Biocompatibility _____</b>	<b>69</b>
4.4.1	<i>In Vitro</i> Cell Viability _____	69
4.4.2	Cell Attachment and Proliferation _____	75
4.4.2.1	Scanning Electron Microscopy (SEM) _____	75
4.4.2.2	Laser Scanning Confocal Microscopy (LSCM) _____	83

<b>CHAPTER 5 CONCLUSIONS</b>	<b>87</b>
<b>5.1 Conclusions</b>	<b>87</b>
<b>5.2 Contribution</b>	<b>93</b>
<b>5.3 Recommendations for Future Research</b>	<b>93</b>
<b>REFERENCES</b>	<b>96</b>
<b>APPENDICES</b>	<b>101</b>
<i>Appendix A</i>	<i>102</i>
<i>Appendix B</i>	<i>103</i>
<i>Appendix C</i>	<i>104</i>
<i>Appendix D</i>	<i>105</i>
<i>Appendix E</i>	<i>106</i>
<i>Appendix F</i>	<i>107</i>

## LIST OF TABLES

<i>Table 2.1.1 Examples of materials currently used in tissue engineering applications</i> .....	9
<i>Table 2.1.2 Implantable polymeric materials</i> <sup>9, 10</sup> .....	9
<i>Table 2.1.3 Investigated potential biomaterials used in cardiac muscle engineering</i> <sup>11</sup> .....	10
<i>Table 2.1.4 Physical and chemical properties of PET regular tenacity fibers</i> <sup>12</sup> .....	11
<i>Table 2.1.5 Example of the average mechanical properties of human tissues</i> <sup>13</sup> .....	13
<i>Table 2.2.6 Comparison of fabrication technologies for pre-made porous scaffolds</i> .....	16
<i>Table 2.2.7 Classifications of 2D and 3D textile structures</i> <sup>17</sup> .....	17
<i>Table 3.1.1 PET yarn properties</i> .....	28
<i>Table 3.1.2 Sample types and parameters for all samples</i> .....	30
<i>Table 3.1.3 Information of commercial samples (confidential information from Gehring) ...</i>	31
<i>Table 3.1.4 Lapping sequence diagram for four knitted samples</i> .....	32
<i>Table 4.1.1 Constructional characteristics of four prototype knitted and two commercial samples</i> .....	54
<i>Table 4.2.2 Maximum and minimum values of pore diameter</i> .....	57
<i>Table 4.2.3 Pore diameter mean and standard deviation values</i> .....	59

## LIST OF FIGURES

<i>Figure 1.1.1</i>	<i>Waiting list of patients for organ transplant at the end of year 2007<sup>1</sup></i>	<i>1</i>
<i>Figure 1.1.2</i>	<i>Parameters for a tissue engineered scaffolds<sup>3</sup></i>	<i>2</i>
<i>Figure 2.2.1</i>	<i>Schematic diagram of different scaffolding approaches in tissue engineering<sup>14</sup></i>	<i>16</i>
<i>Figure 2.2.2</i>	<i>Two dimensional warp knitted mesh used to repair incisional hernias of the abdominal wall<sup>20</sup></i>	<i>19</i>
<i>Figure 2.2.3</i>	<i>A 3D woven fabric structure designed for cartilage tissue engineering application<sup>22</sup></i>	<i>19</i>
<i>Figure 2.2.4</i>	<i>A spacer fabric knitted from multifilament yarns in the face and back layers and showing criss-crossed monofilament yarns in the middle spacer layer.</i>	<i>20</i>
<i>Figure 2.2.5</i>	<i>A cross-sectional view of a single bed latched needle Raschel warp knitting machine<sup>25</sup></i>	<i>21</i>
<i>Figure 2.2.6</i>	<i>A cross-sectional view of the needle bars and guide bars on a double needle bed Raschel knitting machine<sup>25,26</sup></i>	<i>22</i>
<i>Figure 2.2.7</i>	<i>Design mechanism showing how the shogging (back and forth) motion of the guide bars is controlled by the pattern drum with links of different height<sup>26</sup></i>	<i>23</i>
<i>Figure 2.2.8</i>	<i>The vertical needle action of a double needle bed Raschel knitting machine (guide bars are simplified as one)<sup>25</sup></i>	<i>24</i>
<i>Figure 2.2.9</i>	<i>3D spacer fabric used as a compression bandage<sup>32</sup></i>	<i>25</i>
<i>Figure 3.1.1</i>	<i>Experimental approach</i>	<i>28</i>
<i>Figure 3.1.2</i>	<i>Karl Mayer DR 10 warp knitting machine</i>	<i>29</i>

<i>Figure 3.1.3 2D Simulation of 6GB structure in ProCAD and relevant machine parts</i> .....	33
<i>Figure 3.1.4 3D simulation of 24E 6GB in ProCAD software</i> .....	34
<i>Figure 3.1.5 3D simulation of all four prototype knitted structures in ProCAD software</i> .....	34
<i>Figure 3.2.1 SDL 94 thickness gauge in the Biomedical Textile Laboratory at College of Textile, NCSU</i> .....	36
<i>Figure 3.3.1 Model S0015 Cantilever Bending Stiffness Tester from IDM Instruments Pty, Ltd, in the Physical Testing Lab at College of Textile, NCSU</i> .....	42
<i>Figure 3.3.2 Bluehill Instron Model No.5544 with probe bursting strength apparatus attached</i> .....	43
<i>Figure 3.3.3 Bluehill Instron Model No. 5544 Universal Tester with tensile strength apparatus</i> .....	45
<i>Figure 3.4.1 MTT formazan solution in a 96-well plate showing more viable cells on right hand side giving higher formazan production and thus a stronger purple colour<sup>41</sup></i> .....	47
<i>Figure 4.1.1 Surface morphology of four prototype knitted and two commercial samples</i> ....	53
<i>Figure 4.2.1 Optical microscopic image of cross-section cut in the weft direction of the resin embedded 12E4GB fabric showing different layers within the same knitted structure (Magnification 50x)</i> .....	55
<i>Figure 4.2.2 Optical microscopic image of cross-section cut in the weft direction of the resin embedded 12E4GB fabric showing how the pores were identified and constructed in the spacer layer (left) and outer layer (right) (Magnification 50x).</i> .....	55

<i>Figure 4.2.3 Spacer layer Pore distribution trend lines of commercial samples (0-1mm).....</i>	<i>57</i>
<i>Figure 4.2.4 Outer layer (face/back) layer pore distribution trend lines of six samples (0-0.1mm).....</i>	<i>60</i>
<i>Figure 4.2.5 Spacer pore distribution trend lines of six samples (0-0.4mm).....</i>	<i>60</i>
<i>Figure 4.3.1 The level of compression resistance and extent of recovery (Error bars = standard deviation).....</i>	<i>63</i>
<i>Figure 4.3.2 Changes in thickness during compression and recovery testing .....</i>	<i>63</i>
<i>Figure 4.3.3 Flexural rigidity (Stiffness) (Error bars = standard deviation) .....</i>	<i>65</i>
<i>Figure 4.3.4 Bursting strength results (Error bars = standard deviation).....</i>	<i>67</i>
<i>Figure 4.3.5 Tensile strength in warp direction (left) and in weft direction (right) (Error bars = standard deviation) .....</i>	<i>68</i>
<i>Figure 4.3.6 Young's modulus at 20% elongation in warp direction (left) and in weft direction (right) (Error bars = standard deviation).....</i>	<i>68</i>
<i>Figure 4.4.1 Cells attached on 2D plate at Day 3 before (left) and after (right) MTT assay. 70</i>	
<i>Figure 4.4.2 Mean MTT absorbance values at 5 time points in the 15 day study.....</i>	<i>71</i>
<i>Figure 4.4.3 Mean MTT percentage viability values at 5 time points in the 15 day study .....</i>	<i>72</i>
<i>Figure 4.4.4 Cells left on the 3D scaffolds after the MTT assay. ....</i>	<i>73</i>
<i>Figure 4.4.5 Comparison of total porosity (a) with increasing rate of percentage viability from Day1 to Day 6 (b).....</i>	<i>74</i>
<i>Figure 4.4.6 SEM photomicrographs showing changes in cell attachment and proliferation of the 24E 4GB Sample during in vitro cell culture. HDF cells attached to the surface of fabric face from Day 1 to Day 6.....</i>	<i>76</i>

*Figure 4.4.7 SEM photomicrographs showing changes in cell attachment and proliferation of the 24E 4GB Sample during in vitro cell culture. HDF cells attached to the surface of fabric face from Day 10 to Day 15.....77*

*Figure 4.4.8 SEM photomicrographs showing changes in cell attachment and proliferation of the 24E 4GB Sample during in vitro cell culture. HDF cells attached to the side of fabric (weftwise) from Day 1 to Day 6.....78*

*Figure 4.4.9 SEM photomicrographs showing changes in cell attachment and proliferation of the 24E 4GB Sample during in vitro cell culture. HDF cells attached to the side of fabric (weftwise) from Day 10 to Day 15.....79*

*Figure 4.4.10 SEM photomicrographs showing the extent of cell migration before and after 15 days of cell culture on fabric sample 24E 6GB .....80*

*Figure 4.4.11 SEM photomicrographs showing the extent of cell migration before and after 15 days of cell culture on fabric sample 12E 6GB .....81*

*Figure 4.4.12 SEM photomicrographs showing the extent of cell migration before and after 15 days of cell culture on fabric sample SHR 724/5.....82*

*Figure 4.4.13 SEM photomicrographs showing the extent of cell migration before and after 15 days of cell culture on fabric sample SHR 728.....83*

*Figure 4.4.14 LSCM images showing HDF cell proliferation for each sample after Day 1 and Day 15 during in vitro cell culture.....85*

## CHAPTER 1 INTRODUCTION

The traditional approach for patients suffering tissue loss and end-stage organ failure is transplantation and surgical reconstruction, which is associated with major immunological challenges as well as complications following surgery. In the USA there are currently about 90,000 patients waiting for organ transplantation as shown in Figure 1.1.1. The annual healthcare costs for the treatment of these patients exceeds \$500 billion<sup>1</sup>. This healthcare crisis is driving growing interest in regenerative medicine and tissue engineering (TE) research, which is committed to developing viable clinical treatments for the replacement of diseased and injured tissues and organs<sup>1</sup>. What's more, because the current individualized clinical approach is prohibitively expensive, it is foreseen that in the near future, 3D textile fabrication techniques will be harnessed for the commercial production of textile based TE scaffolds and cell culture membranes.

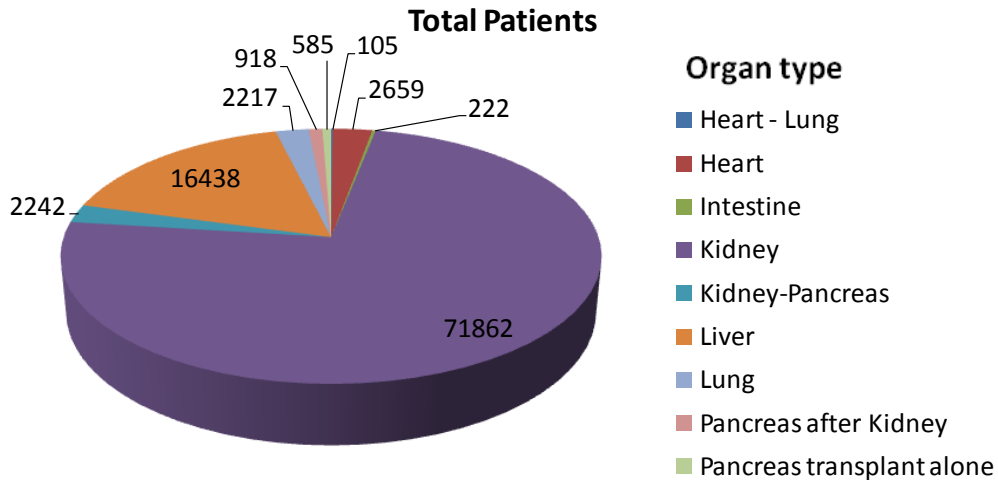


Figure 1.1.1 Waiting list of patients for organ transplant at the end of year 2007<sup>1</sup>

In response to this situation, researchers have developed a tissue engineering approach whereby they harness the body's inherent natural capacity to repair injured tissues by cellular regeneration of viable tissues and organs. In this approach cells are grown on a scaffold in a bioreactor under appropriate conditions in which specific biomolecules are released that induce predictable and desired cell responses and behavior. Clearly the appropriate structural design of the scaffold is critical to the success of this cell culture approach.

In this study we propose to use a three dimensional (3D) scaffold which is able to mimic the native extracellular matrix (ECM) which is vital for cell proliferation and viability<sup>2</sup>. The success of this scaffold is determined by the structural parameters, such as its architecture, total porosity, pore size, shape, geometry and surface topography, as well as its biocompatibility, rate of resorption and mechanical properties (see

Figure 1.1.2).

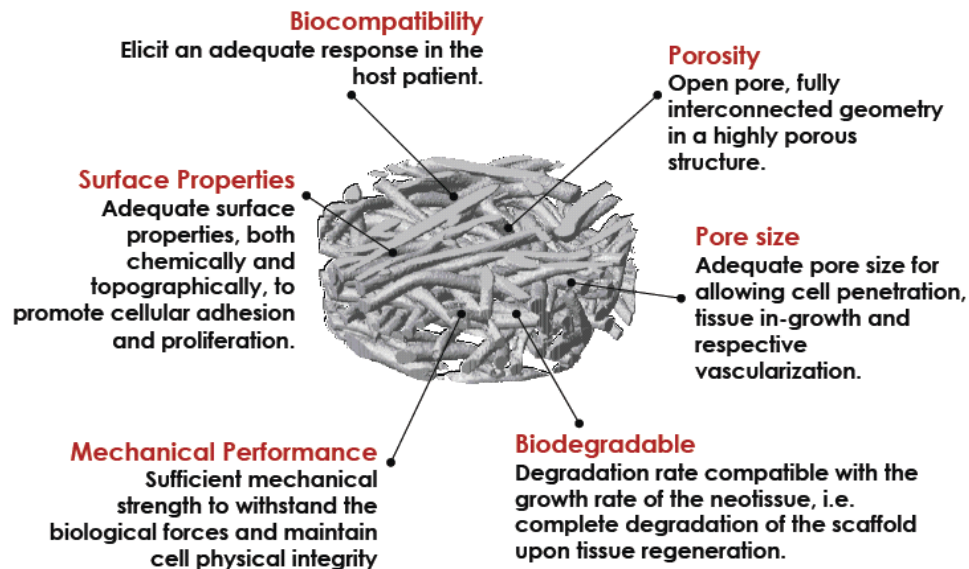


Figure 1.1.2 Parameters for a tissue engineered scaffolds<sup>3</sup>

Scaffolds may be composed of metallic, ceramic, polymeric, natural or composite material, and they are usually porous and biodegradable. Based on a number of different requirements, textile structures in general, and warp knitted spacer fabrics in particular, show relative advantages in providing a 3D shape, high level of porosity, inner connectivity of the pores, a multi-pore size distribution and more than adequate mechanical properties.

This research project proposes to harness the latest warp knitting technologies so as to fabricate 3 dimensional porous tissue engineering scaffolds that will be biocompatible and support the adhesion and proliferation of cells. Four types of polyester spacer fabric samples with different parameters have been produced for this study. Mechanical and biological tests have been conducted to evaluate and optimize the required architecture and properties. Once the manufacturing conditions for this scaffold have been established, then the long term goal is to apply this knowledge to fabricate spacer fabrics for use in a wide range of TE and regenerative medicine applications.

## **1.1 Aims and Objectives**

The main aim for this interdisciplinary research was to find an appropriate textile technology to develop a three dimensional porous structure which will serve as a suitable scaffold for tissue engineering applications. In order to prove the performance and functionality of this structure, it was proposed to use a range of analytical techniques to evaluate the architecture as well as the physical, mechanical and biocompatible properties.

For the purpose of this main aim, three specific objectives have been developed as listed below, and each is followed by a description of the experiments that needed to be performed.

- 1) To design a three dimensional fabric with porous multilayers, high porosity and high interconnectivity of pores using warp knitting technology.
  - 1.2 To discuss the general requirements for tissue engineering scaffolds such as the constructional characteristics and the physical, mechanical and biological properties, based on the review of literature findings.
    - 1.1 To review the literature describing the current methodology to create 3D scaffolds and existing textile fabrications for tissue engineering application, especially technologies for producing spacer fabrics
    - 1.3 To create a practical plan for this experimental study and to define the independent and dependent variables for this study.
- 2) To develop four prototypes with different knitting parameters and to optimize the set-up on the machine to produce the designed structures with the desired properties.
  - 2.1 To create the design for 3D spacer fabric structures and to select the lapping sequences for the face, back and spacer yarns.
  - 2.2 To simulate the 3D fabric design in professional software ProCad to illustrate the yarn spacing and stitch notation in both 2D and 3D formats.
  - 2.3 To optimize the set-up and knitting conditions on the double needle bed, narrow width knitting machine, including the gauge of the needle bars, the number of guide

bars, the distance between needle beds and the chain link sequences to give the lapping diagrams.

2.4 To conduct the fabrication processes which include yarn winding onto bobbins, warping and knitting.

3) To study the constructional characteristics and the physical, mechanical and biological properties of the knitted prototypes as well as two commercial control spacer fabrics.

3.1 To analyze the surface morphology and constructional characteristics using optical microscopy and an image analysis system to view sections through the structure and quantify the pore size distribution.

3.2 To evaluate the mechanical properties including the degrees of compression and recovery, flexural rigidity (stiffness), tensile strength, Young's modulus and bursting strength.

3.3 To assess the biocompatibility of the knitted prototypes and two commercial fabrics by culturing human dermal fibroblast cells on the structure. This will involve conducting in vitro cell tests by means of an MTT bioassay for cell viability, scanning electron microscopy (SEM) and laser scanning confocal microscopy (LSCM) to study cell attachment, proliferation and infiltration on the surface and through the thickness of the scaffolds over a fifteen day culture period.

## **1.2 Outline of Thesis**

This dissertation is organized in five chapters as described below.

Chapter 1 describes the general background and motivation of using 3D textile scaffolds for tissue engineering applications. Aims, specific objectives and unusual definition and terminology are listed. Chapter 2 reviews the important literature of TE applications, scaffold design strategies, current fabrication methodologies and spacer fabric knitting technology. The reason for using a 3D spacer structure for TE applications is highlighted. Chapter 3 describes the experimental design which consists of the materials, fabrication methods and testing approaches used to design, produce and evaluate the spacer fabrics. Chapter 4 reports the result of the investigation into the 3D porous spacer fabrics and the evaluation of the constructional, mechanical and biological properties. Finally, Chapter 5 revisits the main aims and objectives and gives a summary and conclusions of the findings, limitations and the contribution of this research. It also lists recommendations for future research.

## **CHAPTER 2 REVIEW OF LITERATURE**

This chapter reviews the needs, requirement, strategies, technologies, characteristics and properties for scaffold design, fabrication and evaluation. In addition it studies the current textile technologies for use in tissue engineering applications. To better understand the characteristics and performances of scaffolds, this review is divided according to aspects such as material, architecture, structure, mechanical and biological properties. After that, different fabrication technologies are described in an overview and compared with each other. In conclusion it would appear that textile scaffolds have unique advantages over other structures, and so need to be analyzed in greater depth. A general overview is provided that reviews the field of textile fabrication methods for tissue engineering applications both for 2D and 3D structures. A 3D spacer fabric appears to satisfy most of the requirements that were identified in the previous discussion. As a result the chapter ends with a brief introduction to 3D knitted spacer fabrics including their knitting requirements, their equipment mechanism as well as current medical applications.

### **2.1 Tissue Engineering**

#### **2.1.1 Overview**

Since many patients suffer from loss of organ function due to disease, injury or senescence, there is a growing demand for substitute implants which can provide the missing structure and/or function of the diseased organ. The tissue engineering approach to resolving these issues involves a new type of therapy called regenerative medicine<sup>4</sup>. It is design to restore,

maintain, or enhance tissues and organs, in the hope of reducing the need for organ replacement, improving drug delivery and eliminating organ transplants in the future<sup>24</sup>.

## **2.1.2 Characteristics and Demand of Scaffold Design**

When talking about scaffolds used in tissue engineering applications, an important mission and challenging is to control the amount of tissue formation in three dimensions. The design strategy is to develop an optimal microenvironment to mimic the natural extracellular matrix and support neo-tissue genesis which involves cell, attachment, proliferation, differentiation, and regeneration<sup>5, 6</sup>. A highly porous 3D geometry, material with an appropriate chemical composition, adequate physical properties, biocompatibility, and biological functions are all considerable key factors to ensure that this strategy is successful<sup>7</sup>.

### ***2.1.2.1 Materials***

The fundamental approach for tissue engineering is to harness the body's inherent natural capacity to repair injured tissues by cellular regeneration of viable tissues and organs. Synthetic scaffolds need to be absorbed completely by the human body producing non-toxic degradation products over time (usually less than a year) while the new regenerated tissue is remodeling itself into the desired structures<sup>8</sup>. In order to fulfill the diverse needs of tissue engineering, various materials have been exploited as scaffold constructs for tissue regeneration<sup>7</sup>. Table 2.1.1 lists some of the more common materials used frequently for tissue engineering scaffolds. Their advantages and disadvantages are also presented in the Table 2.1.2.

Table 2.1.1 Examples of materials currently used in tissue engineering applications

<b>Materials</b>	<b>Pros</b>	<b>Cons</b>
Certain metal	Superior mechanical properties	Lack of degradability in a biological environment
Certain inorganic/ceramic materials such as hydroxyapatite (HAP) or calcium phosphates	Good osteo-conductivity, being studied for engineering of mineralized tissue	Poor processability into highly porous structures, brittleness
Polymer (e.g. PLLA, PGA )	Good mechanical properties, flexibility in fabrication, variable rate of degradation possible	Structural architecture is limited by fabrication method
Collagen	Biocompatible	Weak tensile properties

Table 2.1.2 Implantable polymeric materials <sup>9, 10</sup>

<b>Fiber Type</b>	<b>Fabrication structure</b>	<b>Application</b>
Collagen, catgut, polyglycolide fiber, polylactide fiber	Monofilament, braided	Biodegradable sutures
Polyester fiber, polyamide fiber, PTFE fiber, polypropylene fiber, polyethylene fiber	Monofilament, braided	Non-biodegradable, sutures
PTFE fiber, polyester fiber, silk, collagen, polyethylene fiber, polyamide fiber	Woven, braided	Artificial tendon
Polyester fiber, carbon fiber, collagen	Braided	Artificial ligament
Low-density polyethylene fiber	Fiber	Artificial cartilage
Chitin/Chitosan	Nonwoven	Artificial skin
Poly(methyl methacrylate) fiber, silicon fiber, collagen	Fiber	Eye-contact lenses, artificial cornea
Silicone, polyacetyl fiber, polyethylene fiber	Fiber	Artificial joints/bones
PTFE fiber, polyester fiber	Woven, knitted	Vascular grafts
Polyester fiber	Woven, knitted	Heart valve/sewing rings

With respect to resorbable polymers for tissue engineering applications, both natural and synthetic materials are used. Among the natural polymers, collagen, alginate and gelatin have been under intensive investigation all over the world<sup>8, 9, 10</sup>. Also systematical studies have investigated a wide range of synthetic polymers, such as polyglycolic acid (PGA), polylactic acid (PLA), co-polymer poly(lactic-*co*-glycolic acid) (PLGA), poly(glycerol sebacate) (PGS) and polyparadioxanone (PDS). The mechanical properties of these biodegradable polymers are listed in Table 2.1.3. The desired degradation rate is the primary criteria which directs the choice of the type of resorbable polymer or the concentration of the component in a copolymer<sup>15</sup>.

Table 2.1.3 Investigated potential biomaterials used in cardiac muscle engineering <sup>11</sup>

<b>Polymer</b>	<b>Elastomer (E) or Thermoplastic (T)</b>	<b>Young's modulus (or stiffness)</b>	<b>Tensile strength</b>	<b>Degradation (Month)</b>
PGA	T	7–10 GPa	70 MPa	2–12
PLLA	T	1–4 GPa	30–80 MPa	2–12
PDS	E	0.6 GPa	12 MPa	6
PGS	E	0.04–1.2 MPa	0.2–0.5 MPa	Degradable
Collagen fibre (Tendon/cartilage/ligament/bone)	E	2–46 MPa	1–7 MPa	Degradable
Collagen gel (calf skin)	E	0.002–0.022 MPa	1–9 kPa	Degradable

However, because these materials will degrade during exposure to ambient air with moisture vapor and water based lubricants and cleaning systems at the time of storage, handling,

production, cleaning, sterilization and testing, it is necessary during preliminary trials to use a non-resorbable polymer to study the knitted structure, architecture and properties of the scaffold. This is why for the purpose of this initial study of the knitted scaffolds' structure and performance it was decided to use a multifilament yarn spun from a non-resorbable polymer. The aromatic polyester, poly(ethylene terephthalate) (PET), was selected for use in this study. It has for many years been widely used for human implantation devices such as sutures, vascular and endovascular prothesis. Its physical and chemical properties are listed in Table 2.1.4.

Table 2.1.4 Physical and chemical properties of PET regular tenacity fibers <sup>12</sup>

<b>Properties</b>	<b>Performance</b>
Melting point	About 260 °C
Density at room temperature	1.38 g/cm <sup>3</sup>
Solubility in water	practically insoluble
Decomposition temperature	340 °C
Young's modulus	2800–3100 MPa
Tensile strength	55–75 MPa

### ***2.1.2.2 Architecture***

In addition to the resorbability and the chemical composition, the architecture plays an important role in the rate of degradation of scaffolds. It also contributes to other physical, chemical, mechanical and biological properties. At the macro scale, it should provide the physical limitation of the scaffold and control the shape of the remodeled tissue. At the micro scale, it should mimic the natural extracellular matrix (ECM) and ensure mass transport of

nutrients and by-products from the cells in order to achieve uniform growth of tissue and to avoid tissue formation only in the peripheral regions of the scaffold<sup>13,14</sup>.

As one of the important architectural parameters, thickness has an important influence on the usefulness and performance of the tissue construct once implanted. Thickness is defined as the distance between one surface of the scaffold and the opposite surface<sup>19</sup>. Since the target tissue being regenerated are inevitably multilayered structures and not monolayers of cells, it is necessary for tissue engineering scaffolds to have a thickness of 1-5mm, and to be able to promote the proliferation of cells through the whole thickness.

### ***2.1.2.3 Mechanical properties***

The mechanical requirements for the engineered scaffolds are determined by the target tissue and the specific clinical or biotechnology applications. Typical examples of the mechanical requirements are listed in Table 2.1.5.

As the scaffold is designed for a specific function, its initial mechanical properties should be similar to those of the tissue it will regenerate. However, over time as the polymer degrades and the scaffold resorbs these initial mechanical properties will deteriorate. Both the selection of the polymer material and the fabrication process play an important role in determining the initial mechanical performance. Take myocardial heart muscle tissue for example. It beats cyclically and continually over life time of the patient. Therefore, the scaffold should be stretchable and have good elastic recovery over the long term. In addition, the material should avoid plastic deformation and failure when exposed to multi cyclic strains<sup>11</sup>. In summary, the basic mechanical properties include tensile strength, Young's modulus, bursting strength, compression resistance, elastic recovery and stiffness.

Table 2.1.5 Example of the average mechanical properties of human tissues <sup>13</sup>

	Ultimate Tensile Strength (MPa)		Ultimate Elongation (%)	
	Longitudinal	Transverse	Longitudinal	Transverse
Femoral artery	1.67	1.37	87	69
Femoral vein	2.16	3.04	82	70
Popliteal artery	1.37	1.18	105	70
Esophagus	0.59	0.18	124	36
Ureter	1.72	0.44	36	98
Stomach	0.55	0.43	93	127
Venous tissue	1.67	2.94	89	66
Bladder	0.24	-	226	-
Skin	7.55	-	78	-

#### ***2.1.2.4 Biological properties***

Besides the mechanical properties, the biological performance also has much influence on the usefulness of tissue engineered scaffolds. Because the scaffold is designed to mimic the natural tissue environment which is dominated by the extra cellular matrix (ECM), it is important to understand the functions of native ECM and to draw parallels with the characteristics of artificial scaffolds. The analogous functions of scaffolds in tissue engineering include:

- a. Provide structural support for seeded cells to attach, proliferate, migrate and differentiate.
- b. Provide mechanical stability during tissue maturation and transmit mechanical cues.

- c. Interact with cells actively to facilitate proliferation or differentiation
- d. Serve as a carrier matrix and reservoir for delivery of growth factors and biomolecules
- e. Provides void volume for angiogenesis, vascularization and new tissue formation during remodeling.

In order to achieve these functions, the scaffold should be able to promote cell attachment and proliferation but should not be toxic to cells (cytotoxicity), or produce toxic by-products during degradation generally speaking. In detail, the scaffolds should realize the following characteristics respectively.

- a. Made of porous biomaterial with open, interconnected pores for cell migration and attachment, nutrient supply and waste diffusion.
- b. Provide sufficient mechanical properties mimicking that of native tissue; tailored substrate stiffness/ flexibility to support direct cell attachment and proliferation.
- c. Provide biological cues such as cell-adhesive binding sites; physical cues such as surface topography, surface stiffness.
- d. Incorporate bioactive agents using nano/ micro encapsulation with controlled release.
- e. Engineered and controllable degradation rate<sup>15</sup>.

## **2.2 Fabrication Methodologies**

### **2.2.1 Overview**

With the objective of realizing the characteristics of scaffolds discussed above, scientists have developed a wide variety of different methods to create 2D and 3D scaffolds. Most of

these methods can be categorized into the four main strategies illustrated in Figure 2.3.1. The first strategy is to first make a porous scaffold and then in a second step to seed cells and generate a cell-seeded scaffold. The second strategy is to use natural tissues from which all living cells have been removed. This leaves behind only an extracellular matrix (ECM) to serve as the porous scaffold which can then be seeded with cells. The third strategy is to create 2D cell sheets using normal cell culturing technologies. Because these monolayers or cell sheets are very thin, they need to be laminated together in multilayered sheets so as to develop 3D architecture. The fourth strategy mixes the cells and self assembling hydrogel components together, and then takes advantage of the self-assembling process by injecting the cells and the gel into the designed tissue shape. This fourth strategy is widely applied in 3D cell printing technology<sup>16</sup>.

Among these four different strategies, various methodologies have been created and have been applied successfully in *in vitro* and *in vivo* studies for different tissue experiments. However among these four strategies we believe that the most promising approach to moving tissue engineering experiments from laboratory bench to routine bedside clinical practice is to select the first strategy and rely on “pre-made porous scaffolds”. Table 2.3.6 lists examples of different types of “pre-made porous scaffolds”. They include electrospun and collagen-elastin matrices, collagen scaffolds and textile scaffolds. These approaches have been selected from the literature because they all have some merit and potential practical use. They can be distinguished from each other by their advantages and disadvantages as listed in Table 2.3.6.

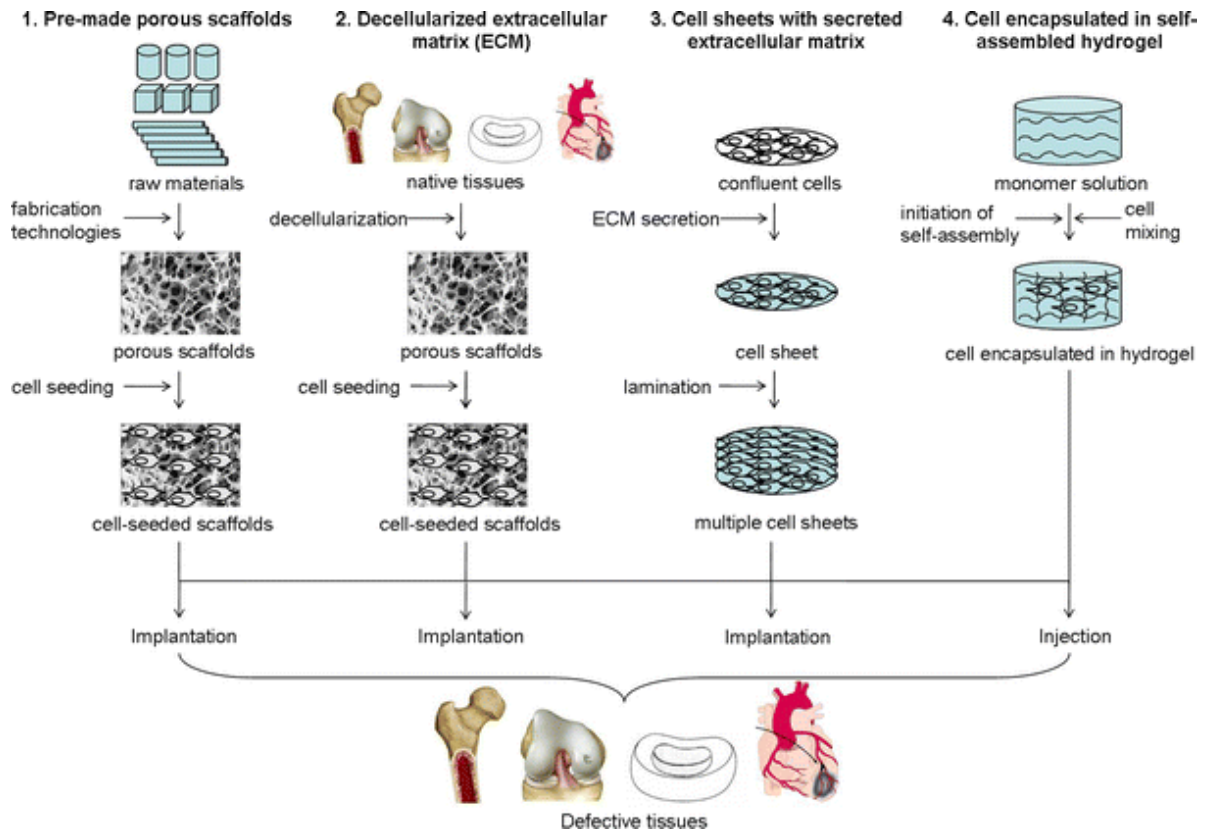


Figure 2.3.1 Schematic diagram of different scaffolding approaches in tissue engineering <sup>14</sup>

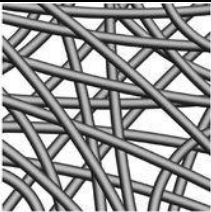
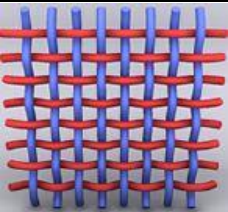
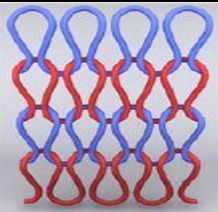
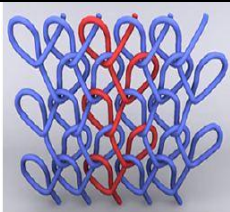
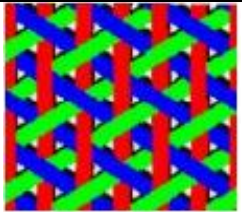
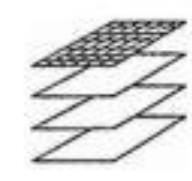

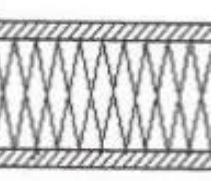
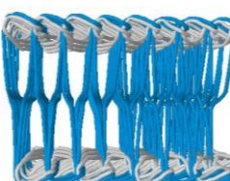
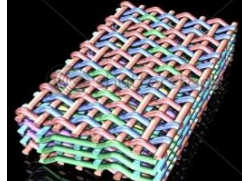
Table 2.3.6 Comparison of fabrication technologies for pre-made porous scaffolds <sup>15</sup>

Fabrication Technologies	Advantages	Disadvantages
Electrospun and collagen-elastin matrices	More tunable properties, low risk of immune response	New approach, need more clinical evidence
Collagen scaffolds	FDA status, good endothelial cell and tissue in-growth	Mechanical properties and degradation rates are not very tunable, risk of immune response
Textile scaffolds	Great design flexibility, capability to be tailored to special needs, various applications, high porosity. 100% open pores	Limited to precise architecture design at micro scale, biocompatibility depends on the yarns and materials.

## 2.2.2 Textile technologies used in medical applications

According to Figure 2.3.6, textile scaffolds have certain advantages over other structures mainly because of the design flexibility and capability to be tailored to most special structural, architectural and performance requirements. This flexibility is due to the wide range of structural variations and patterning technologies available through different textile technologies, whether knitted, woven, braid or nonwoven. Different textile fabrication technologies are summarized in Table 2.3.7. 2D textile structures have been developed for use in various medical textile applications.

Table 2.3.7 Classifications of 2D and 3D textile structures <sup>17</sup>

2D				
				
Nonwoven	Plain weave	Weft knit	Warp knit	Tri-axial weave
3D				
				
Laminate type	3-D braid	Weft knit spacer fabric	Warp knit spacer fabric	3D weave

Bonded nonwoven webs are widely used in hospital operating rooms for protective gowns, surgical drapes, masks and wound dressing. Woven and knitted fabrics are commonly used as bandages, support and compression hosiery and beddings. As surgically implantable

devices, non degradable yarns such as polyester and PTFE have been woven and knitted into artificial arteries, heart valve sewing rings and stent grafts. Warp knits and tri-axial weaves have been generated for use as implantable meshes to repair certain tissue and organs, for example with a hernia defect. Among these variable textile structures, knits have special potential as implantable scaffolds because of their versatility and flexibility.

Currently there are a range of different 2D knitted mesh structures used for implantation<sup>18,19</sup>. Because of the looped stitches, the knitted structure is soft, flexible and stretchable, which makes it adapt to the movement of human body. Besides, it also has high elasticity, tensile strength, bursting strength and excellent porosity, which are key requirements for any implantable device that needs to mimic the biomechanical characteristics of soft tissue. For example, 2D warp knitted structures have been successfully commercialized and used clinically all over the world. Take the warp knitted mesh DynaMesh® Model CICAT (FEG Textiltechnik mbH, Aachen, Germany) for example. It is made from non-absorbable, biostable polyvinylidene fluoride (PVDF) fibers and knitted into a zigzag structure to provide high tear resistance. Regardless of whether it is rolled up and inserted through a narrow trocar during non-invasive endoscopic surgery, or whether it is applied and sutured in place through open extraperitoneal surgery, it serves to support and stabilize the fascial tissue of the abdominal wall for the repair and prophylaxis of incisional hernias<sup>20</sup>(Figure 2.3.2).

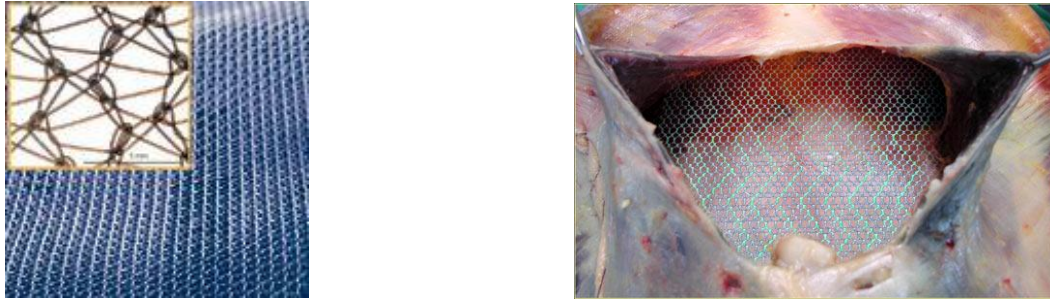


Figure 2.3.2 Two dimensional warp knitted mesh used to repair incisional hernias of the abdominal wall<sup>20</sup>

In contrast, 3D structures are more suitable for tissue engineering as discussed above. For example, Moutos, et al in Duke University have demonstrated the advantages of using a 3D woven structure as a scaffold for cartilage tissue engineering as shown in Figure 2.3.3<sup>21</sup>. It is believed that the dense woven structure has extra compression resistance, tensile strength and Young's modulus, which are key requirement for cartilage tissue<sup>22</sup>. A 3D knitted spacer fabric has a similar mechanical performance, but also has a unique porosity gradient between the layers, which 3D weaves are not able to emulate.

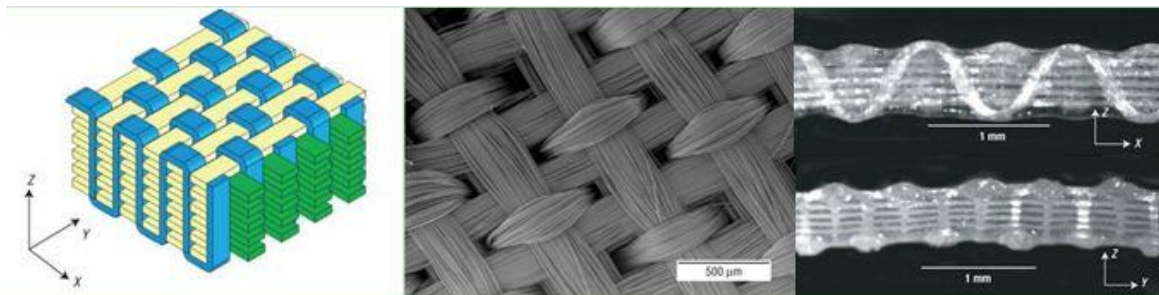


Figure 2.3.3 A 3D woven fabric structure designed for cartilage tissue engineering application<sup>22</sup>

### 2.2.3 Spacer fabric current design and application

The spacer fabric is defined as a 3 layer sandwich structure with two outer layers of fabric and a third inner spacer layer as seen in Figure 2.3.4. Since the technical face, back and

spacer layers are all knitted independently, distinct characteristics can be designed and incorporated into the same fabric by means of changing the yarns and the constructions in each layer.



Figure 2.3.4 A spacer fabric knitted from multifilament yarns in the face and back layers and showing criss-crossed monofilament yarns in the middle spacer layer.

#### **2.2.4 Warp knit spacer fabric technology**

Spacer fabrics can be produced using either weft or warp knitted technologies. Weft knitting spacer fabric is usually knitted on a double jersey circular machine, and fabric width is limited by the needle cylinder<sup>23, 24, 25</sup>. Warp knitting spacer fabric is usually knitted on a rib Raschel machine with two needle bars and a number of guide bars. The warp knitting spacer fabric has a higher thickness<sup>24</sup>.

Figure 2.3.5 shows the cross section view of a single needle bar Raschel warp knitting machine. There are two major classes of warp knitting machines: tricot and Raschel. Because fabric is drawn an angle of 120-160 degrees to the needle on Raschel warp knitting machine, the take-up tension is high and suitable for open fabric structures such as laces and nets. On the other hand, fabric on tricot warp knitting machines is drawn towards the batching roller,

almost at right angles to the needle bar. This creates a gentle and lower tension on the fabric being knitted. The maximum number of beams and guide bars on tricot warp knitting machines is limited to four, and the majority of tricot warp knitting machines operate with only two guide bars<sup>23, 25, 26</sup>.

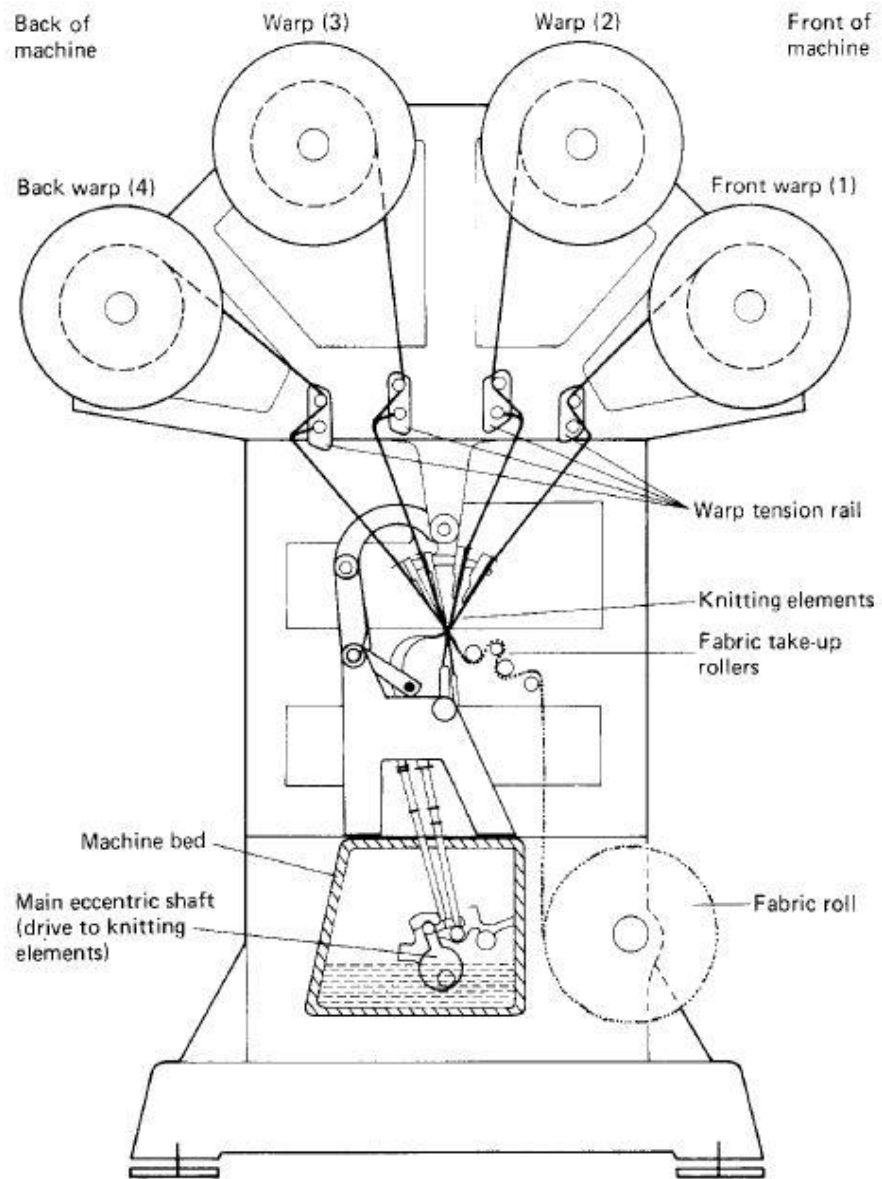


Figure 2.3.5 A cross-sectional view of a single bed latched needle Raschel warp knitting machine<sup>25</sup>

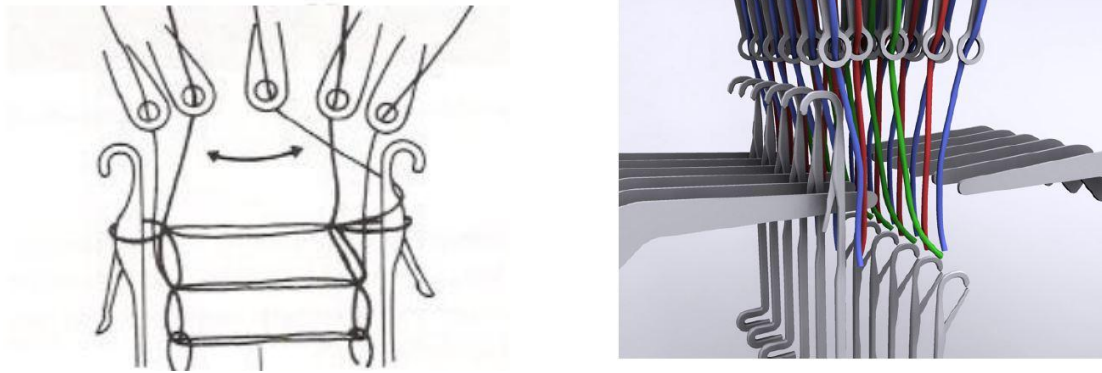


Figure 2.3.6 A cross-sectional view of the needle bars and guide bars on a double needle bed Raschel knitting machine<sup>25,26</sup>.

Double needle bed Raschel machines designed for spacer fabric are built with varying numbers of guide bars one for each yarn supply beam. As can be seen in the Figure 2.3.5 and Figure 2.3.6, the needle bars are operated independently in an up-and-down movement, while the guide bars “shog” alternately back and forth across the needles of each bar. The warp knit fabric design and lapping sequence is controlled by the links, whose height is defined between each course and directs the shogging (back and forth) movement on each of guide bar independently<sup>25,26</sup>.

The shogging movements of the guide bars control different warp knit designs. *“Different shogging movements are initiated by varying the radius of a continuously turning pattern shaft, either in the form of different heights of pattern links that pass over a pattern drum attached to the shaft, or in the form of carefully shaped solid metal circular cams, termed pattern wheels.”*<sup>26</sup> Figure 2.3.7 shows a pattern drum that can be rotated with links of different heights controlling the shogging movements of an associated guide bar. The movement of each guide bar is controlled by a separate sequence of chain links whose height is different in certain order according to the pattern. The height difference produces a thrust

against the end of the push rod, resulting in movement of the associate guide bar. An increase in height from one link to the next produces a positive shog in a direction away from the pattern device while a decrease in height produces a negative shog. A constant height will produce no shog and the guide bar will continue to swing through the same needle space, producing a pillar stitch.

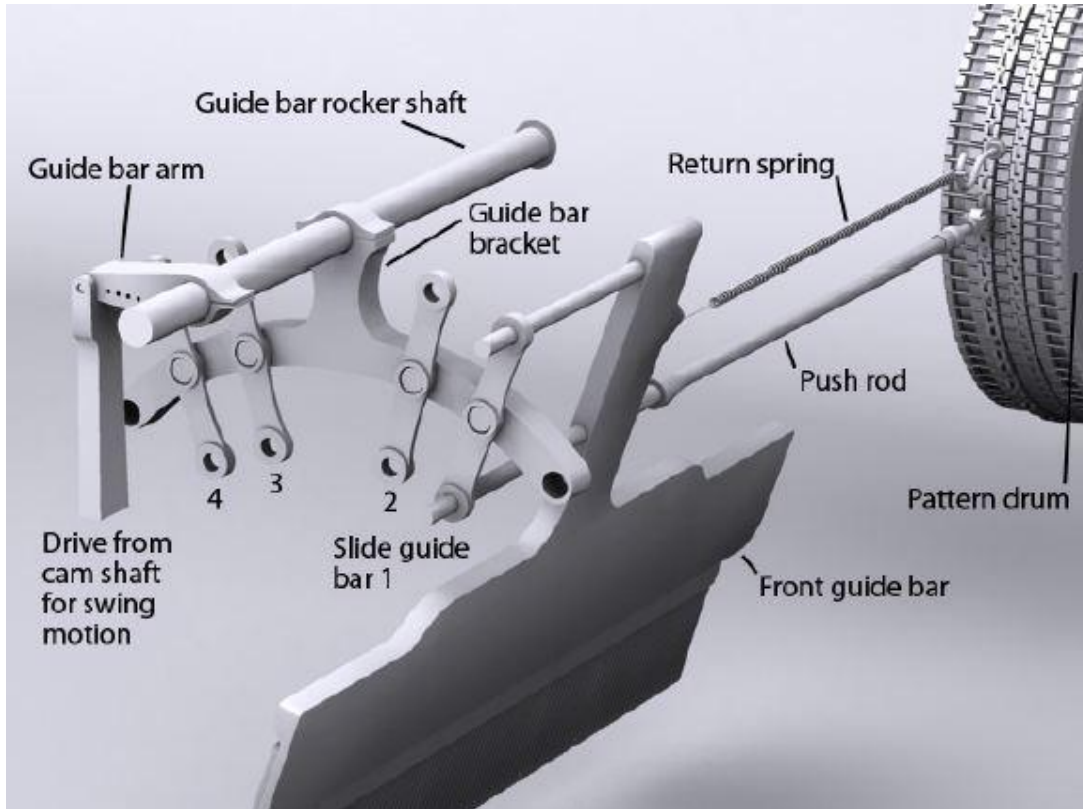


Figure 2.3.7 Design mechanism showing how the shogging (back and forth) motion of the guide bars is controlled by the pattern drum with links of different height <sup>26</sup>.

The guide bars swing or shog in front and at back of needs at the mean while the needles move up and down to form continuous loops. The movement of needle bar is illustrated in Figure 2.3.8<sup>25</sup>.

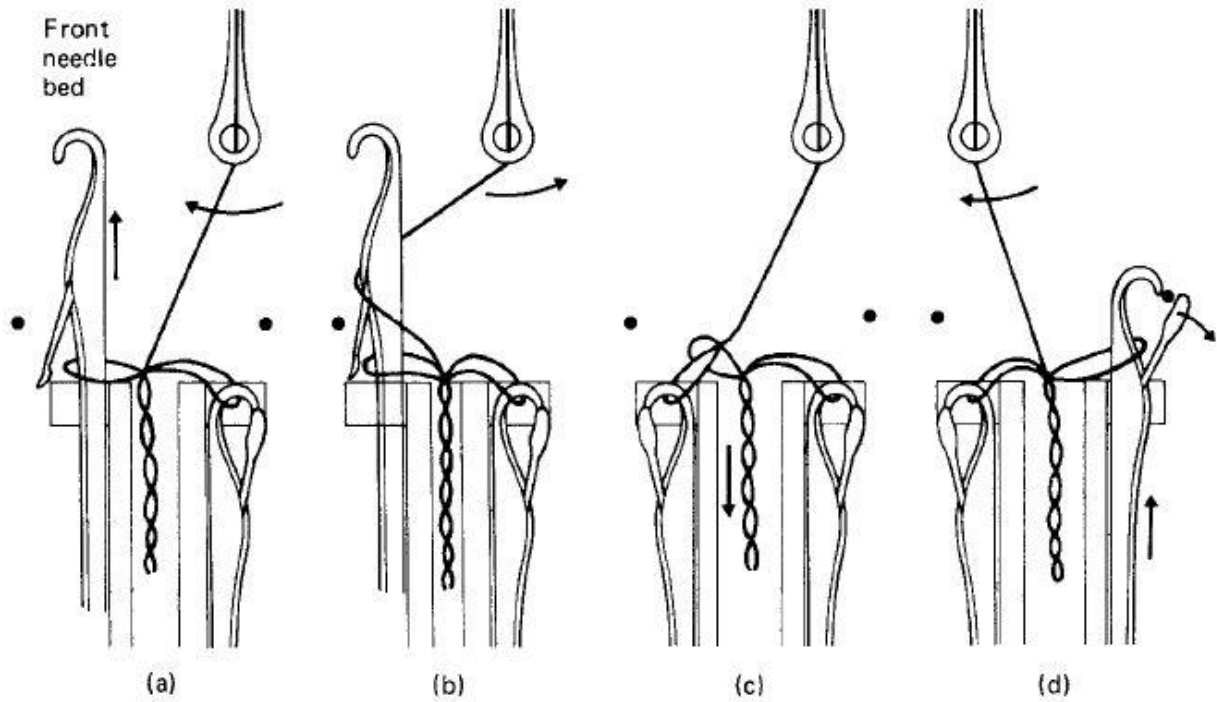


Figure 2.3.8 The vertical needle action of a double needle bed Raschel knitting machine (guide bars are simplified as one) <sup>25</sup>

## 2.2.5 Biomedical application of spacer fabric

As described earlier, the 3D knitted spacer fabric construction performs in a different manner to that of the traditional 2D knits. As a 3D structure, the spacer fabric contains a considerable amount of space inside the fabric, and the spacer yarns oriented in the Z or thickness direction provide superior compression and recovery properties<sup>24</sup>. In addition to having the well-known advantages of knitted structures, such as high bursting strength, high elongation, low Young's modulus and high porosity, the 3D spacer fabric stands out as a one piece multi-layered structure with high volume to weight ratio, softness, breathability, moisture conductivity, compression resistance and excellent recovery properties <sup>28, 29</sup>. This unique

architecture with its impressive physical and mechanical performance has been discovered by medical textile researchers and applied to both internal and external end-uses.

In various external applications, the spacer layer allows consistent air circulation to reduce heat build-up and increase moisture transfer<sup>30</sup>. Under applied pressure, it shows sustained graduated compression and uniform pressure distribution. So it is ideally suited for use as a compression bandage, for comfort cushioning<sup>30,31</sup>, and shock absorbency<sup>32</sup>. When used as a compression bandage, for example, the spacer fabric provides lightweight, non-fraying and breathable support with enhanced thermophysiological properties and protective cushioning. In addition, it shows excellent transference of pressure and the sub-bandage compression applied to the limb does not appear to be as severely influenced by the number of layers as it is with the traditional 2D bandages (Figure 2.3.9)<sup>32</sup>.



Figure 2.3.9 3D spacer fabric used as a compression bandage<sup>32</sup>

For internal applications, spacer yarns can provide a layered surface area for cell attachment and guide the cell migration through the thickness of the fabric. The numerous interconnecting pores will allow fluids carrying nutrients and waste by-products to flow

through the entire structure, hence providing superior fluid transport performance. However, there is no published research data to support this claim at the present time.

Another key advantage of using a spacer fabric as a tissue engineering scaffold is that it is a one-piece multilayer structure with different pore size distributions in the layers but without an “interface”. This means that it successfully avoids thermal bonding, toxic organic solvents or chemical adhesives that would be used to assemble traditional foams and combine multilayer fabrics. The spacer fabric may also facilitate different cell lines so as to generate separate types of tissue in the different layers. The engineered pore size distribution and porosity gradient could also provide physical guidance for the differentiation of progenitor and stem cells. In summary, the future possibilities of applying knitted spacer fabrics to a wide range of different tissue engineering end-uses looks promising, since various properties can be incorporated into the scaffold structure by changing the type of polymer, changing the type of yarns, modifying manufacturing process or activating the fibers with a surface treatment. For instance, the total porosity and the pore size distribution can be controlled by a number of manufacturing parameters, such as the gauge of the needle bed, the number of or the yarn guides, the type or combination of yarns, the gap between the needle beds and the orientation of the spacer yarns to parallel or crossed<sup>23, 24</sup>.

## CHAPTER 3 EXPERIMENTAL

### 3.1 Experimental Design

The main aim for this interdisciplinary research has been to design, produce and evaluate an appropriate three dimensional porous structure according to the experimental approach illustrated in Figure 3.1.1. First, in order to meet the requirements for tissue engineering applications, a knitted structure was designed and simulated using professional software ProCAD WarpKnit 3D. From the results of this simulation the basic knitting parameters were selected and applied to the set-up on a double needle bar Karl Mayer knitting machine. Second, 72 bobbins were wound and mounted on a creel. They were then warped on four beams with 72 ends per beam, threaded into the knitting machine and knitted into 4 samples with different knitting parameters (Table 3.1.1). After the prototype samples were produced and conditioned, the characteristics and various properties were evaluated using different standard test methods. Besides the dimensional and mechanical characteristics, the biological properties were also measured, including tests for cell viability, attachment and proliferation. Last but not the least, the results for all the tests mentioned above were statistically analyzed. Conclusions will be drawn on how these properties were influenced by the knitted structure and the knitting parameters. This will provide constructive recommendations for future research.

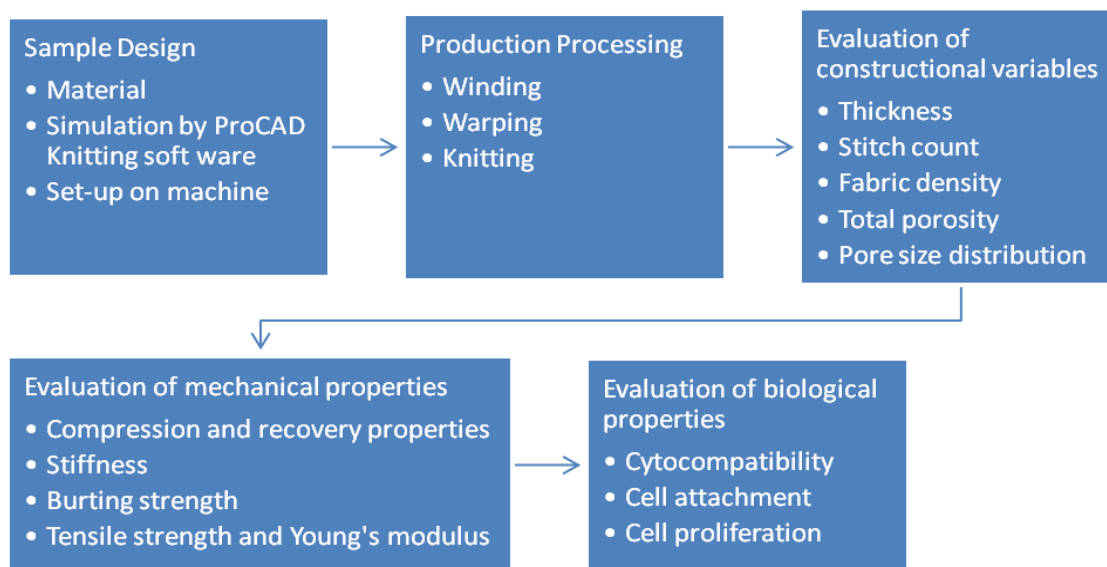
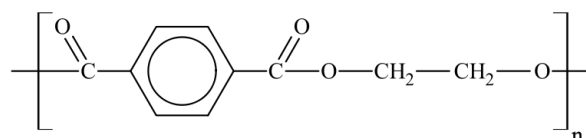


Figure 3.1.1 Experimental approach

### 3.1.1 Material

Poly(ethylene terephthalate) (PET), molecular formula  $(C_{10}H_8O_4)_n$  as shown below, was used in this study due to its permanent nature (i.e. non-resorbability), good mechanical stability, biocompatibility and comparative lower cost.



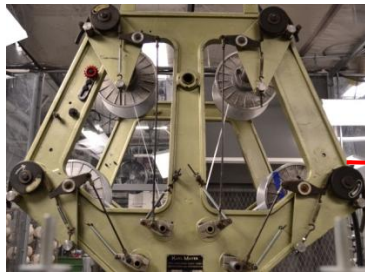
The 150 denier, 48-filament textured polyester (PET) yarn used in this study was obtained from Unifi Inc., Yadkinville, NC, USA, and its technical details supplied by the company are listed in Table 3.1.1.

Table 3.1.1 PET yarn properties

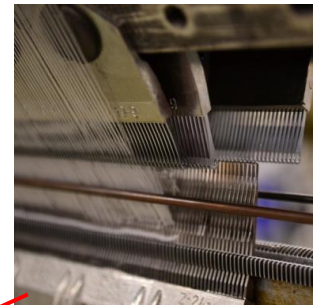
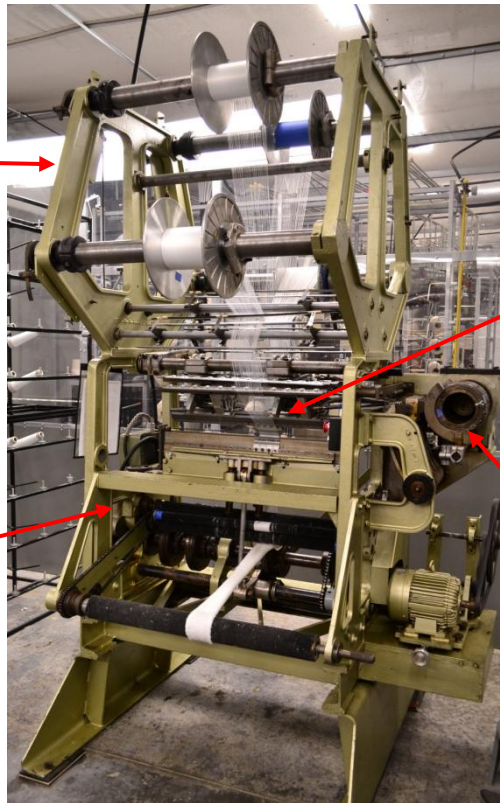
Properties	Cross-section	Tenacity	Elongation	Shrinkage	Density	Twist direction
PET yarn	Round	4.7 (gpd)	20.4%	14.8% (180F)	1.38 (g/cm <sup>3</sup> )	S

### 3.1.2 Spacer Fabric Design and Production

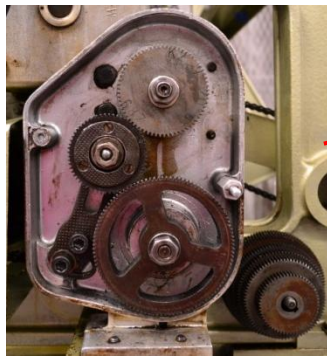
The prototype spacer fabric samples were knitted on a double needle bed, narrow width (26 inches) Rasche Karl Mayer DR 10 warp knitting machine with two interchangeable sets of needles for the two needle beds, having both 12 gauge and 24 gauge sets of needles (Figure 3.1.2).



Yarn tension control



Guide bars and needles



Fabric tension control



Links

Figure 3.1.2 Karl Mayer DR 10 warp knitting machine

The four prototype knitted samples were identified as follows: 24E6GB, 24E4GB, 12E6GB and 12E4GB, according to the gauge (E) and the number of guide bars (GB) as shown in Table 3.1.2. All of the four samples were knitted with 72 ends. In addition, two 100%

polyester commercial spacer fabric control samples, identified as SHR 724/5 and SHR 728, were introduced in the study. These two commercial samples were obtained from Gehring Textiles Inc, Garden City, NY, USA, and were included because they contained monofilament spacer yarns instead of the multifilament yarns used for the prototype knitted samples. Their technical information is listed in Table 3.1.3. From the literature review, it is believed that a denser spacer layer would contribute to the compression resistance and would be able to support cell attachment. Also, the higher gauge and the higher number of guide bars, as well as the multifilament spacer yarns, would increase the density of the spacer fabric. Therefore a hypothesis is proposed that the higher gauge and the higher number of guide bars as well as the multifilament spacer yarns will have an impact on the spacer fabric's performance with respect to constructional characteristics, mechanical and biological properties.

Table 3.1.2 Sample types and parameters for all samples

<b>Parameters</b>	<b>Gauge (needles per inch)</b>	<b>Number of Guide Bars</b>	<b>Spacer yarns</b>	<b>Ends/ fabric width</b>	<b>Sources</b>
<b>24E 6GB</b>	24	6			
<b>24E 4GB</b>	24	4	Multi-filament	72 ends	Knitted at NCSU
<b>12E 6GB</b>	12	6			
<b>12E 4GB</b>	12	4			
<b>SHR 724/5</b>	22	5	Mono-filament	Wide width	Gehring Textiles Inc.
<b>SHR 728</b>	22	6			

Note: Four guide bar means only guide bars No. 2-5 were used (see Table 3.1.4 ).

Table 3.1.3 Information of commercial samples (Information supplied confidence by Gehring textiles Inc.)

Sample	Properties	Technical Face	Spacer	Technical Back
	Percentage of the yarn in the fabric	15.10%	68.30%	16.60%
<b>SHR 724/5</b>	Yarn type	70D-36F texture polyester, SD	30D-1F polyester, SD	70-36 texture polyester, SD
	Structure	2 bar diamond face structure	1 bar pile connector	2 bar solid plain back face
	Percentage of the yarn in the fabric	34.90%	38.10%	27.00%
<b>SHR 728</b>	Yarn	100D-54F polyester, bright, round	30D-1F polyester, SD	40D-17F polyester, SD
	Structure	2 bar solid plain back face	2 bar pile connector	2 bar solid plain back face

Note: In the table “D” is short for denier, “F” for filament and “SD” for semi dull.

Prototype samples for both needle gauges were knitted into the same structure and thickness with the spacer yarns lying with both cross and parallel orientations. The lapping sequence used for the different gauges and the different numbers of guide bars are shown in Table 3.1.4 and Figure 3.1.3. Since the height of the links (Figure 3.1.3) was different for 12 and 24 gauge needles, the lapping sequences were modified as shown in Table 3.1.4 so as to obtain the same cross and parallel spacer yarn orientation on Bars 3 and 4 (Figure 3.1.3).

Table 3.1.4 Lapping sequence diagram for four knitted samples

<b>12 E 6 GB :</b>	<b>24 E 6 GB :</b>
Front:	Front:
Bar 1 : 0-0/1-2/1-1/1-0	Bar 1 : 1-2/0-0/1-0/0-0/1-2/2-2/1-0/2-2/
Bar 2 : 0-0/1-0/1-1/1-2	Bar 2 : 1-0/0-0/1-2/2-2/1-0/0-0/1-2/2-2/
Spacer Yarns:	Spacer Yarns:
Bar 3 : 2-3/3-2/1-0/1-2	Bar 3 : 1-2/2-3/3-2/1-0/1-2/2-3/3-2/1-0/
Bar 4 : 1-0/1-2/2-3/3-2	Bar 4 : 3-2/1-0/1-2/2-3/3-2/1-0/1-2/2-3/
Back:	Back:
Bar 5 : 1-0/1-1/1-2/0-0	Bar 5 : 1-1/1-0/1-1/1-2/1-1/1-0/1-1/1-2/
Bar 6 : 1-2/1-1/1-0/0-0/	Bar 6 : 0-0/1-2/1-1/1-0/0-0/1-2/1-1/1-0/
<b>12 E 4 GB:</b>	<b>24 E 4 GB:</b>
Front:	Front:
Bar 2 : 0-0/1-0/1-1/1-2	Bar 2 : 1-0/0-0/1-2/2-2/1-0/0-0/1-2/2-2/
Spacer Yarns:	Spacer Yarns:
Bar 3 : 2-3/3-2/1-0/1-2	Bar 3 : 1-2/2-3/3-2/1-0/1-2/2-3/3-2/1-0/
Bar 4 : 1-0/1-2/2-3/3-2	Bar 4 : 3-2/1-0/1-2/2-3/3-2/1-0/1-2/2-3/
Back:	Back:
Bar 5 : 1-0/1-1/1-2/0-0	Bar 5 : 1-1/1-0/1-1/1-2/1-1/1-0/1-1/1-2/

Based on the lapping sequence and the other knitting parameters mentioned above, the spacer fabric samples were first simulated using the professional fabric design software ProCAD and presented in Figure 3.1.3, Figure 3.1.4 and Figure 3.1.5, so as to obtain a direct illustration of each structure before knitting. The 2D simulations provided the loop notations

for the face (Guide bars 1 and 2), spacer (Guide bars 3 and 4), and back yarns (Guide bars 5 and 6). The color of the face and back yarns was set at white while the spacer yarns were shown in blue to make a clear distinction. Next, the 3D simulations gave a valuable direct-view of the knitted stitches and yarn spacing, which are hard to observe in the real knitted prototype fabrics due to the variable yarn tension and deformation.

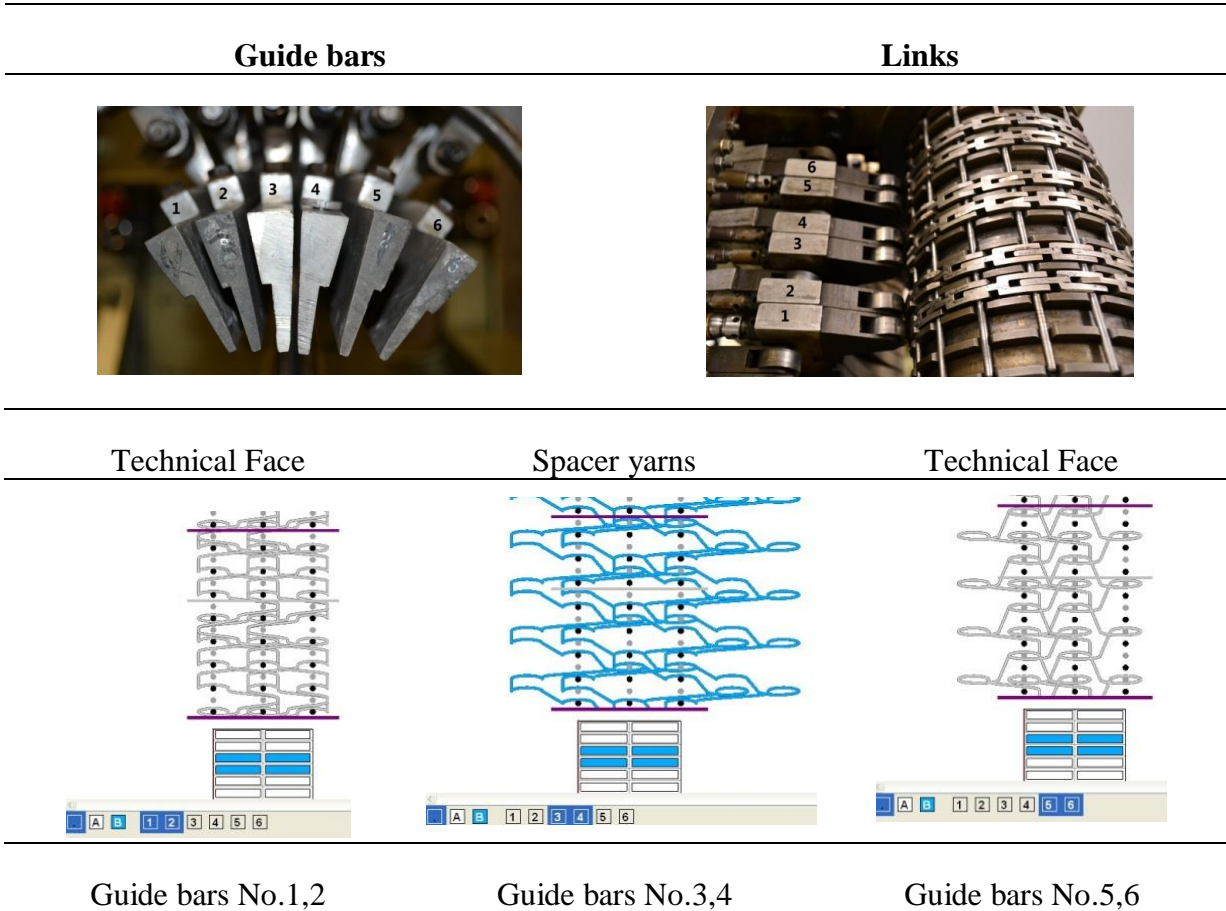


Figure 3.1.3 2D Simulation of 6GB structure in ProCAD and relevant machine settings

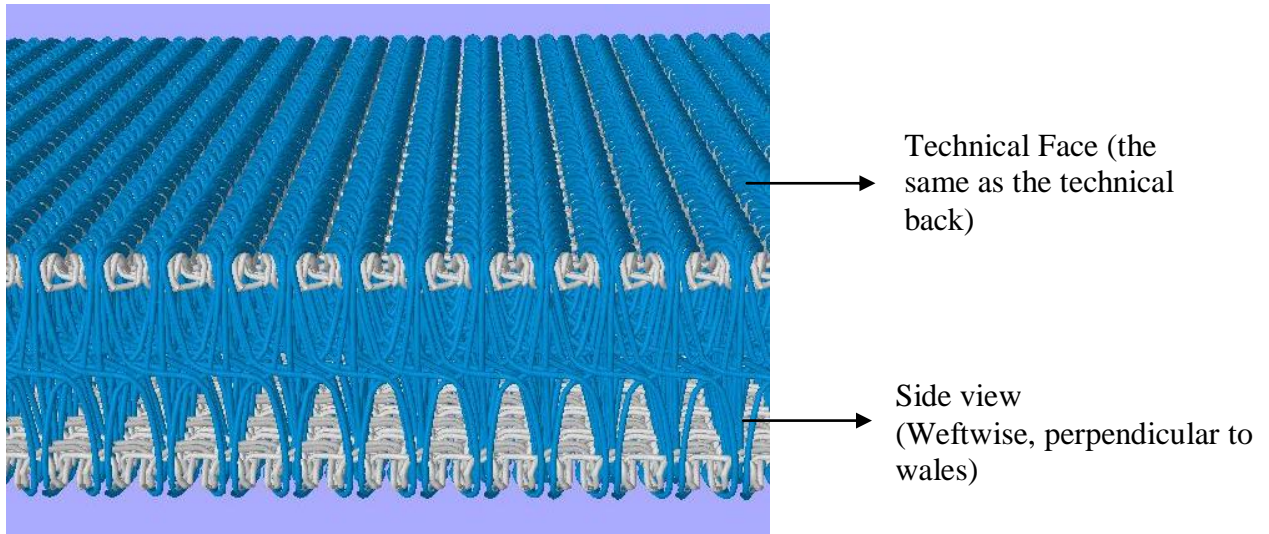


Figure 3.1.4 3D simulation of 24E 6GB in ProCAD software

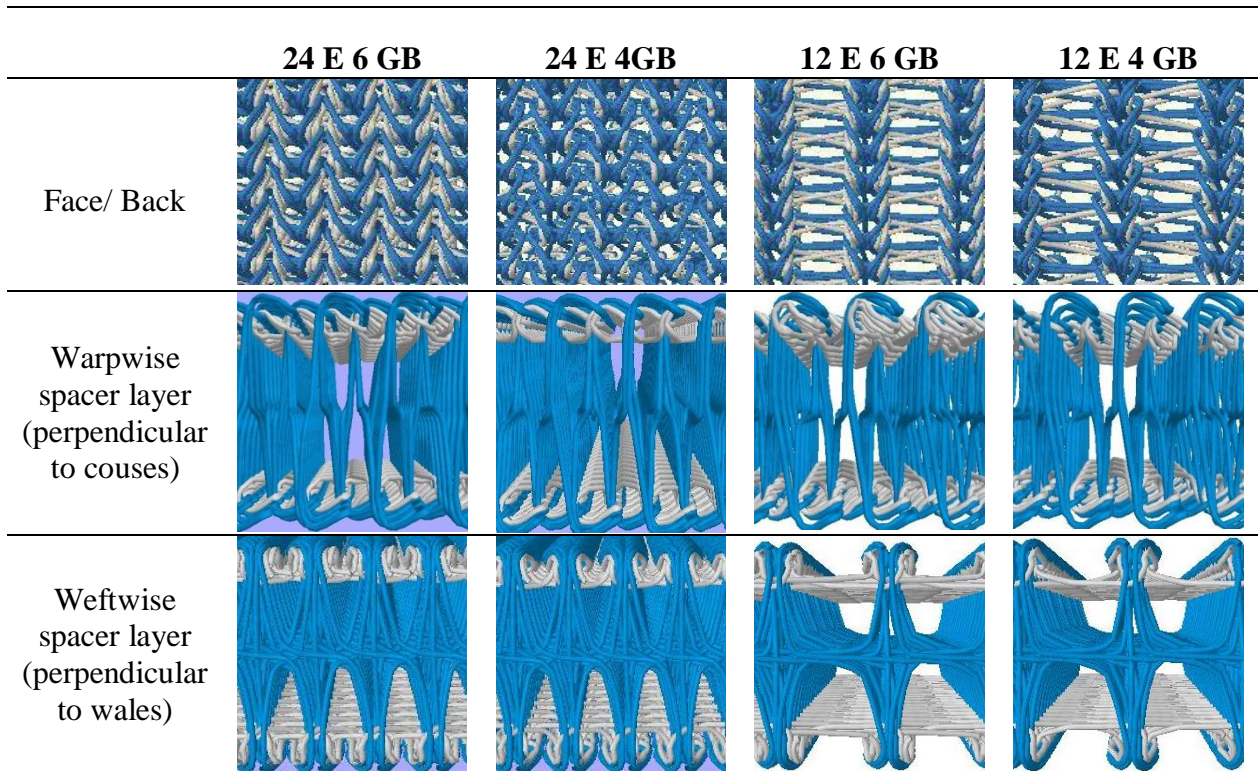


Figure 3.1.5 3D simulation of all four prototype knitted structures in ProCAD software

## **3.2 Evaluation of Constructional Characteristics**

The following constructional characteristics: fabric stitch count, fabric density, thickness, total porosity, pore size distribution and surface morphology were measured on the prototype knitted grey fabrics and the two finished commercial samples. These properties were considered critical to understanding the different structures generated by the different knitting parameters.

### **3.2.1 Fabric Structure and Surface Morphology by Optical Image**

#### **Analysis**

After conditioning overnight at  $65\pm 3$  % RH and a temperature of  $20 \pm 2$  °C, the knitted spacer fabric structures were analyzed using a Nikon SMZ 1000 optical microscope under magnifications of 10 times and 20 times. Five images were taken of the fabric, namely the technical face and back, and the spacer layer in cross-section for each sample.

### **3.2.2 Fabric Count, Thickness, and Density**

Based on these images, fabric stitch counts were determined by counting the number of wales and courses per inch according to the *ASTM D 3887–96 (Reapproved 2008) Standard Specification for Tolerances for Knitted Fabrics*<sup>33</sup>. The specimens were chosen at random from different locations all at least 1 inch from the edges of the samples. Five specimens of each sample were counted four times each and the values averaged.

The thickness of the spacer fabrics was determined using an SDL 94 thickness gauge from Shirley Developments Ltd, Stockport, England (Figure 3.2.1) which was able to apply a

range of pressures from 20-2000 g/cm<sup>2</sup>. The area of the presser foot was 412mm<sup>2</sup>, and the gauge measured thickness to a precision of 0.01mm. The test was conducted according to *ASTM D 1777 – 96 (2007) Standard Test Method for Thickness of Textile Materials*<sup>34</sup>.

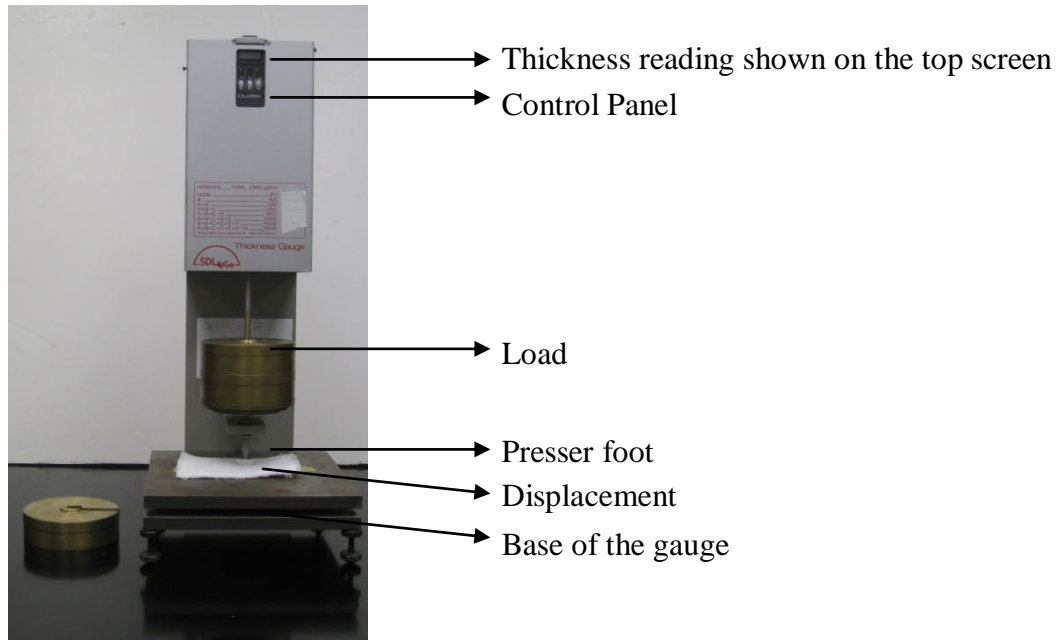


Figure 3.2.1 SDL 94 thickness gauge in the Biomedical Textile Laboratory at College of Textile, NCSU

The displacement between the base and the circular weighted presser foot was read on the top screen as the thickness value of the specimen. Specimens measuring 16cm by 10cm were cut from the center of the rolls of grey knitted samples and were left free of folds, creases, or wrinkles, for 24 hours before testing to relax and condition in a standard atmosphere of  $21 \pm 1^{\circ}\text{C}$  ( $70 \pm 2^{\circ}\text{F}$ ) and  $65 \pm 2\%$  relative humidity. Since the thickness value of all textiles will vary according to the pressure applied to the surface, any thickness value discussed later will specify the pressure at the time the measurement was taken. For thickness testing in this study the pressure applied to presser foot was 20 g/cm<sup>2</sup> for all specimens. Each fabric sample

was measured 10 times and the average of these 10 readings represents the mean thickness of the sample.

The density ( $D$ ,  $\text{g}/\text{cm}^3$ ) of the fabric was determined from the fabric mass ( $M$ ,  $\text{g}$ ) per unit area ( $S$ ,  $\text{cm}^2$ ) which was calculated from length ( $L$ ,  $\text{cm}$ ) and width ( $W$ ,  $\text{cm}$ ) of the specimen and divided by the thickness ( $h$ ,  $\text{cm}$ ) as shown in Equation 3.1 according to *ASTM F2450 – 10 Standard Guide for Assessing Microstructure of Polymeric Scaffolds for Use in Tissue-Engineered Medical Products*<sup>35</sup>.

$$D = \frac{M}{S * h} = \frac{M}{L * W * h} \quad (3.1)$$

### 3.2.3 Total Porosity

The nature and extent of the porous macrostructure and microstructure of a tissue engineering scaffold will affect both the cellular response and the functionality of the generated tissue. According to ASTM F2150-10, the Standard Guide for Characterization and Testing of Biomaterial Scaffolds Used in Tissue-Engineered Medical Products, the porosity is defined as the “property of a solid which contains an inherent or induced network of channels and open spaces. Porosity can be measured by the ratio of pore (void) volume to the apparent (total) volume of a porous material and is commonly expressed as a percentage.” However, since it is difficult to measure the total porosity directly, it was calculatedly using the Equation 3.2 which relies on the density of the 3D fabric scaffold and the density of the polymer *ASTM F2450 – 10 Standard Guide for Assessing Microstructure of Polymeric Scaffolds for Use in Tissue-Engineered Medical Products*<sup>35</sup>.

$$p = \left(1 - \frac{d_s}{d_p}\right) \times 100 = \left\langle 1 - \left\{ \frac{\left(\frac{m_s}{v_s}\right)}{d_p} \right\} \right\rangle \times 100 = \left\langle 1 - \left\{ \frac{\left(\frac{m_s}{w \times l \times h}\right)}{d_p} \right\} \right\rangle \times 100 \quad (3.2)$$

Where,

$p$  = total porosity

$d_s$  = the density of the scaffold in (g/cm<sup>3</sup>),

$d_p$  = the density of the polymer in (g/cm<sup>3</sup>),

$m_s$  = the mass of the scaffold (g),

$v_s$  = the volume of the scaffold (cm<sup>3</sup>),

$w$  = the width of the scaffold (cm),

$l$  = the length of the scaffold (cm),

$h$  = the thickness of the scaffold (cm)

The density of the polyester ( $d_p$ ) was assumed to be 1.38 (g/cm<sup>3</sup>)<sup>36</sup>. Each sample was cut into sixteen 4.00 cm by 5.00 cm specimens and conditioned overnight at 65±3 % RH and 20 ±2 °C. The width and length were measured using vernier calipers, while the thickness was measured using the SDL 94 Thickness Gauge as described above. The mass of the specimen was measured on a weighing balance (Model AG 245) with a precision of 0.1 mg, and the total porosity,  $p$ , for each sample was reported as a mean +/- standard deviation value.

### 3.2.4 Pore size Characterization

A pore is defined as an inherent or induced network of channels and open spaces within an otherwise solid structure as explained in *ASTM F2150*. But the pore size is difficult to

measure directly due to its variations in type, the irregular shape and tortuosity. Although various methods have been reported in the literature, there is still a lack of agreement on a reliable and representative methodology for evaluating the average pore size and its distribution under a standardized method that would facilitate comparison of results. The method used in this study was selected and adapted to evaluate the influence of the various knitting parameters on the pore size and its distribution among the samples included in this research.

Because a knitted fabric is flexible and deformable, it is difficult to measure the pore size and its distribution directly from the cross section. Specimens of each sample were cut into squares measuring 4 cm x 4 cm and embedded in epoxy resin with 5% methyl ethyl ketone peroxide (MEKP) initiator. They were allowed to harden overnight at 44% relative humidity and 19°C and then cut into sections with a Buehler IsoMet® low speed saw (Buehler LTD, Lake bluff IL, USA). The sections were polished in a series of steps using polishing paper from 120 to 1200 grit on a MetPrep 3™ Grinding/Polishing Machine (Allied High Tech Products, Inc, Rancho Dominguez, CA, USA). Images of embedded scaffold sections of all six samples were taken using a Nikon Eclipse L150 optical microscope with a Nikon DXM1200 digital capture camera at magnifications of 50 and 100 times. The images were analyzed using the java-based image processing software ImageJ (NIH). Pores are defined and constructed in each plane by making the biggest inscribed circle connecting at least three different fiber surfaces. Before undertaking these measurements, the contrast and threshold of each image were optimized. The diameters of the individual pores were calculated using ImageJ. Twenty images were taken of the section slices in any one plane and 600 pores were

analyzed based on those images per sample. The average pore diameter was calculated and statistically reported as a mean  $\pm$  standard deviation. The pore size distribution has been presented in graphical form using a six order polynomial trend curves.

### **3.3 Mechanical Tests**

#### **3.3.1 Compression and Recovery**

The method of measuring compression resistance and recovery properties was developed from ASTM D6571-01 Standard Test Method for Determination of Compression Resistance and Recovery Properties of High loft Nonwoven Fabric Using Static Force Loading<sup>37</sup>. Samples were tested on the SDL 94 thickness gauge from Shirley Developments Ltd, Stockport, England, which was the same instrument used for the thickness test described above. This was undertaken by measuring the thickness of the knitted fabric after applying a series of defined pressures onto the fabric. In half-minute intervals a series of weights (20, 50, 100, 200, 700, 1200, 1700g) was added in succession, and the thickness values were recorded. For the unloading cycle, the weights were removed in half minute intervals over the same sequence (1700, 1200, 700, 200, 100, 50, 20g), and the thickness values were measured again. This procedure was repeated 10 times for each sample. The thickness values of each sample were averaged at all 13 time points and reported as a trend curve for analysis. The level of Compression resistance was defined as the ratio of the thickness at 1700g loading point divided by the initial thickness at 20g loading. The extent of recovery was defined as the ratio of the final removed 20g thickness divided by the initial 20g thickness. The level of compression resistance and the extent of recovery were used to present the changes in

thickness during the test and are reported as a percentage in terms of a mean  $\pm$  standard deviation.

### 3.3.2 Flexural Rigidity (Stiffness)

The stiffness of all the six fabric samples was obtained using a Model S0015 Cantilever Bending Stiffness Tester from IDM Instruments Pty Ltd., Melbourne, Victoria, Australia (Figure 3.3.1). The test was run according to the *ASTM D1388-08 Standard Test Method for Stiffness of Fabric*<sup>38</sup>. The only deviation from the standard method was that the samples were cut into specimens measuring 4cm x 20 cm instead of 2.5cm x 20 cm. A specimen was moved forward at a specified rate in a direction parallel to its long dimension, until its leading edge projected from the edge of a horizontal surface. The length of the overhang was measured when the tip of the specimen fell under its own mass to the point where the line joining the top to the edge of the platform makes a 0.724 rad (41.5°) angle with the horizontal. For each sample four specimens were measured and four readings were taken from each specimen, one in each direction and two from each side. From these measured overhang length values  $O$ , the bending length  $c$  was calculated according to Equation 3.3.

$$c = \frac{O}{2} \quad (3.3)$$

Where,

$c$  = bending length (cm);  $O$  = length of overhang (cm)

The flexural rigidity  $G$  of the fabrics was obtained using Equation 3.4

$$G = 1.421 * 10^{-5} * W * c^3 \quad (3.4)$$

Where,

$W$  = fabric mass per unit area ( $\text{g}/\text{cm}^2$ );  $c$  = bending length (cm)

The stiffness value for each sample was reported as the mean  $\pm$  standard deviation.

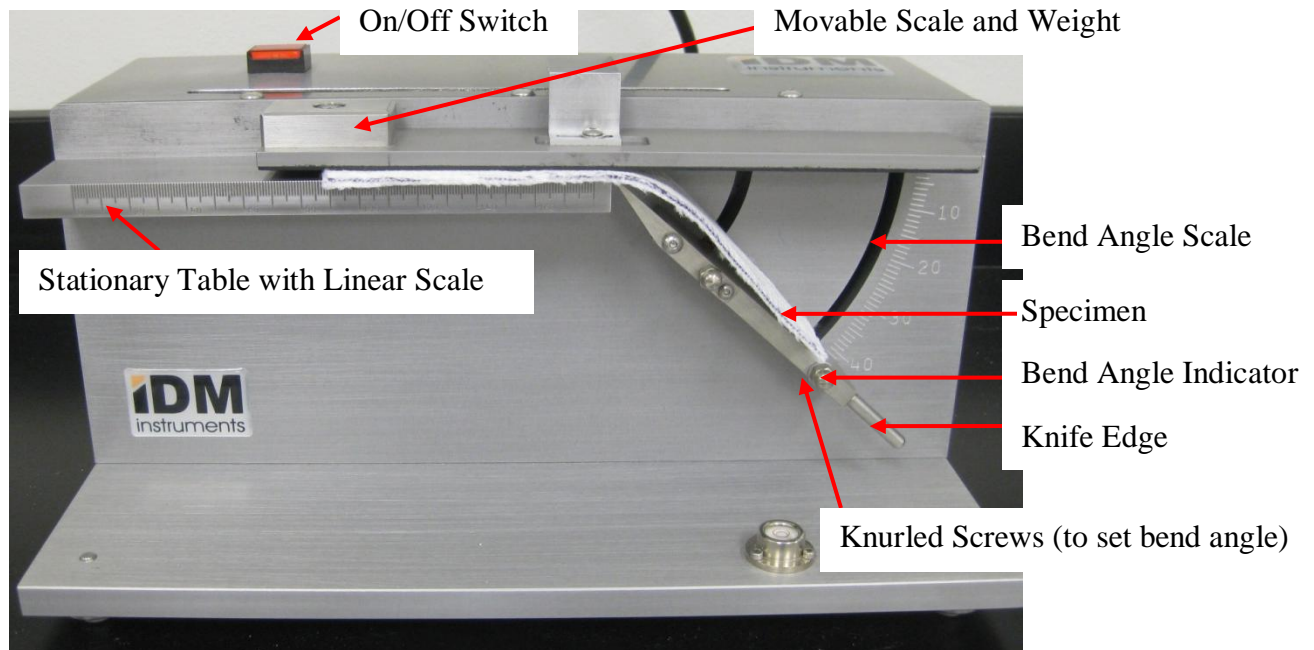


Figure 3.3.1 Model S0015 Cantilever Bending Stiffness Tester from IDM Instruments Pty, Ltd, in the Physical Testing Lab at College of Textile, NCSU

### 3.3.3 Bursting Strength

The probe bursting strength of the specimens was determined by using a modified standard ASTM D3787 Bursting Strength of Textiles—Constant-Rate-of-Traversal (CRT) Ball Burst Test Method<sup>39</sup>. The maximum bursting strength was defined as the absolute force applied at right angles to the plane of the fabric at the failure point. After conditioning for 24 hours in a standard atmosphere, the samples were cut into 4 cm x 4 cm squares. A specially designed bursting strength apparatus with a probe and two mounting plates (ISO 7198:1998 International Standard Cardiovascular implants — Tubular vascular prostheses<sup>40</sup>) were mounted on a Model # 5544 Bluehill Instron Universal Tester (Instron, Norwood, MA, USA)

as showing in Figure 3.3.2. The test was started with the probe just touching the surface of the specimen. An increasing force was exerted at right angle to the plane of the specimen by a polished, hemispherical shaped hardened steel probe that was attached to the top fixed clamp of the machine until rupture occurred. The metal probe utilized for all bursting strength testing had a diameter of 6.25 mm, whereas the diameter of the hole in the middle of the two mounting plates was 11.45mm. Between the two mounting plates there was a black O-rings use to clamp the fabric specimen. The inside and outside diameters of this O-ring were 18.72 mm and 24.98 mm respectively. In order to perform the bursting strength testing, the rate of traverse was set to 305 mm/min. The maximum bursting strength was averaged from the 16 specimens tested and reported in terms of the mean  $\pm$  standard deviation.

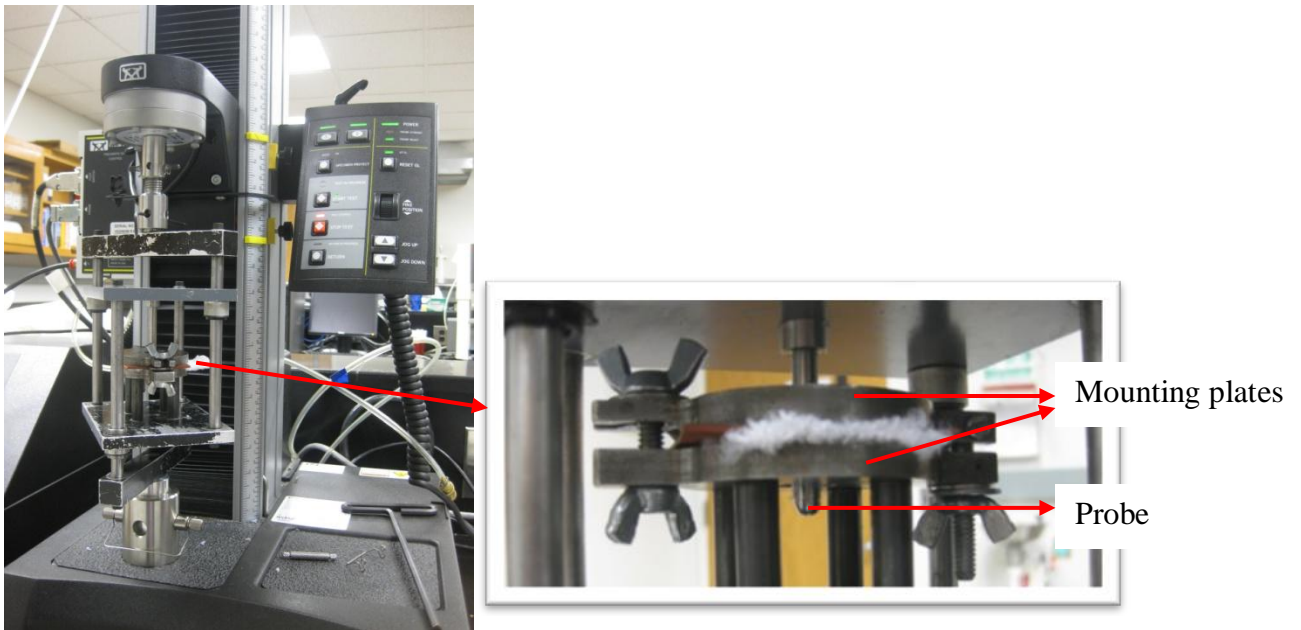


Figure 3.3.2 Bluehill Instron Model No.5544 with probe bursting strength apparatus attached

### 3.3.4 Tensile strength

In order to study the maximum tensile strength in the warp and weft directions, samples were tested on the Model # 5544 Bluehill Instron Universal Tester (Instron, Norwood, MA, USA) following the standard *ASTM D 5035-11 Standard Test Method for Breaking Force and Elongation of Textile Fabrics (Strip Method)*<sup>39</sup>. A test specimen was mounted between two clamps which were initially 2.45 cm apart and a force was applied to the specimen (Figure 3.3.3). Once the test started the two clamps moved in opposite directions at a constant speed of 305mm/min until the specimen broke. Values for the breaking force and elongation of the test specimen were obtained from the computer recorder and controller which were interfaced with the universal tester. Based on these values, the maximum tensile strength and Young's modulus were calculated and stress/ strain curves were created. The maximum tensile strength (stress) is defined as the absolute force per unit area at the failure point.

Young's modulus, E, was determined from the slope of the stress/strain curve in the initial linear portion of the curve, and the modulus was reported as the steepest slope between the lower and upper bounds. For example, the 20% Young's modulus is the modulus calculated between the origin and 20% of the maximum tensile strength as calculated by Bluehill 2 Software following the Equation 3.5

$$E = \frac{\text{tensile stress}}{\text{tensile strain}} = \frac{\sigma}{\epsilon} = \frac{F/A}{\Delta L / L} = \frac{F * L}{A * \Delta L} \quad (3.5)$$

Where,

$E$  = the Young's modulus (MPa),

$F$  = the absolute force applied to the fabric (N),

$A$  = the original cross-sectional area through which the force is applied ( $\text{mm}^2$ )

$\Delta L$  = the amount by which the length of the object changes (mm),

$L$  = the original length of the object (mm).

In this test, 12 specimens were cut into 2.5cm x 8cm strips in both directions (6 in the warp direction and 6 in the weft direction) from each fabric sample unit. The maximum tensile strength (N) and 20% Young's modulus (MPa) were averaged and reported as a mean  $\pm$  standard deviation.

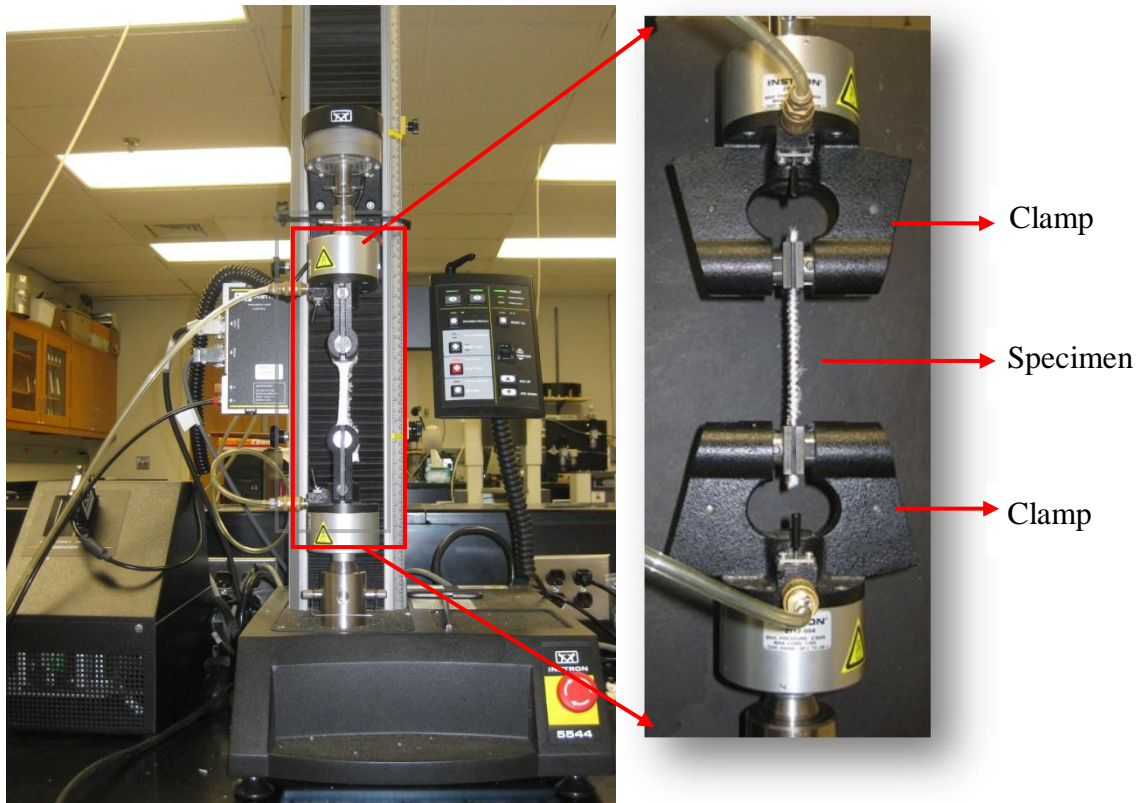


Figure 3.3.3 Bluehill Instron Model No. 5544 Universal Tester with tensile strength apparatus

### **3.4 *In Vitro* Cell Culture Study**

#### **3.4.1 Preparation of Sample**

All the six samples were cut into 16mm diameter circles to fit into 24-well plates and be sterilized in an Anprolene Model AN74ix sterilizer (Anderson Products, Inc, Cresco, PA, USA). Ethylene oxide gas was used as the sterilant and released from a 20 cc ampoule inside the sterilizer bag, slowly diffusing out over a 12 hr sterilization period at ambient temperatures (approximately 70 °F).

Before cell seeding, the specimens were pre-wetted in 70 % aqueous ethanol solution for 48 hours, rinsed twice with ultrapure water and twice with sterile Hanks™ solution, and then immersed in 1.00 ml FGM-2 fibroblast medium (Lonza Walkersville, Inc Basel, Switzerland) in 24-well plates for 2 hours in an incubator at 37°C. The specimens were then seeded with Clonetics® Human Fibroblast Cell Systems (Lonza Walkersville, Inc Basel, Switzerland) at 10,000 cells per well according to routine cell-culture methods. The plates were incubated at 37°C and 5% CO<sub>2</sub> for fifteen days. For each fabric sample, four specimens were used as well as one for the 2D well (no specimen) control and one for the no cell (with specimen) control were included in this study.

The biological performance was evaluated by 3-(4,5-dimethylthiazol-2-yl)-2,5-diphenyltetrazolium bromide (MTT) viability assay, scanning electron microscopy (SEM) and laser scanning confocal microscopy (LCSM) analysis at time points of Day 1, Day 3, Day 6, Day 10 and Day 15.

### 3.4.2 Cell Viability (MTT Assay)

At each time point, samples were taken from the 24-well plates and transferred into new plates for the MTT study. The MTT solution (Promega Corporation, Madison, WI, USA) was prepared by dissolving the powder in phosphate buffered saline at a concentration 1 mg/ml. After 1 hr of incubation, the purple crystals were dissolved by adding sodium dodecylsulphate (SDS) in a 1: 1 mixture of water and dimethylformamide (DMF) at a concentration of 20% w/v.

After adding 1ml of MTT medium (0.0005mg/ml) to each well, the plates were incubated for 3hrs, rinsed and desorbed in 100ul of 70% isopropanol. After being agitated rapidly at 400 revolutions /min for 40min, the dyed medium was transferred to 96-well plate, and read at 550nm. The viability is expressed as a percentage of the control sample (100%).

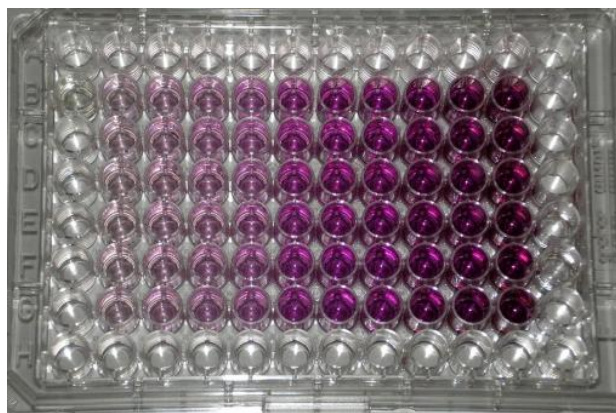


Figure 3.4.1 MTT formazan solution in a 96-well plate showing more viable cells on right hand side giving higher formazan production and thus a stronger purple colour<sup>41</sup>

### **3.4.3 Scanning Electron Microscopy (SEM)**

In order to observe the morphology of the cells attached to the surface yarns and spacer yarns, specimens were viewed under a JEOL JSM-6360LV scanning electron microscope from JEOL USA, Inc., Peabody, MA, USA using the variable pressure mode at high vacuum with an accelerating voltage of 5 kV.

Prior to viewing, the cell seeded specimens were fixed with the 4F: 1G fixative<sup>42</sup>, a mixture containing 4% formaldehyde and 1% glutaraldehyde in a monobasic phosphate buffer with a final pH of 7.2-7.4 and a final osmolality of 176 mosmol. They were left for 1-2 hr at room temperature and then dehydrated in a graded aqueous ethanol series to 100% ethanol, at which time they were critical point dried with liquid CO<sub>2</sub>. Finally, specimens were mounted on aluminum stubs using conductive carbon tape and sputter-coated with gold-palladium for viewing in a JEOL JSM-6360LV scanning electron microscope<sup>43-45</sup>.

In order to get representative results, images were taken at random on the top and bottom surfaces and of the cross-sectional side-view of the specimens at various magnifications.

### **3.4.4 Laser Scanning Confocal Microscopy (LSCM)**

In order to visualize the cell population throughout the thickness of the scaffold, a Zeiss Model LSM 710 laser scanning confocal microscope (Carl Zeiss MicroImaging, New York, NY, USA) was used with a 10 X 0.45 NA dry Plan Apochromat objective. The scan head was attached to a Zeiss Axio Observer Z1 inverted microscope with a motorized x, y, z stage. Sections of 2D images were generated from the surface to the inside of the specimen cross

section. The spatial resolution of the images was 512 x 512 pixels. ZEN software (Carl Zeiss MicroImaging, New York, NY, USA) was used for 3D image reconstruction and analysis.

At each time point prior to viewing, the cell seeded specimens were removed from their seeding plates and cut in order to obtain the cell morphology of the internal cross-section. Then specimens were washed three times in Hanks™ solution before and after being stained in 300 µm Live/Dead double-stain solution (LIVE/DEAD® Viability/Cytotoxicity Kit from Invitrogen™, Carlsbad, CA, USA) for 30 minutes while being covered in aluminum foil so as to prevent fading.

### 3.5 Statistics

Key knitting parameters such as gauge and number of guide bars have been selected as independent factors, and the selected constructional characteristics, mechanical and biological properties have been selected as the dependent variables in this study. The statistical regression analysis was performed on all six samples, and the data are represented as a mean ± standard deviation. Statistical difference was analyzed using software R version 2.13.1. For the two-way analysis of variance (ANOVA), a p value less than 0.05 was considered statistically significant.

As to the general linear regression test, the Equation (3.6) is used to describe the model.

$$Y(E, GB) = \varepsilon + \beta_1 E + \beta_2 GB + \beta_3 E GB \quad (3.6)$$

Where,  $Y$  represents the discrete dependent variable of each evaluation;  $E$  and  $GB$  are discrete independent variables gauge and number of guide bars;  $\varepsilon$  is the intercept;  $\beta_1$  is the coefficient of  $E$ ;  $\beta_2$  is the coefficient of  $GB$ ; and  $\beta_3$  is the coefficient of  $E*GB$ .

## CHAPTER 4 RESULTS AND DISCUSSION

All the knitting parameters that were varied in this study, such as the number of guide bars, the gauge, the yarn type and yarn size (linear density), stitch counts, the loop length and the lapping sequence, had some impact on the architecture, dimensions and constructional properties of the resulting knitted structures, which resulted in a range of different mechanical and biological performances. This chapter begins with an evaluation of each of these critical properties and then discusses how these properties can be controlled and predicted from the knitting parameters used.

### 4.1 Effect of Knitting Parameters on Constructional Characteristics

Views of the face and back structures of the greige spacer fabric samples as well as cross-sectional views in the warpwise and weftwise directions are shown in Figure 4.1.1. These images show the range of different structural morphologies included in this study. The fabrics knitted from six guide bars show straight and uniformly spaced wales, while those knitted on four guide bars have a zigzag configuration. The two commercial samples, SHR 724/5 and SHR 728, show a more open cross-sectional structure due to the monofilament spacer yarns. The two designed samples knitted with multifilament yarns from 4 guide bars appear to have a less dense structure so that the individual yarns can be seen more clearly in the spacer layer.

The constructional characteristics, which included thickness, fabric density, total porosity and fabric stitch count, have been listed in Table 4.1.1. Both gauge and number of guide bars have a positive impact on thickness but a negative impact on total porosity, and for both the

difference is significant ( $p < 0.05$ ). When comparing the thickness values of the four prototype knitted samples, the 6 guide bar group was thicker than the 4 guide bar group, pointing to the fact that the number of guide bars has a bigger impact on thickness than the needle gauge (coefficient GB > coefficient E). However, this result needs to be studied further with different yarn types and yarn sizes, as there are other factors such as yarn feed tension, fabric take-down tension and heat setting conditions that also influence fabric thickness. The values of fabric density and total porosity for the four prototype knitted samples were fairly close to each other. This is surprising given that the two 24 gauge samples had theoretically twice as many yarns knitted together in the same width as the two 12 gauge samples. Yet the differences in total porosity were only minor, primarily because of the highly porous structure. The two commercial samples had high porosity values because more space existed between the monofilament fibers lying in the spacer layer. SHR 724/5 had the highest porosity also due in part to the monofilament spacer yarns and to its open diamond face structure (Figure 4.1.1), but also due to the finer 70 denier yarns contained on the fabric's technical face and back. The total porosity values for all six spacer fabric samples lay between 86% and 94%. It is believed this is in the correct range for tissue engineering 3D scaffold structures.

According to the regression analysis, the equations below are the two relationships of independent variables gauge (E) and number of guide bars (GB) with dependent variable

$Y_{\text{thickness}}$  and  $Y_{\text{total porosity}}$ , where E and GB are discrete value.

$$Y_{\text{thickness}} = 2.5309 + 0.2200 E + 0.4401 \text{GB} - 0.3120 E * \text{GB}$$

$$Y_{\text{total porosity}} = 0.88399 - 0.02501 E - 0.01646 \text{GB} + 0.01383 E * \text{GB}$$


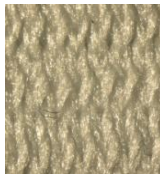

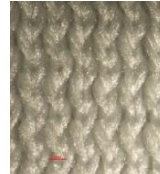
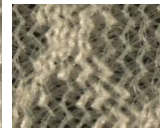

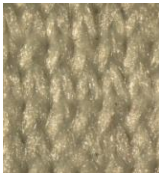
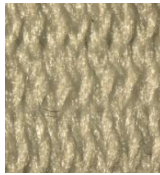

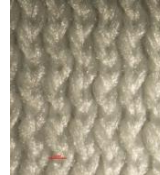
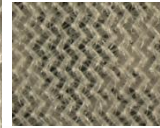

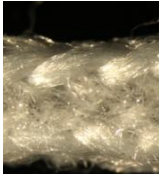
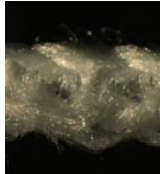

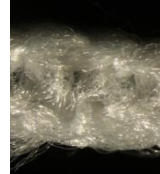
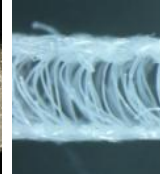




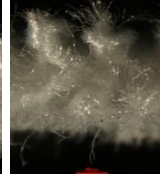

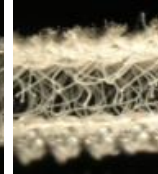
Sample name	24 E 6 GB	24 E 4 GB	12 E 6 GB	12 E 4 GB	SHR 724/5	SHR 728
<b>Gauge</b>	24	24	12	12	22	22
<b>Guide bars</b>	6	4	6	4	5	6
<b>Stitch type on face and back</b>	Tricot stitch	Single guide bar tricot stitch	Tricot stitch	Single guide bar tricot stitch	Diamond front (lace) / Single guide bar tricot back	Sharkskin tricot stitch front/ Tricot stitch back
<b>Technical face structure (Mag 10x)</b>						
<b>Technical back structure (Mag 10x)</b>						
<b>Cross section cut warpwise (Mag 20x)</b>						
<b>Cross section cut weftwise (Mag 20x)</b>						

Figure 4.1.1 Surface morphology of four prototype knitted and two commercial samples

Table 4.1.1 Constructional characteristics of four prototype knitted and two commercial samples.

Variables		24 E 6GB	24 E 4 GB	12 E 6 GB	12 E 4 GB	SHR 724/5	SHR 728
Thickness (mm)	Mean	3.013	2.751	2.971	2.531	2.133	2.255
	Std Dev.	0.131	0.120	0.084	0.163	0.071	0.153
Fabric density (g/cm <sup>3</sup> )	Mean	0.198	0.191	0.184	0.160	0.080	0.160
	Std Dev.	0.004	0.003	0.004	0.004	0.000	0.003
Total porosity (%)	Mean	85.63%	85.90%	86.75%	88.40%	94.14%	87.96%
	Std Dev.	0.01%	0.02%	0.02%	0.01%	0.00%	0.01%
Fabric stitch count	Wales per inch	19.5	15.5	17.0	14.5	31.0 face/ 22.5 back	30.0 face/ 43.0 back
	Course s per inch	21.0	25.5	19.0	20.5	35.5 face/ 34.5 back	29.5 face/ 29.0 back

Note: Calculated porosity assumes density of polyester = 1.38 g/cm<sup>3</sup>

## 4.2 Pore Size Characterization by Image Analysis

Because of the lack of agreement between various image analysis technologies, no attempt was made to measure the actual pore size directly. As explained previously in Chapter 3, a best approximation was undertaken by first embedding the spacer fabric samples in resin and then cutting them along the courses and the wales, and polishing them in order to see the cross-sectional structure in the warp and weft directions respectively. In this research, individual pore size was defined as the diameter of the biggest inscribed circle connecting at least three individual fiber surfaces observed in the cross-sectional images (Figure 4.2.1). This provided an objective standard procedure within this study to measure quantitatively the

microscopic space inside the knitted fabrics and to evaluate its influence on the fabric's biological properties.

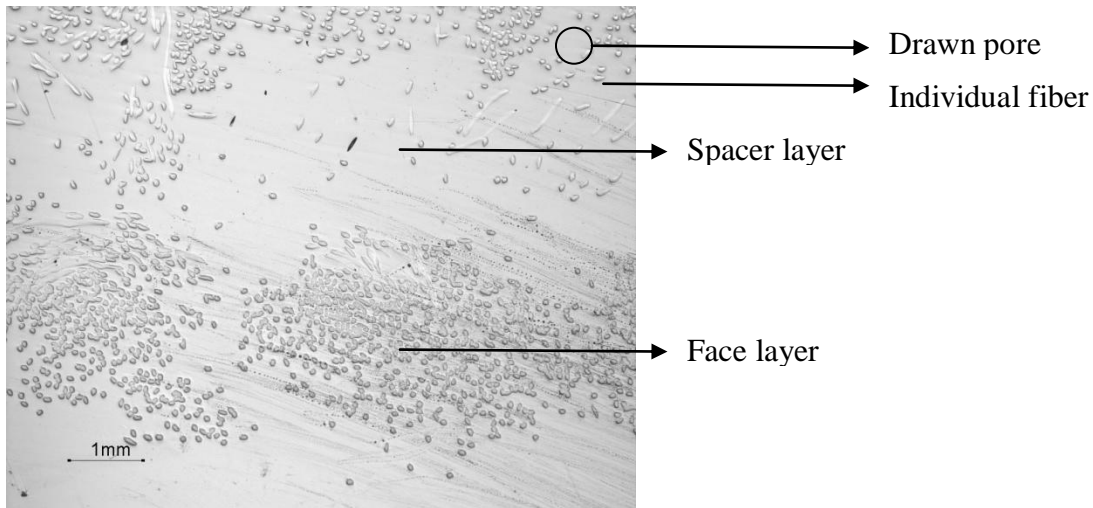


Figure 4.2.1 Optical microscopic image of cross-section cut in the weft direction of the resin embedded 12E4GB fabric showing different layers within the same knitted structure (Magnification 50x).

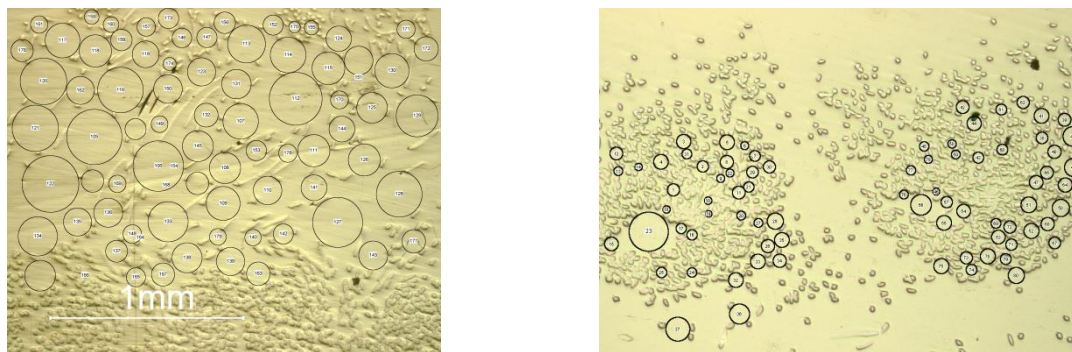


Figure 4.2.2 Optical microscopic image of cross-section cut in the weft direction of the resin embedded 12E4GB fabric showing how the pores were identified and constructed in the spacer layer (left) and outer layer (right) (Magnification 50x).

In terms of analyzing the textile structure, the cross section of a spacer fabric consists of three layers; the face layer, the spacer layer and the back layer as shown in Figure 4.2.2. Although separate and distinctive, these three layers are actually all interconnected. In fact the pores in this 3D structure are all 100% open, which will ensure the transportation of

oxygen, nutrition and cellular by-products through the porous scaffold so as to promote cell proliferation, angiogenesis (the formation of new capillaries) and vascular growth. A unique geographical feature of this structure is the bimodal distribution of pore sizes, including bigger pores in the spacer layer and smaller pores between the knitted yarns and the knitted filaments in the face and back layers.

In order to better describe this unique multilevel structure, the results of the pore size measurements were divided into four groups; the weft outer layer, the warp outer layer, the weft spacer layer and the warp spacer layer. These groupings have permitted us to measure and report the pores in the two outer layers (face and back) separately from the pores in the inner or spacer layer. Since pores in the outer layer also contain the very small ones between filaments in the same yarn the pores which were taken into account are those larger than the filament cross section within a yarn.

The largest pores were all located in the spacer layers and the largest one was 1.37 mm in diameter of SHR724/5. However, only the commercial samples have more than 20% spacer pores larger than 0.4 mm of diameter and 10% outer pores larger than 0.1 mm of diameter. Therefore, the distribution of outer pores focuses on the section 0-0.1mm while spacer pores on the section 0-0.4mm. The maximum and minimum diameter are calculated and listed in Table 4.2.2. According to the distribution trend in Figure 4.2.3, the pores in the spacer layer of commercial sample SHR724/5 appear frequently within range 0-0.3mm, but still a considerable number of pores are larger than 0.6mm. Another interesting detail is the number of extremely large pores (>1mm) increasing at the end of the trend line.

Table 4.2.2 Maximum and minimum values of pore diameter

Pore diameter (mm)		24E 6GB	24E 4GB	12E 6GB	12E 4GB	SHR724/ 5	SHR72 8
Weft –outer layer	Min	0.025	0.019	0.02	0.028	0.013	0.013
	Max	0.107	0.087	0.18	0.167	0.129	0.178
Warp-outer layer	Min	0.160	0.185	0.087	0.151	0.294	0.113
	Max	0.067	0.071	0.050	0.080	0.062	0.050
Weft-spacer layer	Min	0.080	0.205	0.080	0.062	0.107	0.071
	Max	0.657	1.027	1.065	0.579	1.366	1.358
Warp- spacer layer	Min	0.025	0.071	0.107	0.087	0.124	0.080
	Max	0.320	0.924	0.510	0.546	1.337	1.270

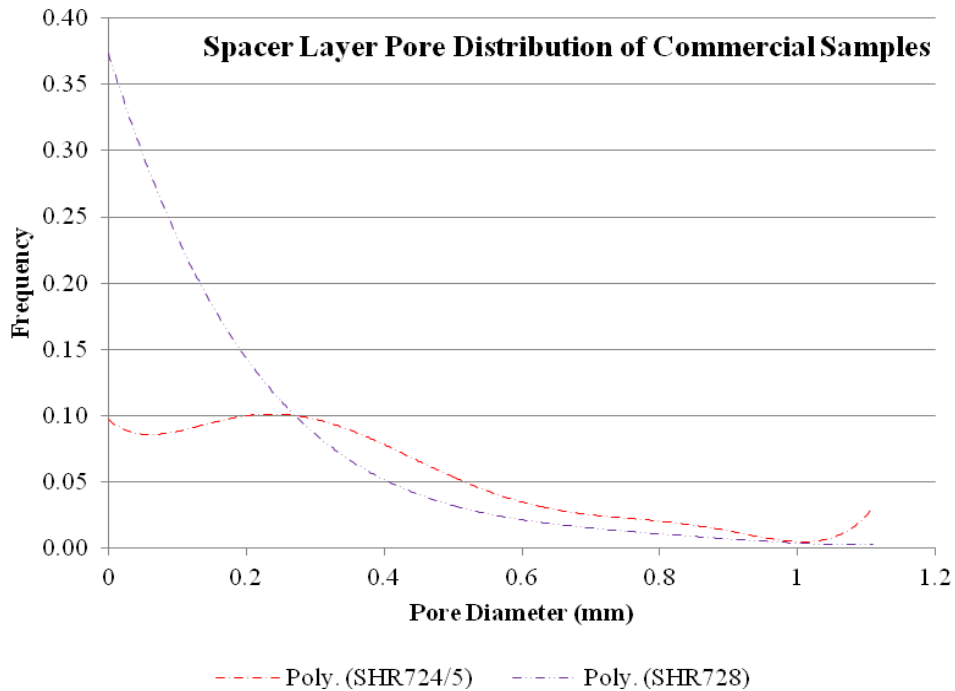


Figure 4.2.3 Spacer layer pore distribution trend lines of commercial samples (0-1mm)

The means and standard deviations of the pore diameters have been calculated and are listed in Table 4.2.3, and the pore size distributions for the outer two layers and the spacer layer have been plotted as polynomial trend lines in Figure 4.2.4 and Figure 4.2.5 respectively.

Compared with the 4 guide bar group, the 6 guide bar group shows larger pores in the weft direction, but smaller pores in most cases in the warp direction with the exception of the 24 gauge samples. This means that the number of guide bars has a positive impact on the mean pore size in the weft cut direction (i.e. across the wales), but a negative impact in the warp cut direction (i.e. across the courses) in both the face and back layers. When the number of guide bars remains constant, the mean pore size increases in the face and back layers as the gauge decreases. This means that the gauge has a negative effect on the space between the yarns, which has been confirmed by ANOVA statistical analysis. See ANOVA print-out in the Appendix. As one might expect the impact of the gauge and the number of guide bars on the pore size distribution in the spacer layer was not based on the mean values. However, as shown in the ANOVA results, the pore size distribution was impacted by fabric thickness which in turn was determined by both the gauge and the number of guide bars during warp knitting production.

Table 4.2.3 Pore diameter mean and standard deviation values

Pore diameter ( $\mu\text{m}$ )		<b>24E 6GB</b>	<b>24E 4GB</b>	<b>12E 6GB</b>	<b>12E 4GB</b>	<b>SHR724 /5</b>	<b>SHR728</b>
<b>Weft cut outer layer</b>	<b>Mean</b>	46.60	45.59	71.32	55.67	44.99	46.68
	<b>StdDev</b>	0.01	0.01	0.03	0.02	0.02	0.03
<b>Warp cut outer layer</b>	<b>Mean</b>	68.42	72.82	54.36	78.11	70.34	51.97
	<b>StdDev</b>	0.02	0.03	0.02	0.02	0.04	0.02
<b>Weft cut spacer layer</b>	<b>Mean</b>	209.25	147.12	211.10	195.44	375.94	147.12
	<b>StdDev</b>	0.07	0.15	0.20	0.08	0.27	0.23
<b>Warp cut spacer layer</b>	<b>Mean</b>	257.31	242.01	231.25	238.54	617.01	487.95
	<b>StdDev</b>	0.04	0.10	0.08	0.08	0.29	0.29

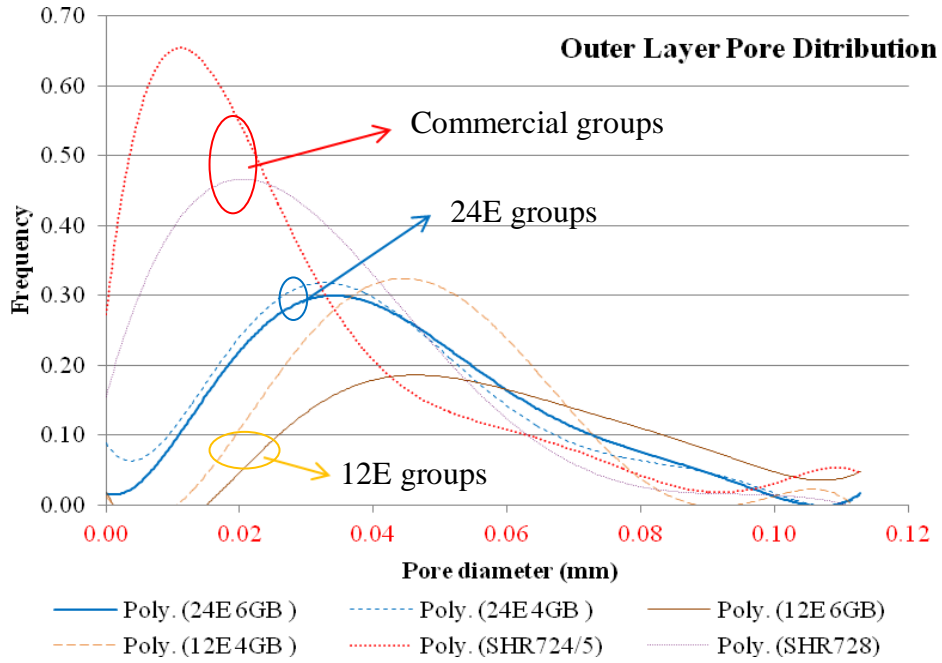


Figure 4.2.4 Outer layer (face/back) layer pore distribution trend lines of six samples (0-0.1mm)

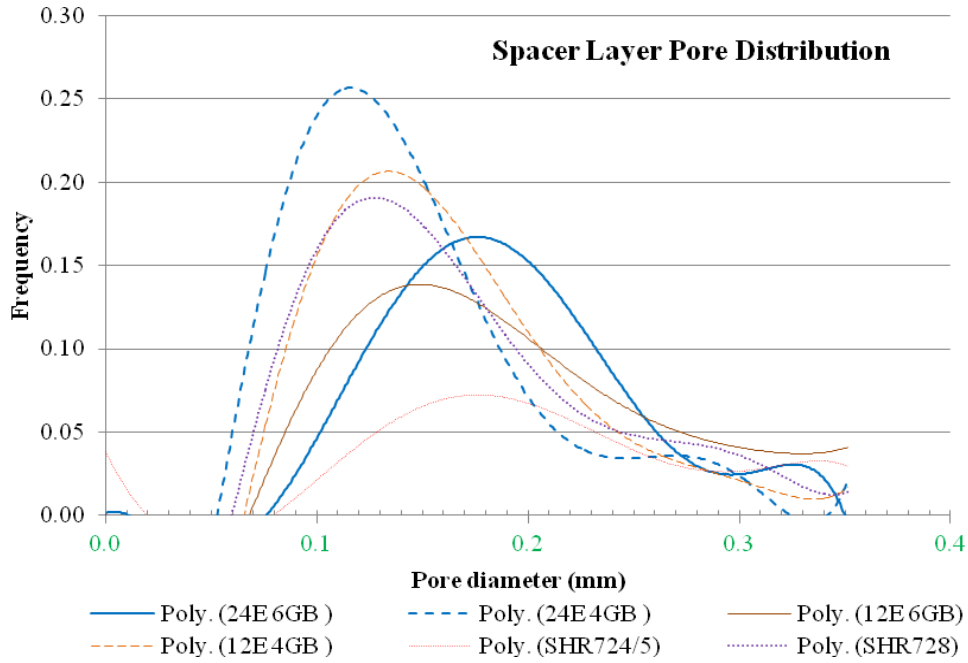


Figure 4.2.5 Spacer pore distribution trend lines of six samples (0-0.4mm)

The two distributions of pore size diameters in both the warp and weft directions were combined, analyzed and then converted into a six order polynomial trend line using Microsoft® Excel 2010. Based on these trend lines, the 12 gauge group had the most amount of large pores and the commercial fabrics had the most amount of small pores in the outer layers (Figure 4.2.4). As to the spacer layer, the 24 gauge 6 guide bar knitted sample, and the commercial SHR 724/5 sample had the most large pores, while the other prototype knitted structures gave similar distributions with the mode value around 0.120 mm (Figure 4.2.5).

### **4.3 Mechanical Properties**

#### **4.3.1 Compression and Recovery**

As mentioned in Chapter 3 the values for the level of compression resistance and the extent of recovery were used to describe the deformation in thickness, as the applied pressure was increased and decreased. As the level of compression resistance increased at higher pressures so the thickness deformation decreased. On the other hand, the extent of recovery remained stable for most spacer fabrics as the applied pressures were reduced from 700 to 20 g/cm<sup>2</sup> (Figure 4.3.1).

Based on the results shown in Figure 4.3.2, both the number of guide bars and the gauge have a positive impact on the level of compression resistance and particularly on the extent of recovery ( $p < 0.05$ ). As for the four prototype knitted samples, the level of compression resistance ranged from 34.7% to 43.3%, while the extent of recovery varied from 76.2% to 80.6%. Clearly the 24 gauge and 6 guide bar samples gave superior compression resistance and recovery properties compared to their 12 gauge and 4 guide bar counterparts. This

observation is understandable because those structures with better compression resistance and recovery performance were those with a higher fabric density (Table 4.1.1). Surprisingly the commercial sample SHR724/5, with its thicker monofilament spacer yarns, exhibited the least compression resistance. Clearly its compression performance was more dependent on the total porosity, the mean pore size in the spacer layer and/or the thickness of the fabric, rather than the thickness of the spacer yarns. Both commercial samples gave equivalent recovery properties to those of the prototype knitted samples. The reason may have been due to the fact that in all six spacer fabrics some of the spacer yarns were aligned in a cross-cross orientation.

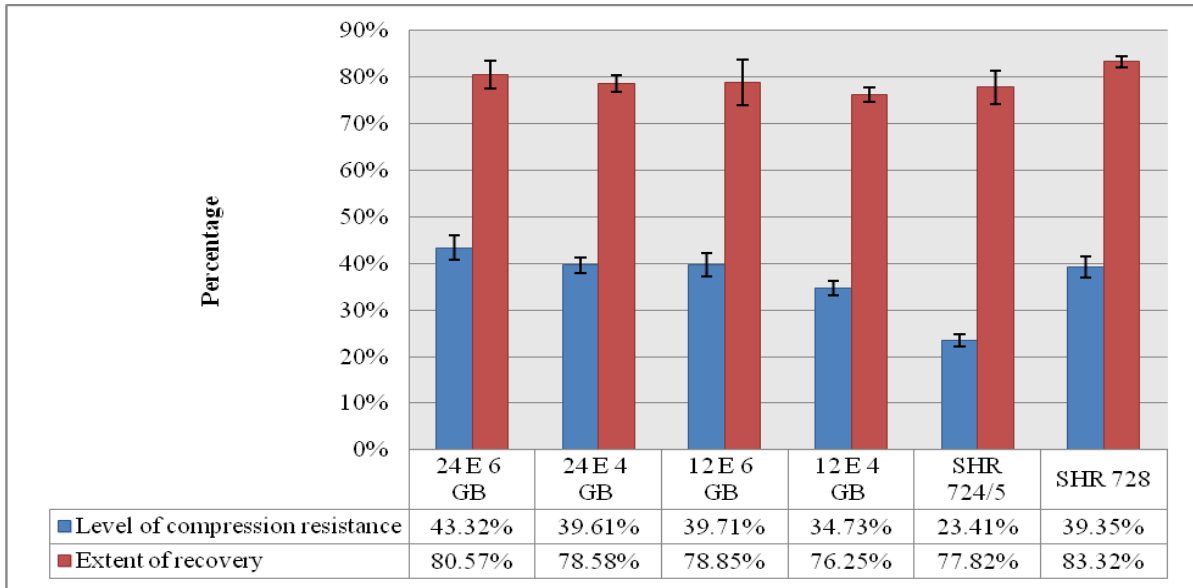


Figure 4.3.1 The level of compression resistance and extent of recovery (Error bars = standard deviation)

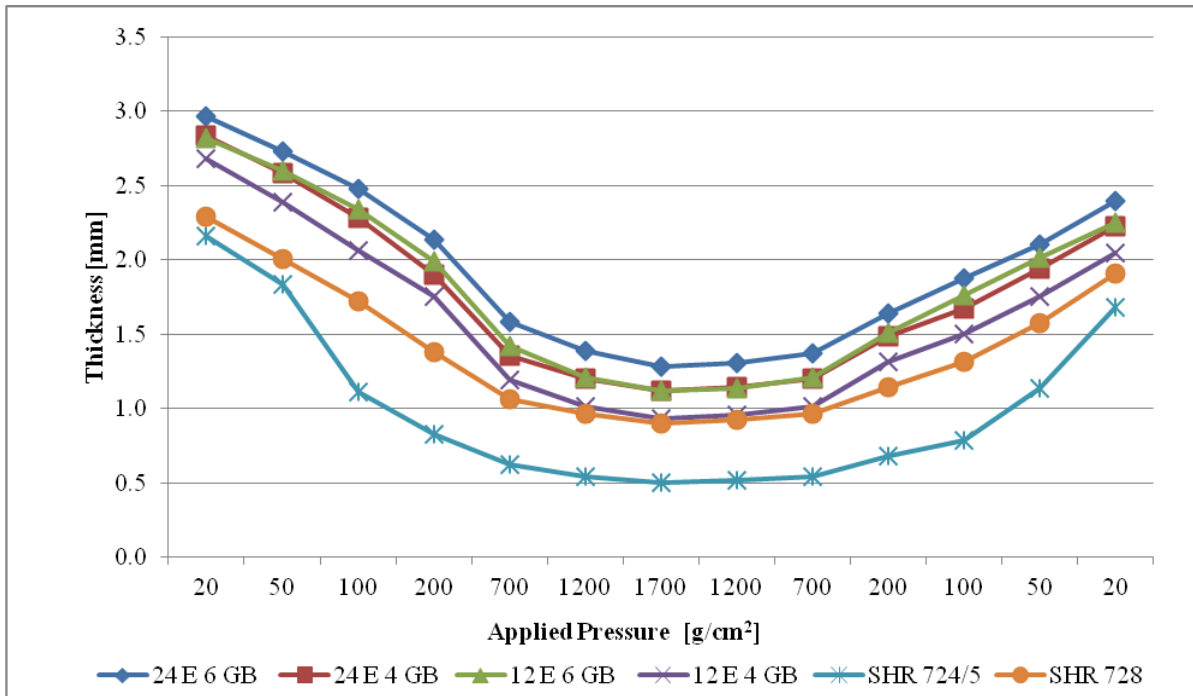


Figure 4.3.2 Changes in thickness during compression and recovery testing

The mean values of thickness were calculated from all 10 readings of each sample at each applied compressive load. These mean values were then plotted on a thickness vs. applied pressure curve to show the deformation performance (Figure 4.3.2). All four prototype knitted spacer fabrics regardless of gauge and number of guide bars followed similar changes in thickness deformation throughout the whole test sequence. The thinner, lighter weight, more porous commercial sample, SHR724/5, did exhibit less compression resistance than the other commercial spacer fabric and the prototype knitted samples, but was able to show equivalent recovery on unloading.

According to statistical regression analysis, the following equations are the relationship of independent variables gauge (E) and number of guide bars (GB) with dependent variables level of compression resistance ( $Y_{\text{level of compression resistance}}$ ) and extent recovery ( $Y_{\text{extent recovery}}$ ), where E and GB are discrete values.

$$Y_{\text{level of compression resistance}} = 0.34744 + 0.04869 E + 0.04945 GB - 0.01230 E*GB$$

$$Y_{\text{extent recovery}} = 0.762478 + 0.023340 E + 0.026039 GB - 0.005949 E*GB$$

### **4.3.2 Flexural Rigidity (Stiffness)**

The flexural rigidity, or stiffness, represents the resistance of a fabric to bending when a force is applied along one edge while the opposite edge is held in a fixed position as defined in ASTM D1388-08. In other words, a structure with high flexural rigidity does not bend easily. According to the statistical ANOVA test, both gauge and number of guide bars have positive impacts on flexural rigidity, and the difference is statistically significant ( $p < 0.05$ ). Figure 4.3.3 presents a bar chart of the mean values for the flexural rigidity of each of the six

spacer fabric samples. Prototype knitted fabrics with the same gauge, but more guide bars have been shown in this study to result in stiffer fabrics with higher flexural rigidity. Likewise the samples with the same number of guide bars, but a higher gauge, we have shown that the same situation applies. Therefore, both the number of guide bars and the gauge have a positive impact on the flexural rigidity of spacer fabrics. It can be seen that the two commercial samples gave the lowest flexural rigidity of all six samples. This may have been a consequence of being thinner fabrics with lower fabric densities and finer yarns, and for the SHR 724/5 fabric, due to its very high total porosity.

According to statistical regression analysis, the following equation is the relationship of independent variables gauge (E) and number of guide bars (GB) with dependent variable Flexural rigidity ( $Y_{\text{flexural rigidity}}$ ), where E and GB are discrete values.

$$Y_{\text{flexural rigidity}} = 0.06673 + 0.12381 E + 0.09027 GB - 0.06897 E*GB$$

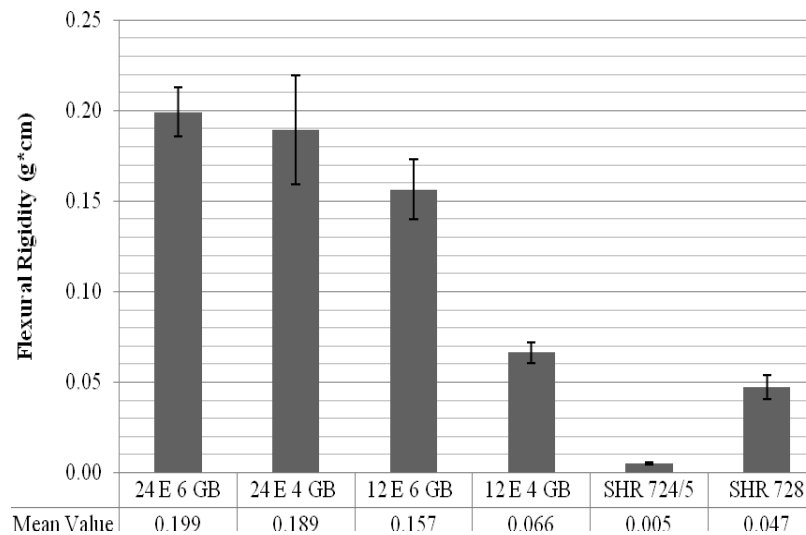


Figure 4.3.3 Flexural rigidity (Stiffness) (Error bars = standard deviation)

### 4.3.3 Bursting Properties

The bursting strength measured in this test represents the resistance to a force applied at right angles to the plane of the fabric until the fabric breaks and failure occurs. However, according to the standard deviation error bars in Figure 4.3.4, the data are spread over a wide range of values, possibly due to the high elongation of the spacer fabric structure. So a statistical analysis of variance (ANOVA) test was performed to demonstrate that significant differences in the mean bursting strength were found at the 95% confidence interval ( $p < 0.05$ ) (Appendix E). It was also possible to conclude that the number of guide bars had a more significant positive impact on the bursting strength than the gauge. The two commercial samples had significantly different performances. The SHR 728 sample was at least 3 times stronger than the SHR724/5 sample which, although knitted on the same gauge machine, used only 5 guide bars instead of 6, had the lowest fabric density, only 70 denier polyester yarns, and a total porosity of 94%. The superior bursting strength performance of SHR728 may have been the result of a high fabric count, 6 guide bars, a 22 gauge needle bed and a 100 denier yarn linear density. According to the statistical regression analysis, the following equation is the relationship of the independent variables gauge (E) and number of guide bars (GB) with the dependent variable  $Y_{\text{bursting strength}}$ , where E and GB are discrete values.

$$Y_{\text{bursting strength}} = 232.72 + 31.38 E + 107.85 GB - 43.00 E * GB$$

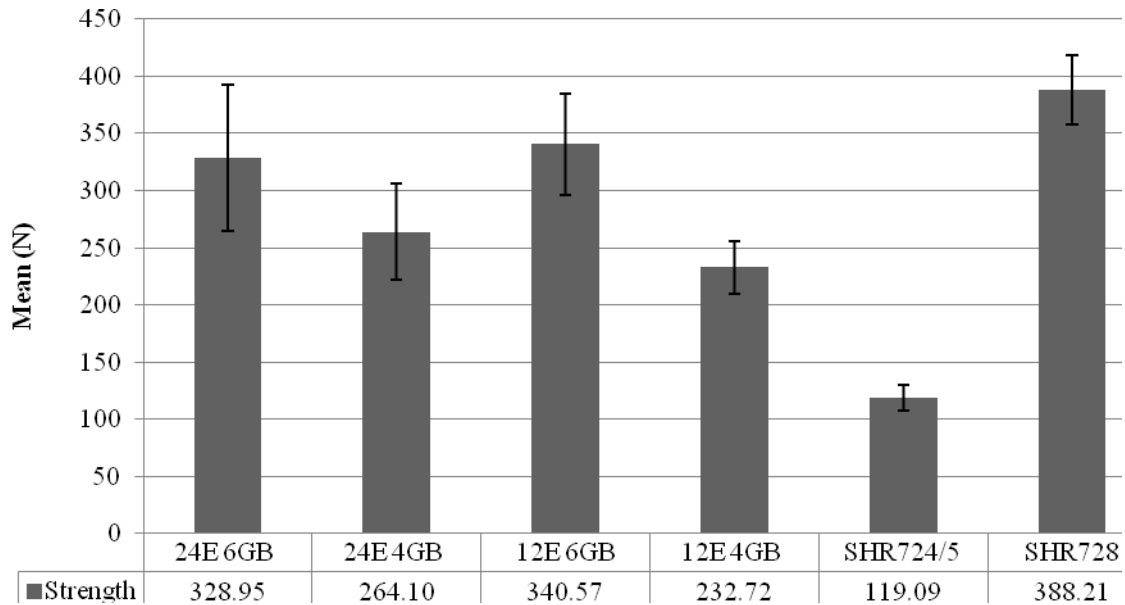


Figure 4.3.4 Bursting strength results (Error bars = standard deviation)

#### 4.3.4 Tensile Properties

The mean values for tensile strength and Young's modulus at 20% elongation in both the warp and weft directions are shown in Figure 4.3.5 and Figure 4.3.6. Note that the y axes of these 4 figures have different scales, so care should be taken when comparing the height of the bars between the different figures. According to Figure 4.3.5, the knitted prototype spacer fabrics could withstand higher tensile strength in the warp direction than in the weft direction. Both the gauge and the number of guide bars are seen to have significant positive impact on this property. With respect to the knitted samples, both 6 guide bar samples show the highest tensile strength in the warp direction and a low tensile strength value in the weft direction. It is known that these structures have larger elongations in the weft direction, which result in lower weft Young's modulus values. The different face vs. back structures

may have contributed to the strong tensile performance for both commercial samples in the weft direction.

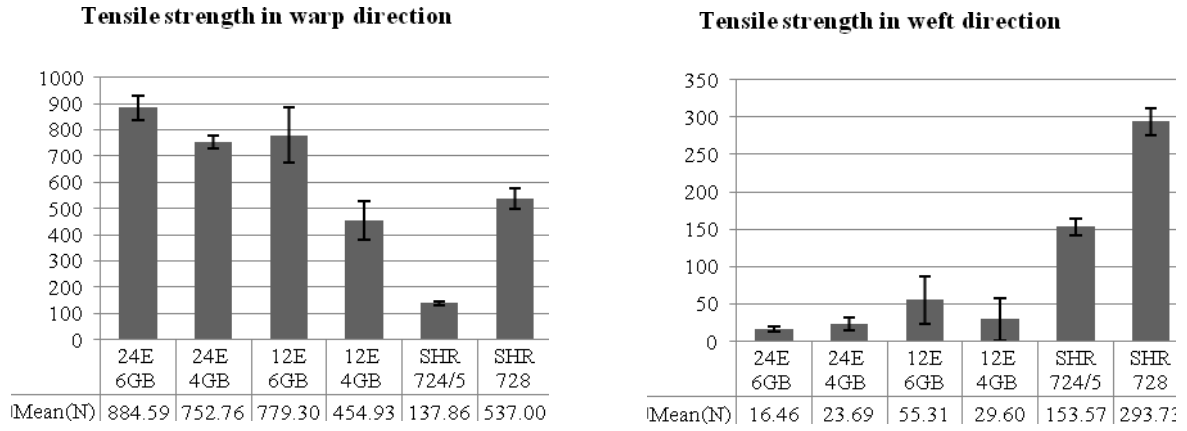


Figure 4.3.5 Tensile strength in warp direction (left) and in weft direction (right) (Error bars = standard deviation)

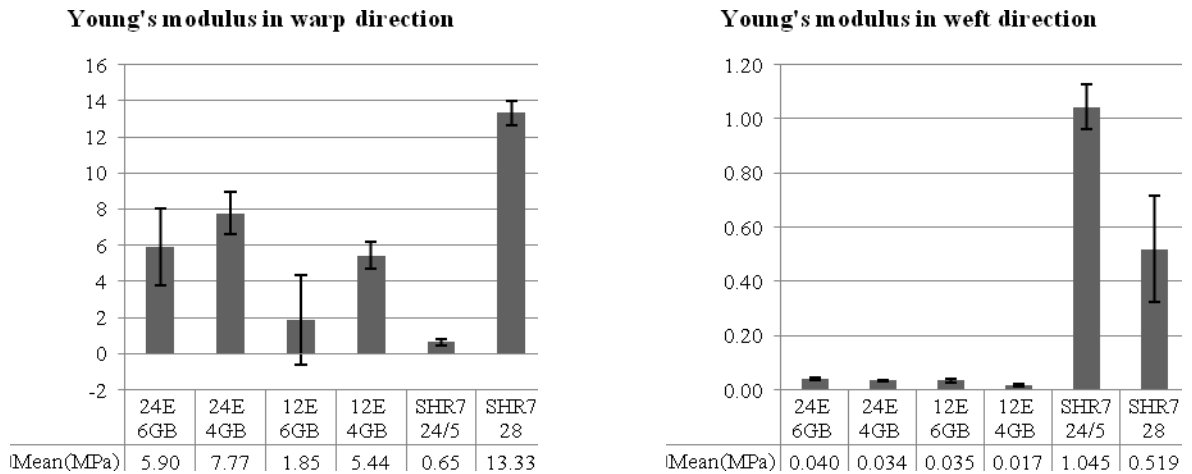


Figure 4.3.6 Young's modulus at 20% elongation in warp direction (left) and in weft direction (right) (Error bars = standard deviation).

As to the tensile modulus at 20% elongation, the performance in the warp direction is influenced primarily by the clearly aligned wales. Both factors, gauge and number of guide bars have statistically significant impacts on the weft and warp directions ( $p < 0.05$ ). The

results for Young's modulus in Figure 4.3.6 suggest that the gauge shows a positive impact, while the number of guide bars exhibits a negative impact on the resistance to tensile deformation. Since the 4 guide bar sample has a lower wale count and more space between yarns, the force is more easily shared, which leads to improvements in tensile modulus by either increasing the gauge or decreasing the number of guide bars. According to the statistical regression analysis, the following equations provide the relationship of the independent variables gauge (E) and number of guide bars (GB) with the dependent variable tensile strength in the warp direction ( $Y_{\text{warp tensile strength}}$ ), tensile strength in weft direction ( $Y_{\text{weft tensile strength}}$ ), Young's modulus in warp direction ( $Y_{\text{warp Young's modulus}}$ ) and Young's modulus in the weft direction ( $Y_{\text{weft Young's modulus}}$ ), where E and GB are discrete values.

$$Y_{\text{warp tensile strength}} = 649.3 + 105.3 E + 130.1 GB$$

$$Y_{\text{weft tensile strength}} = 454.9 - 431.2 E - 399.6 GB + 392.4 E * GB$$

$$Y_{\text{warp Young's modulus}} = 7.65567 + 0.05319 E - 5.80183 GB + 3.99660 E * GB$$

$$Y_{\text{weft Young's modulus}} = 0.01650 + 0.01750 E + 0.01850 GB - 0.01225 E * GB$$

## **4.4 Biocompatibility**

### **4.4.1 *In Vitro* Cell Viability**

The biocompatibility of the scaffolds was confirmed by the successful results from the semi-quantitative study of cell viability using the MTT assay. The cells gave a blue/purple color since the nuclei were dyed by the MTT reagent (Figure 4.4.1). At each time point, cells were detached from the fabric samples and the absorbance of the solution with detached cells indicated the initial cellular growth on the corresponding structure. In this cytocompatibility

test method the absorbance value in a control well without a scaffold indicates the extent of cell growth on a two dimensional surface. This value was used as a benchmark for comparison with the MTT analysis. The absolute value determined by the MTT assay represents the total cell counts. It can be used to calculate the percentage viability, which is the ratio of the 3D absorbance value to the 2D absorbance. This enables us to compare the efficiency of cellular growth in a 3D scaffold compared to a 2D well plate.

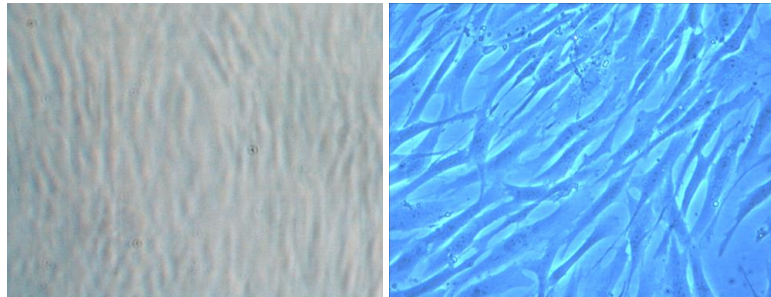


Figure 4.4.1 Cells attached on 2D plate at Day 3 before (left) and after (right) MTT assay.

Note: Since the light could not pass through the thick 3D spacer fabric, the cellular growth could not be the same observed the same way under optical microscope.

The MTT absorbance of samples exposed to 2D well plates and 3D spacer fabric scaffolds show an increase in cell count over time (Figure 4.4.2). This confirms that in spite of being composed of polyester (PET) fibers, the 3D spacer fabric structure is compatible with fibroblast cells. However, there was a hiatus in the increase between Day 6 and Day 10, which is believed to be due to a lack of medium and nutrients. Originally the changing of the medium was planned for a 2 day cycle, which was discovered by Day 8 not to be frequent enough. Therefore the feeding frequency increased to a daily basis and cellular growth continued to increase from Day 10 onwards. After increasing the nutrition supply Figure

4.4.2 shows that the cell counts increased but the capacity limitation of confluent cellular growth was not achieved on either the 2D well plate or the 3D fabric scaffold.

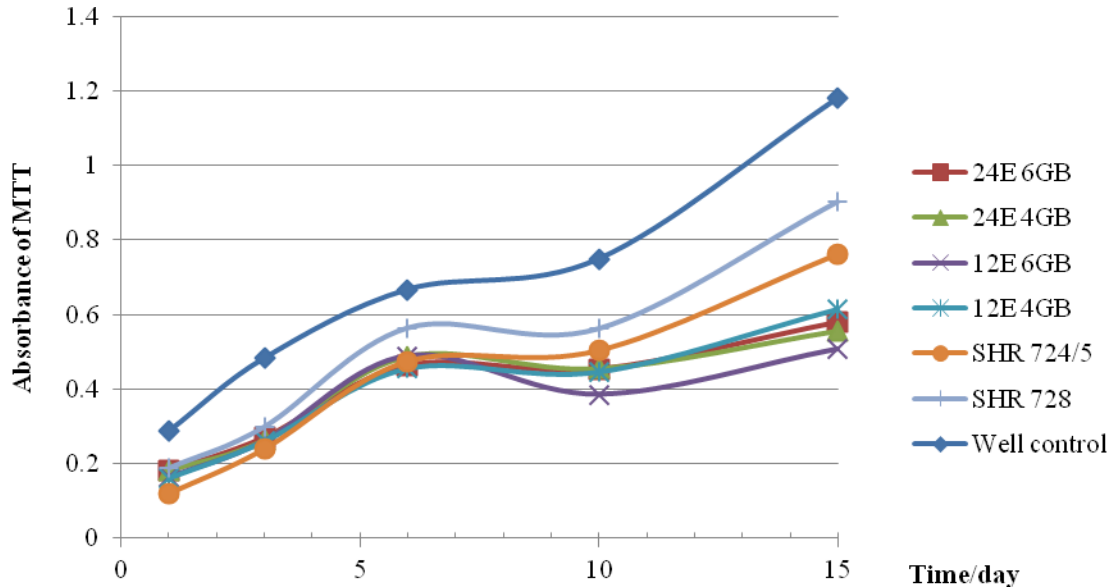


Figure 4.4.2 Mean MTT absorbance values at 5 time points in the 15 day study

On the other hand, the value of percentage cell viability compares the rate of change of cellular growth between the seven samples (Figure 4.4.3). The curve for the 3D scaffolds sees a dramatic increase up until Day 6, which suggests that 3D scaffold structures can improve cell attachment and proliferation at the beginning of the experiment under conditions of adequate nutrition supply. Ideally there would be a point in time when the MTT curve for the 2D well plate and the curve for the 3D scaffold would cross each other and demonstrate the ability of 3D scaffold material to exceed that of the 2D well plate. Unfortunately, this point was never reached during this MTT assay due in part to the lack of nutrition on Day 8 and the limited amount of time for continuing this study.

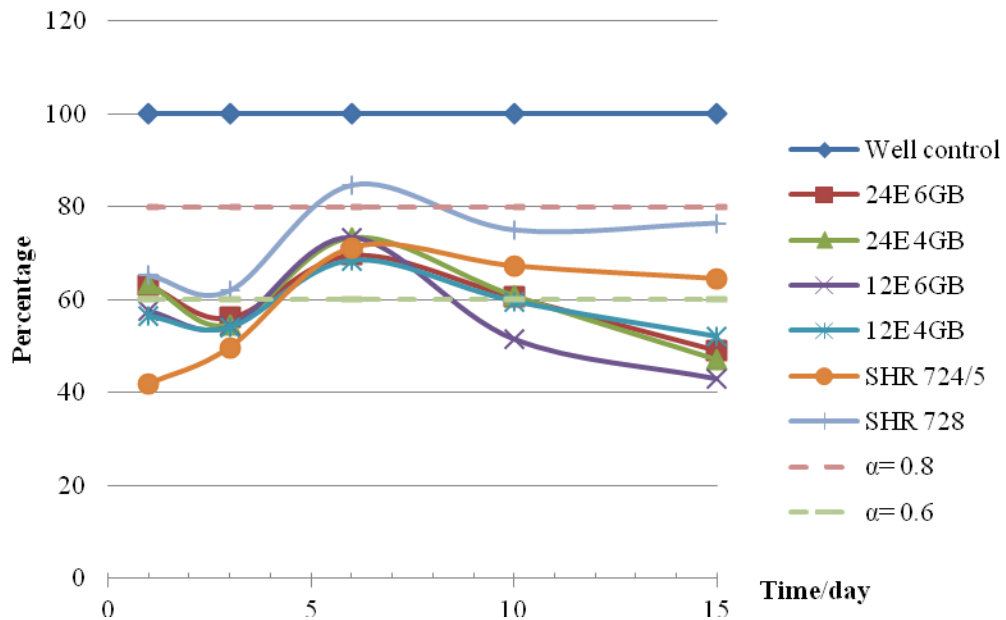


Figure 4.4.3 Mean MTT percentage viability values at 5 time points in the 15 day study

In addition, the MTT assay is based on the concentration of cells which have been washed and detached either from the scaffold or the 2D plate and it is assumed that the ratio of detached cells over total cells is the same from the same unit area. However, cells were not able to be completely detached from the 3D scaffolds compared to the 2D plates, according to the observation that MTT dyed cells were left on the PET scaffolds as seen in Figure 4.4.4 (PET could not be dyed by MTT). This might have been caused by two possible reasons. First, the 3D scaffold had a much larger specific surface area than the 2D plate in terms of unit volume, which caused many more cells to be left on the surface. If the ratio of detached cells over all cells grown in the wells is denoted as  $\alpha$ ,  $\alpha$  equals to 1 in the ideal 2D condition,

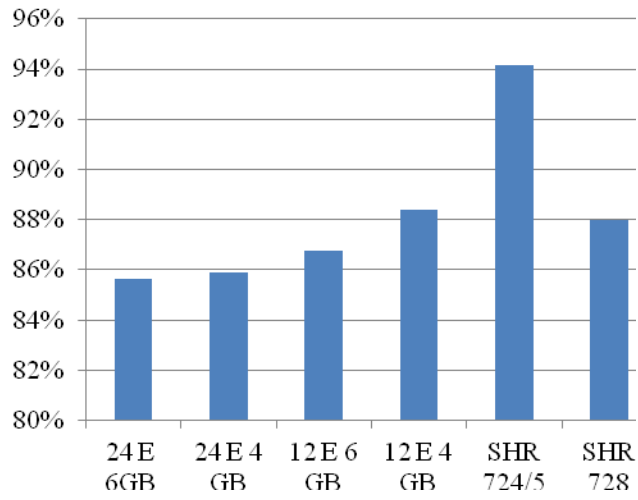
which means that all cells in 2D well plates are aspirated. Then the detaching ratio of the 3D scaffolds lies between 0 and 1, which means that not all the cells could be detached. As such,  $\alpha$  could depend on the specific surface area of the cell seeded structure and the percentage of the cell solution aspirated from the well. According to the observations made during this study,  $\alpha$  is assumed to lie between 0.6 and 0.8 (i.e. between line  $\alpha= 0.6$  and  $\alpha= 0.8$  in Figure 4.4.3). This needs to be confirmed in a further study.



Figure 4.4.4 Cells left on the 3D scaffolds after the MTT assay.

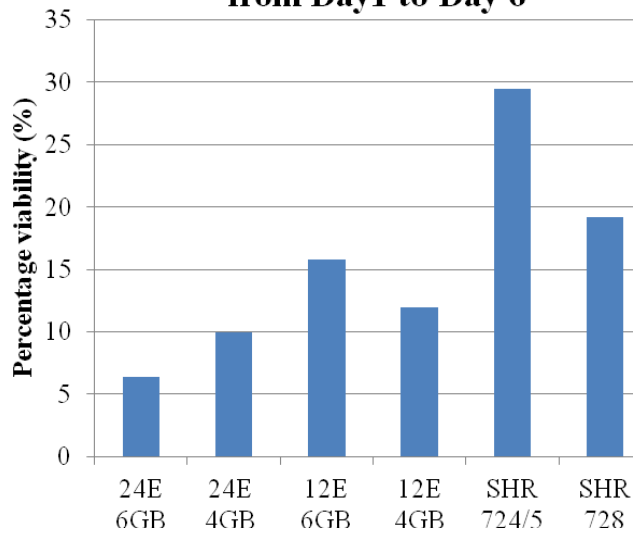
Owing to the reasons discussed above, the increasing rate of percentage viability from Day 1 to Day 6 (the difference of percentage viability between Day 1 and 6) was used to describe the difference in cellular growth between the spacer fabric scaffolds. It was found to agree with the value for total porosity with the exception of sample 12E 6GB (Figure 4.4.5).

### Total Porosity



(a)

### Increasing rate of cellular growth from Day1 to Day 6



(b)

Figure 4.4.5 Comparison of total porosity (a) with increasing rate of percentage viability from Day1 to Day 6 (b)

## **4.4.2 Cell Attachment and Proliferation**

Since the MTT assay was used as a semi-quantitative method, SEM and LSCM were also employed as qualitative methods to study the surface morphology and visualize through the thickness of the spacer fabrics during the 15 day *in vitro* cell study.

### ***4.4.2.1 Scanning Electron Microscopy (SEM)***

SEM photomicrographs were taken to show views of the face and back surfaces as well as the cross sections of the cell-seeded fabrics at different time points throughout the 15 day experiment. The 24 gauge 4 guide bar sample was selected as an example to illustrate how the adhesion, growth and proliferation of cells advanced over the 15 days (Figure 4.4.6 -Figure 4.4.9). During the 15-days in culture the cells started attaching themselves to the crossed filaments and micro-spaces between filaments (Day 3), and then migrated along the filaments in order to reach neighboring yarns (Day 6). Proliferating cells were in contact with each other between the filaments mostly within the same wale (Day 10), and the wide valley between the wales was finally bridged by a confluent sheet of cells on the top surface by Day 15.

Surface photomicrographs of four of the other samples before and after seeding cells (at Day1 and Day 15) are presented in Figure 4.4.13. Note that by Day 15 the cells had migrated to a point where they fully cover the yarns on the surfaces of all the spacer fabric samples. Their ability to proliferate through the thickness of these spacer fabrics is less certain.

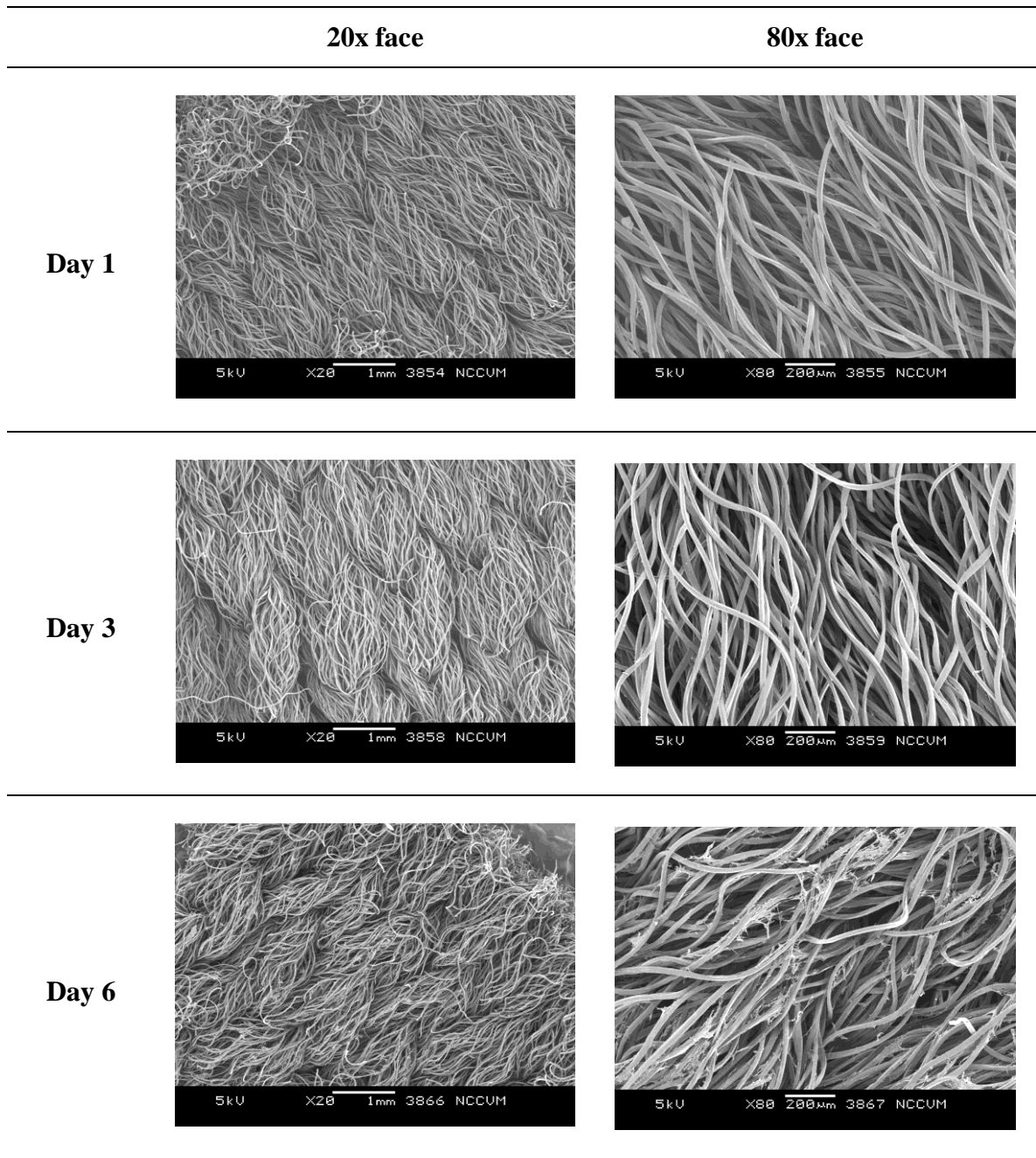


Figure 4.4.6 SEM photomicrographs showing changes in cell attachment and proliferation of the 24E 4GB Sample during *in vitro* cell culture. HDF cells attached to the surface of fabric face from Day 1 to Day 6.

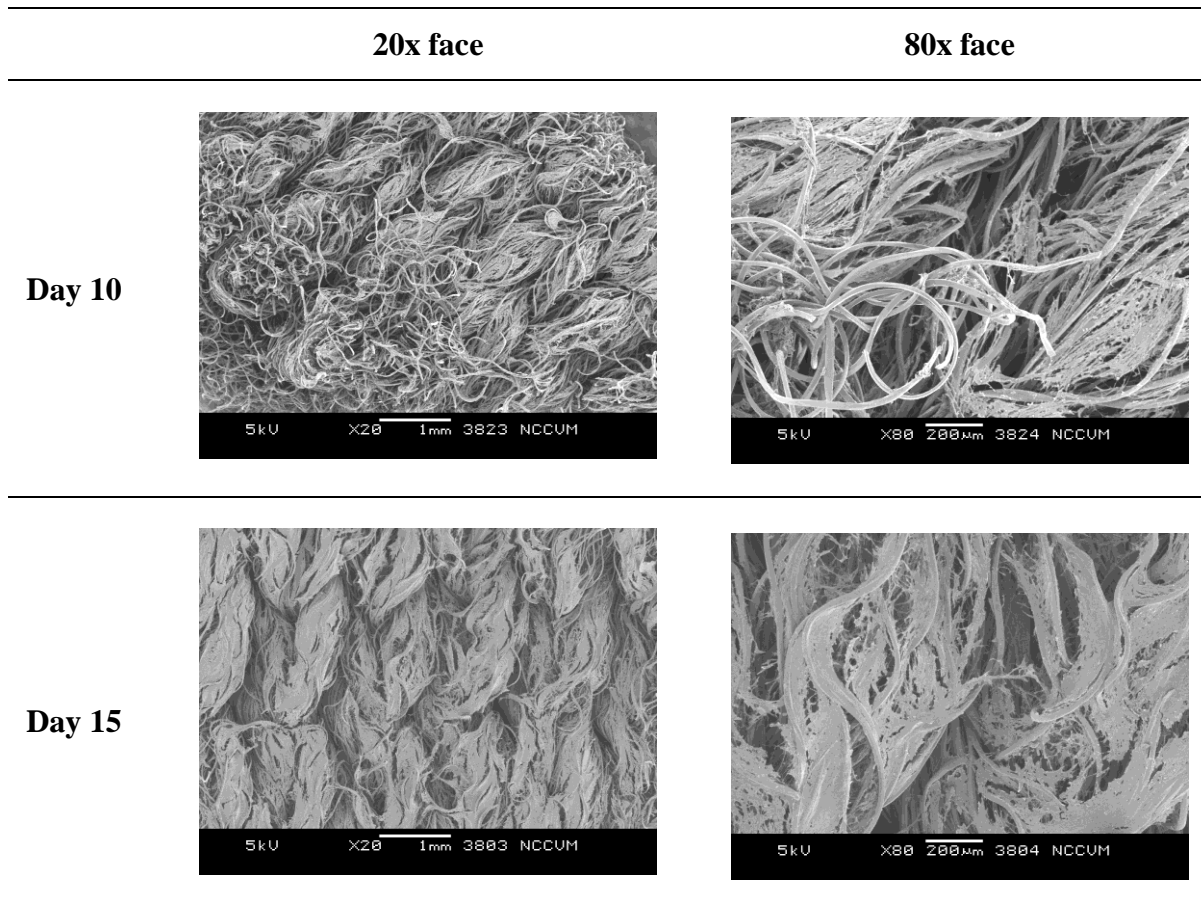


Figure 4.4.7 SEM photomicrographs showing changes in cell attachment and proliferation of the 24E 4GB Sample during *in vitro* cell culture. HDF cells attached to the surface of fabric face from Day 10 to Day 15.

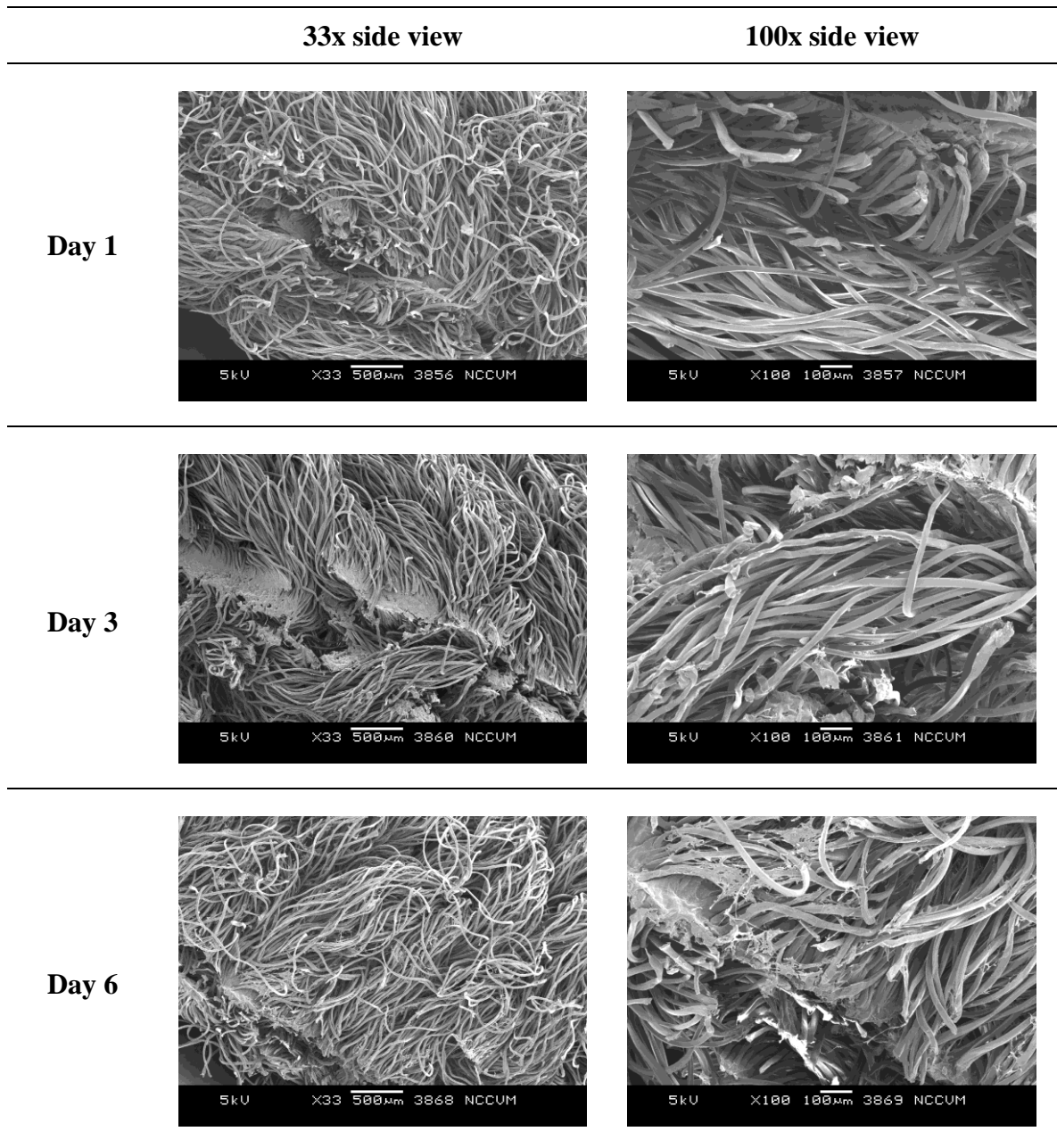


Figure 4.4.8 SEM photomicrographs showing changes in cell attachment and proliferation of the 24E 4GB Sample during *in vitro* cell culture. HDF cells attached to the side of fabric (weftwise) from Day 1 to Day 6.

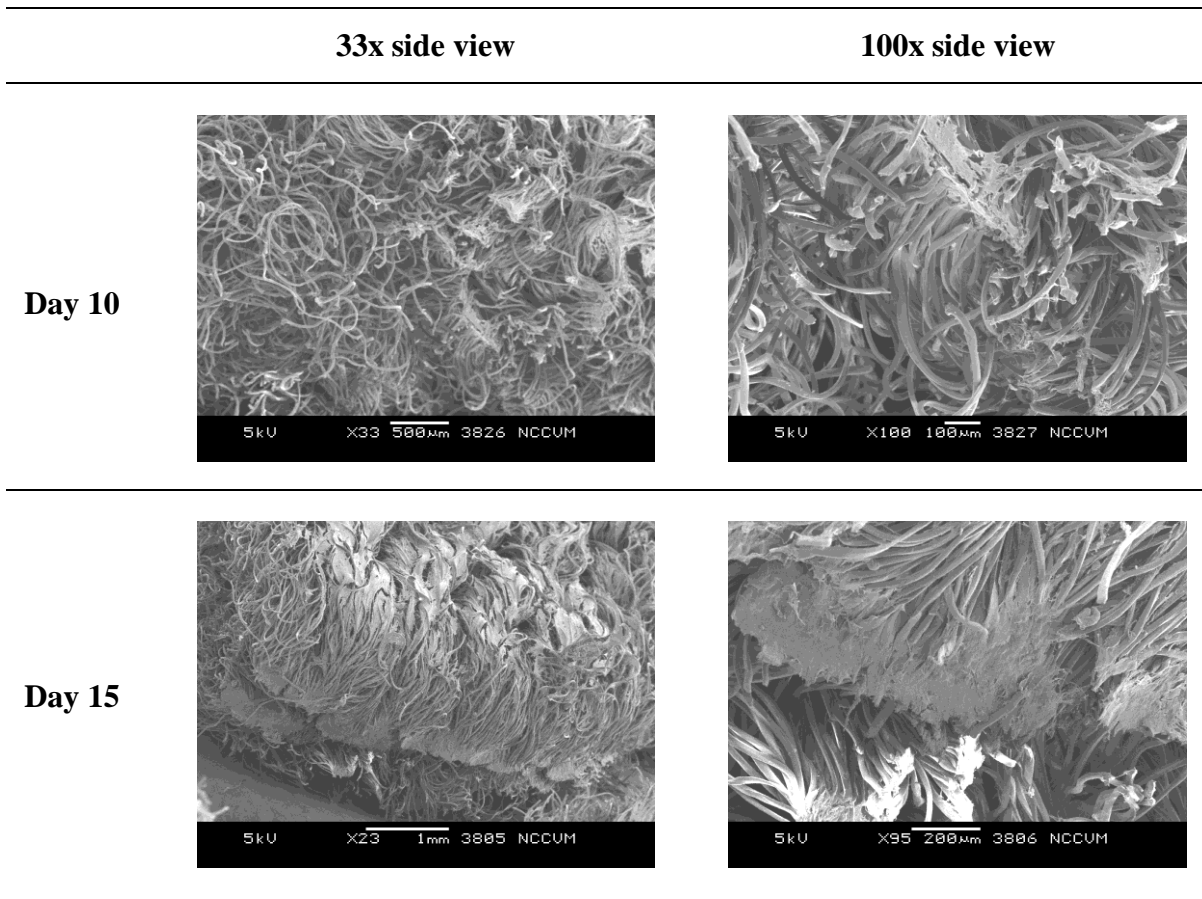


Figure 4.4.9 SEM photomicrographs showing changes in cell attachment and proliferation of the 24E 4GB Sample during *in vitro* cell culture. HDF cells attached to the side of fabric (weftwise) from Day 10 to Day 15.

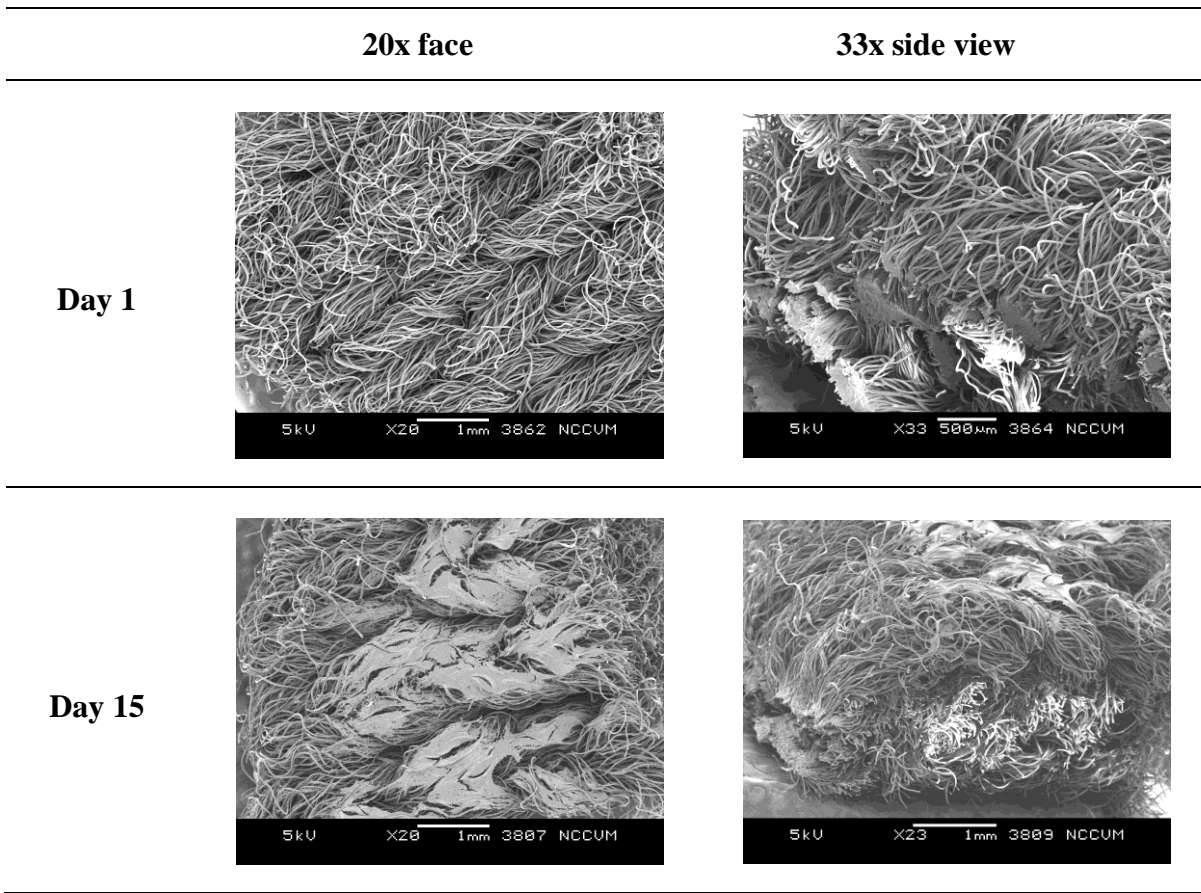


Figure 4.4.10 SEM photomicrographs showing the extent of cell migration before and after 15 days of cell culture on fabric sample 24E 6GB

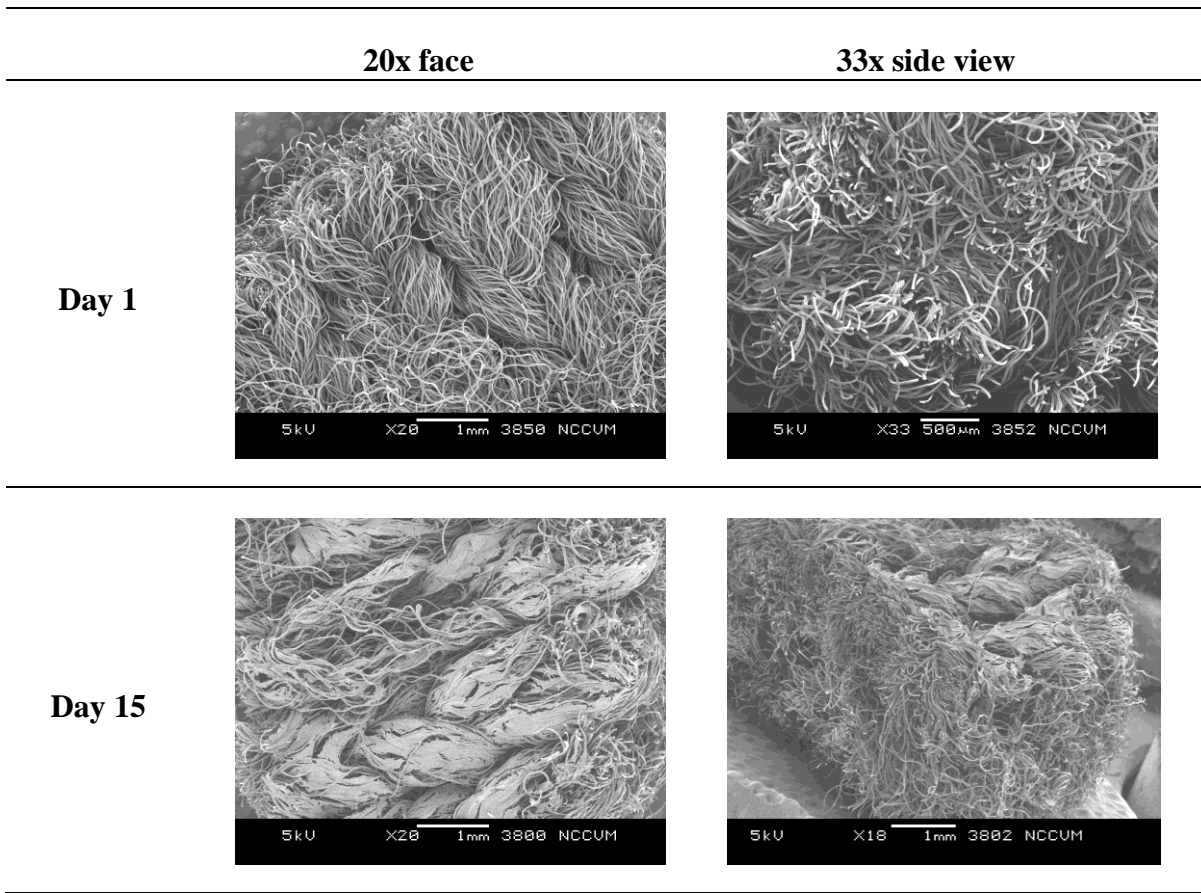


Figure 4.4.11 SEM photomicrographs showing the extent of cell migration before and after 15 days of cell culture on fabric sample 12E 6GB

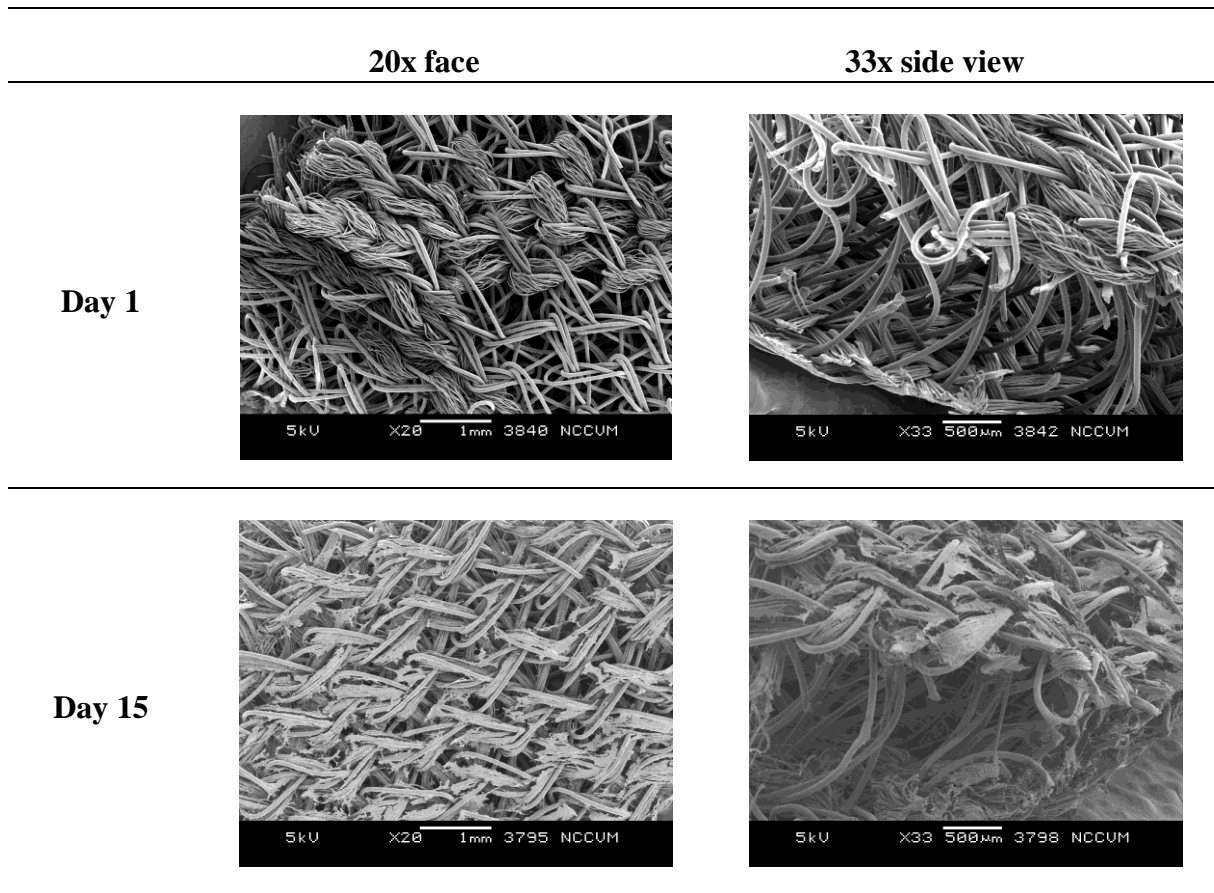


Figure 4.4.12 SEM photomicrographs showing the extent of cell migration before and after 15 days of cell culture on fabric sample SHR 724/5

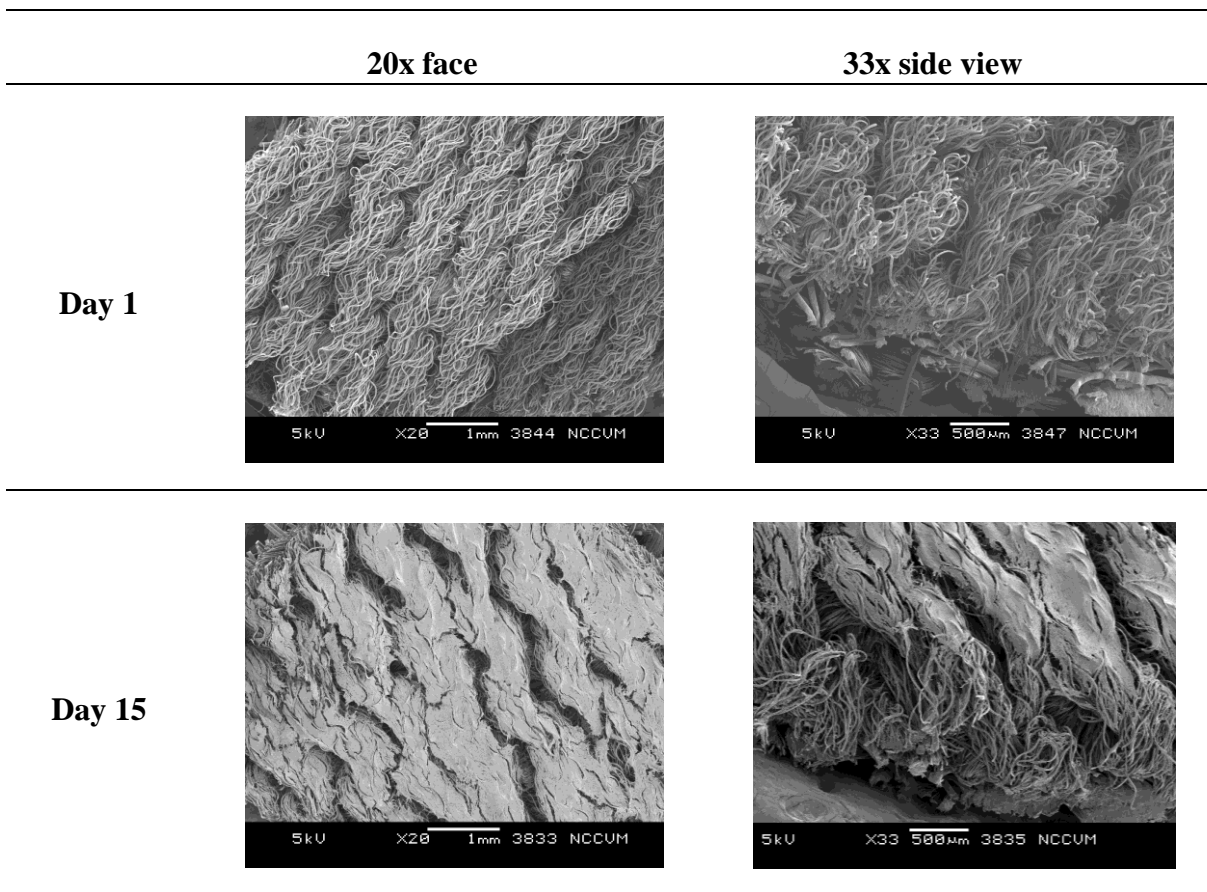


Figure 4.4.13 SEM photomicrographs showing the extent of cell migration before and after 15 days of cell culture on fabric sample SHR 728

#### ***4.4.2.2 Laser Scanning Confocal Microscopy (LSCM)***

The live/dead double-stain is capable of dyeing the nuclei of cells so as to distinguish the live ones (green) from the dead cells (red) under laser scanning confocal microscope. Unlike SEM, which was used to observe surface cell attachment, the LSCM scanned inside the structures so as to provide valuable information of cell proliferation along the spacer yarns through the thickness. The images of each sample were taken at all 5 time points during the 15 day *in vitro* study. Figure 4.4.14 summarizes only those images at Day 1 and Day 15 for all six spacer fabric samples. Because the PET fibers reflect blue light under LSCM, these

images can be visualized by seeing both the fibrous structure (in blue) and the nuclei of the live/dead cells in the same images.

When the spacer fabric specimens were placed in the culture well plates, the bottom of the fabric (the technical face) was in contact with the 2D surface of the cell culture plates. From Figure 4.4.14 it can be seen that the cells proliferate through the whole thickness of the spacer fabrics and attach well to both outer layers after 15 days. According to the images at Day 15, the four prototype knitted fabric scaffolds supported more cells through the thickness, while for the commercial samples the cells were gathered near the top and bottom surfaces. At Day 1, the cells were seen attached to the spacer yarns of all six scaffolds, but they were more abundant on the four prototype knitted spacer fabric samples. This confirms that spacer fabric scaffolds are able to support cell proliferation through the thickness of a 2-3 mm thick construct, and that multifilament spacer yarns can increase the level of cell attachment in the spacer layer compared to the use of monofilament spacer yarns.

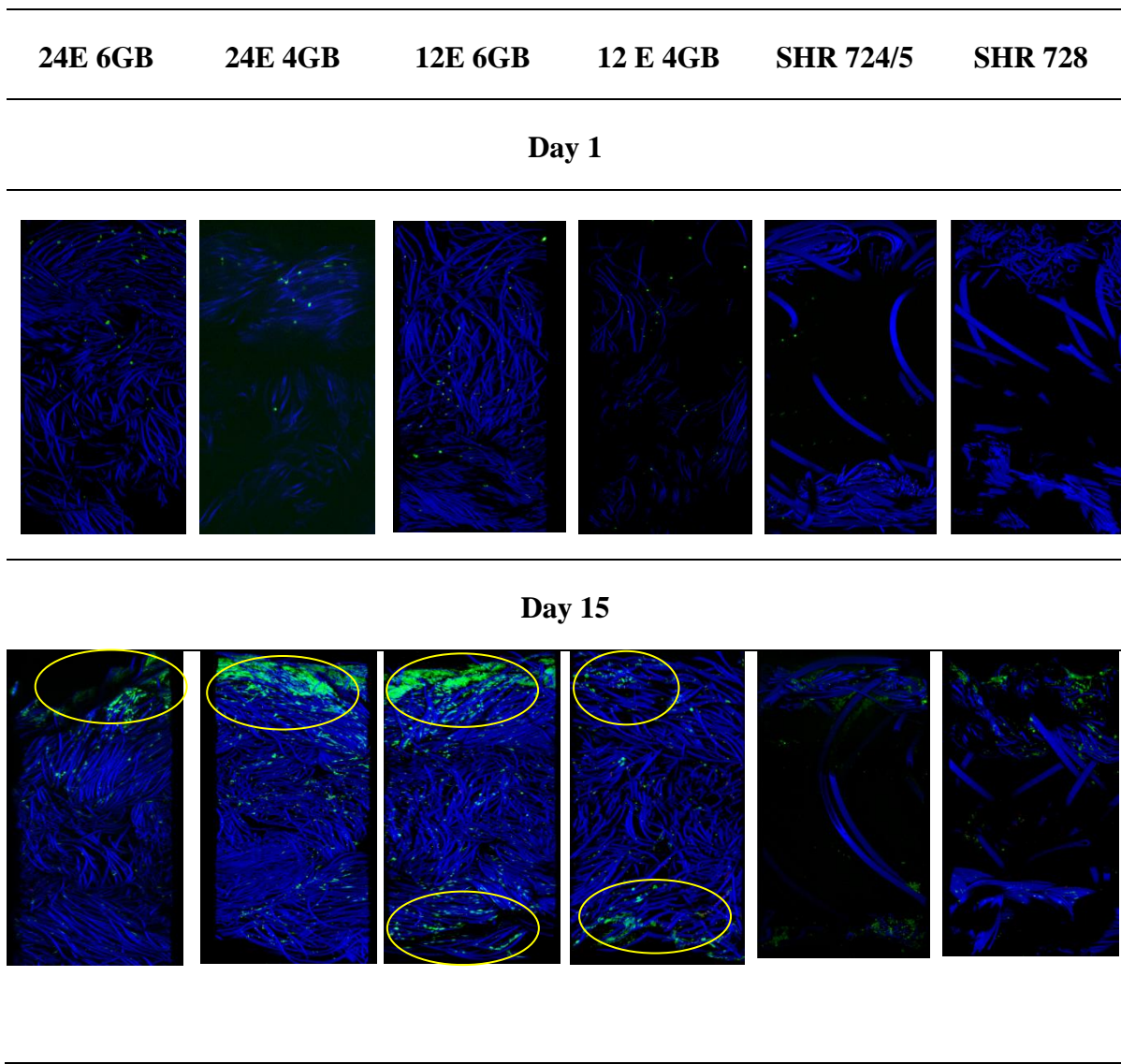


Figure 4.4.14 LSCM images showing HDF cell proliferation for each sample after Day 1 and Day 15 during *in vitro* cell culture



## CHAPTER 5 CONCLUSIONS

In this chapter, the main aims described previously in Chapter 1 are revisited and discussed as the main conclusions. Each of the specific objectives is addressed in turn with particular concluding statements following the main conclusion. At the end the findings, contribution, and limitations of the study are addressed as well as recommendations for future research.

### 5.1 Conclusions

**Main conclusion:** A novel 3D spacer fabric structure with multifilament spacer yarns has been creatively designed and produced to fulfill the desired requirements for tissue engineered scaffolds which were discovered and presented in Chapter 2, the literature review. An experimental procedure has been developed and followed using the latest analytical techniques. This has enabled the completion of a comprehensive study on the performance and functionality of these tissue engineering scaffold structures.

*Conclusion 1: A 3D flat spacer fabric has been successfully designed with three porous multilayers, high porosity and high interconnectivity of the pores using warp knitting technology.*

1.1 From the relevant literature, general requirement for tissue engineering scaffolds have been summarized. This has included the constructional characteristics as well as physical, mechanical and biological properties.

1.2 Based on the relevant literature, the current methodology to create 3D scaffolds has been reviewed and compared. The pros and cons of existing textile fabrications

for tissue engineering applications have been highlighted. The warp knitted spacer fabric shows certain advantages over other textile structures. They include the one-piece multilayer, high specific surface area, high porosity, 100% inner connected pores, and adequate compression and recovery properties.

1.3 A practical approach to the experimental study has been undertaken, which consists of four steps: sample design, production and fabrication of prototypes, evaluation and analysis of results. Key knitting parameters such as the gauge and number of guide bars have been selected as independent factors, and selected constructional characteristics, mechanical and biological properties have been selected as the dependent variables.

***Conclusion 2: Four prototypes with different knitting parameters were successfully designed and produced, as well as the set-up on the warp knitting machine was optimized before production.***

2.1 A 3D flat spacer fabric structure was successfully created. A 150 denier 48 filament polyester (PET) yarn was selected for the technical face, back and spacer yarns. The lapping sequence was designed according to a tricot stitch face and back structure, as well as controlling the cross and parallel spacer yarns in cross and parallel orientations.

2.2 The 3D fabric design was simulated in professional software ProCad to illustrate the yarn spacing and stitch notation in both 2D and 3D formats. Key knitting

conditions on the machine were selected according to the optimized design which was generated from the simulation.

2.3 A double needle bed, narrow width warp knitting machine was prepared and the set-up for operation was established. The knitting conditions were set up using 12 and 24 needle bar gauges and both 4 and 6 guide bars. A 2 mm distance between the needle beds was kept constant throughout the prototype production.

2.4 The fabrication processes included the winding of polyester (PET) yarns onto 72 bobbins, the warping of the 72 ends onto 4 beams, and the knitting of four different prototype samples.

***Conclusion 3: Two additional commercial control samples were included in the evaluation procedures. All six samples were tested for their constructional characteristics as well as physical, mechanical and biological properties, followed by statistical analysis.***

3.1 Optical microscopy was used for the purpose of analyzing the surface morphology and constructional characteristics. In addition, an image analysis system was adapted to view sections through the structure and quantify the pore size distribution.

Comparing the four knitted samples, both the gauge and the number of guide bars have a positive impact on the thickness, fabric density and fabric count. But both have a significant negative impact on total porosity ( $p < 0.05$ ). As to the pore size

characterization by image analysis, the gauge has a significant negative impact on the mode of the pore size distribution in the outer layers. The number of guide bars did not significantly affect pores in outer layer, but contributed to the multi-mode distribution of pores in the spacer layer. Considering the commercial samples, both of them had low fabric densities, a narrow thickness but high porosity and high fabric count. The SHR 728 sample has pore characteristics that were closer to the prototype knitted samples. And the SHR 724/5 sample had more large pores particularly in the spacer layer.

3.2 The mechanical properties of all six samples were tested, including the extent of compression and recovery, the flexural rigidity (stiffness), the tensile strength and Young's modulus as well as the maximum bursting strength. The relationship of independent variables such as the gauge (E) and the number of guide bars (GB) to the dependent variables, Y, have been generated by each test and follow the equations listed below.

Given that the commercial samples contained finer polyester yarns on the face and back, a different gauge and monofilament spacer yarns, most of their test results did not compare with the four prototype knitted samples except for the weft tensile strength. In addition, the SHR728 sample had advantages in terms of the extent of recovery, the warp Young's modulus and the bursting strength.

Comparing the mechanical performance of the four prototype knitted samples, both the number of guide bars and the gauge had significant positive impacts on the

compression resistance, the extent of recovery, flexural rigidity (stiffness), tensile strength in the warp direction, Young's modulus and bursting strength, but a negative impact on the tensile strength in the weft direction ( $p < 0.05$ ). The 24E 6GB sample ranked top in compression resistance and extent of recovery, stiffness, and warp tensile strength, while the 12E 6GB sample gave the highest bursting strength among all the six samples.

It was concluded that the mechanical properties could be enhanced by increasing the gauge (E) and the number of guide bars (GB). The summary below provides the relationship between the independent factors E and GB and each of the measured mechanical properties, where both E and GB were discrete whole integers. These equations will contribute to the future studies related to changes in gauge and the number of guide bars.

$$Y_{\text{thickness}} = 2.5309 + 0.2200 E + 0.4401 \text{GB} - 0.3120 E * \text{GB}$$

$$Y_{\text{total porosity}} = 0.88399 - 0.02501 E - 0.01646 \text{GB} + 0.01383 E * \text{GB}$$

$$Y_{\text{compression resistance}} = 0.34744 + 0.04869 E + 0.04945 \text{GB} - 0.01230 E * \text{GB}$$

$$Y_{\text{recovery rate}} = 0.762478 + 0.023340 E + 0.026039 \text{GB} - 0.005949 E * \text{GB}$$

$$Y_{\text{flexural rigidity}} = 0.06673 + 0.12381 E + 0.09027 \text{GB} - 0.06897 E * \text{GB}$$

$$Y_{\text{bursting strength}} = 232.72 + 31.38 E + 107.85 \text{GB} - 43.00 E * \text{GB}$$

$$Y_{\text{warp tensile strength}} = 649.3 + 105.3 E + 130.1 \text{GB}$$

$$Y_{\text{weft tensile strength}} = 454.9 - 431.2 E - 399.6 \text{GB} + 392.4 E * \text{GB}$$

$$Y_{\text{warp Young's modulus}} = 7.65567 + 0.05319 E - 5.80183 \text{GB} + 3.99660 E * \text{GB}$$

$$Y_{\text{weft Young's modulus}} = 0.01650 + 0.01750E + 0.01850 \text{ GB} - 0.01225 E * \text{GB}$$

3.3 As to biocompatibility, a 15 day human dermal fibroblast cell culture study was completed on all six samples, followed by the quantitative *in vitro* cell viability MTT bioassay and qualitative observations by scanning electron microscopy (SEM) and laser scanning confocal microscopy (LSCM) to study cell attachment, proliferation and infiltration on the surface and through the thickness of the scaffolds.

All six samples were successful in promoting cellular growth as demonstrated by increasing absorbance in the MTT assay. Cell attachment on the face and the cross-sections was confirmed by the SEM images and the cell proliferation through the thickness was observed by LSCM images and animation movies. It was clear that the small pore size on the outer layers had a positive impact on the initial cell attachment on the surface since confluent cell sheets were observed on the faces with smaller pores after only a few days in culture. Compared with the monofilament spacer yarns in the commercial samples, it was clear that the textured multifilament yarns were better able to support cell attachment and proliferation in the spacer layer since more cells were observed migrating along the fibers through the thickness of the prototype spacer fabrics than through the commercial samples with monofilament spacer yarns.

It was concluded that spacer fabric scaffolds could satisfy the biocompatibility requirement and could contribute to cellular growth on the surface and through the thickness of the scaffolds. The multifilament spacer yarns, the higher gauge and the higher number of guide bars are all positive contributing factors that encourage cell

attachment and proliferation to occur through the thickness of these 3D textile scaffolds.

## **5.2 Contribution**

In addressing the aim of design, production and evaluation of novel three dimensional porous knitted scaffolds, this study has for the first time been successful in integrating the latest warp knitting technologies with biological assays and developing an experimental procedure to evaluate the performance of these tissue engineering constructs. It has now been successfully demonstrated by this study that a 3D flat warp knitted spacer fabric with multifilament spacer yarns has the potential to be used as a porous scaffold for tissue engineering applications. The relationship between the knitting parameters and the mechanical performance has been determined statistically. These mathematical equations will serve as valuable references for the further advanced design of spacer fabric scaffolds for various specific tissues engineering applications.

As such, this study has clearly provided a novel design for the porous 3D structure, an interdisciplinary approach and a significant contribution to research in the field of medical textiles and tissue engineering.

## **5.3 Recommendations for Future Research**

The goals in this study focused on designing, developing, fabricating and evaluating 3D fibrous scaffold structures for tissue engineering applications. The experimental approach which is described in Chapter 3 investigated the design, simulation, fabrication and evaluation of flat spacer fabrics using warp knitting technologies for potential use as tissue

engineered scaffolds. Some recommendations for continuing studies can be drawn and are listed below:

- 5.3.1 As flat structures are limited to certain applications, tubular spacer fabric structures need to be studied in the future to satisfy the demand for hollow and tubular shaped scaffolds with multilayered walls. This is particularly relevant for vascular and urological applications.
- 5.3.2 Also further studies need to include the use of resorbable materials, such as PLA, PGA or PCL and their copolymers. Their inclusion will expand the research to include a comparison of molecular weight and mechanical performance before and after yarn preparation, knit fabrication, cleaning and testing. What is more, the rate of degradation of such synthetic resorbable polymers can lead to questions about biological properties such as cytotoxicity which can be negatively impacted by the rate of resorption.
- 5.3.3 Because this preliminary study was based on the general requirements for tissue engineering applications, it is recommended that further studies consider the advanced design of spacer fabrics for specific tissues with certain precise functions in the future. For example, the design of spacer fabrics to support the growth of pancreatic islets and the production of insulin would be a worthwhile objective.
- 5.3.4 Based on the mathematical equations that relate the mechanical properties with the independent factors of knitting machine design and operation, it is likely that

additional factors will be needed to adjust the knitting parameters and control the fabric's characteristics and performance properties in future studies.

- 5.3.5 With respect to the *in vitro* study, it is recommended that cell culture experiments be conducted over longer periods and with a larger number of replicates. In addition, *in vivo* animal studies will be needed as some future time point. This will call for a series of mechanical and biological tests to be performed both before and after the *in vivo* studies to monitor the performance during the resorption process.

## REFERENCES

1. Living and Deceased Donors -- All Organs 2000-2009 [Internet]: Arbor Research Collaborative for Health, [www.ustransplant.org](http://www.ustransplant.org), Nov 16, 2011
2. Griffith LG. Emerging design principles in biomaterials and scaffolds for tissue engineering. *Ann N Y Acad Sci* 2002 06;961: 83-95.
3. Lee J, Cuddihy MJ, Kotov NA. Three-dimensional cell culture matrices: State of the art. *Tissue Eng Part B Rev* 2008 Mar;14(1):61-86.
4. Griffith LG, Naughton G. Tissue engineering--current challenges and expanding opportunities. *Science* 2002 February 08;295(5557):1009-14.
5. Ramalingam M, Ramakrishna S. Design strategies of tissue engineering scaffolds with controlled fiber orientation. *Tissue Eng* 2007 08;13(8):1845-66.
6. Courtney T, Sacks MS, Stankus J, Guan J, Wagner WR. Design and analysis of tissue engineering scaffolds that mimic soft tissue mechanical anisotropy. *Biomaterials* 2006 07;27(19):3631-8.
7. Ma PX. Biomimetic materials for tissue engineering. *Adv Drug Deliv Rev* 2008 Jan 14;60(2):184-98.
8. Jones JR, Lee PD, Hench LL. Hierarchical porous materials for tissue engineering. *Philos Transact A Math Phys Eng Sci* 2006 Jan 15;364(1838):263-81.
9. Robert Czajka. Development of medical textile market. *Fibres & Textiles in Eastern Europe* 2005;13(1):13.

10. Rajendran S, Anand SC, Harrison PW. Developments in medical textiles A critical appreciation of recent developments. In: Manchester (United Kingdom): Textile Institute; 2002. .
11. Chen QZ, Bismarck A, Hansen U, Junaid S, Tran MQ, Harding SE, Ali NN, Boccaccini AR. Characterisation of a soft elastomer poly(glycerol sebacate) designed to match the mechanical properties of myocardial tissue. *Biomaterials* 2008 Jan; 29(1):47-57.
12. Polyethylene terephthalate - IDENTIFICATION [Internet] Bonn, Germany: German Institut für Arbeitsschutz, IFA; c2010. <http://www.dguv.de/ifa/en/index.jsp>, 2011
13. Hiroshi Y. Comparison of the mechanical properties of human organs and tissues. In: Evans F. Gaynor, editor. *Strength of biological materials* Baltimore. Baltimore, Maryland, USA: The Williams and Wilkins Company; 1970.
14. Chan BP, Leong KW. Scaffolding in tissue engineering: General approaches and tissue-specific considerations. *Eur Spine J* 2008 12;17 Suppl 4:467-79.
15. Chung S. *Fibrous scaffolds for tissue engineering applications*. NC, USA: North Carolina State University; 2010.
16. Baker SC, Atkin N, Gunning PA, Granville N, Wilson K, Wilson D, Southgate J. Characterisation of electrospun polystyrene scaffolds for three-dimensional in vitro biological studies. *Biomaterials* 2006 06; 27(16):3136-46.
17. Badawi M Sc, Said Sobhey AM. Development of the weaving machine and 3D woven spacer fabric structures for lightweight composites materials. ; 2008.

18. Van Lieshout M, Peters G, Rutten M, Baaijens F. A knitted, fibrin-covered polycaprolactone scaffold for tissue engineering of the aortic valve. *Tissue Eng* 2006 03;12(3):481-7.
19. Elsner P, Hatch KL, Wigger-Alberti W. *Textiles and the skin*. Basel ; New York: Karger; 2003. volume editors, Peter Elsner, Kathryn Hatch, Walter Wigger-Alberti.
20. Application of DynaMesh-CICAT [Internet] Aachen, Germany, 2011, en.dyna-mesh.com.
21. Moutos FT, Estes BT, Guilak F. Multifunctional hybrid three-dimensionally woven scaffolds for cartilage tissue engineering. *Macromol Biosci* 2010 Nov 10;10(11):1355-64.
22. Moutos FT, Freed LE, Guilak F. A biomimetic three-dimensional woven composite scaffold for functional tissue engineering of cartilage. *Nat Mater* 2007 Feb;6(2):162-7.
23. Wheatley B, Development of tricot and Raschel machinery over the past 50 years, *Knit Outwear*. *Times Y'r Bk*, 1968, 242-57.
24. Yip J, Ng S. Study of three-dimensional spacer fabrics: Physical and mechanical properties. *J Mater Process Technol* 2008 09/12;206(1-3):359-64.
25. Darlington KD. The production of raschel crochet fabric. *Knit Outwear Times*; 1968.
26. Workbook-warp knitting (textile extension) document Presentation.
27. Darlington KD, The production of Raschel crochet fabric, *Knit Outwear Times*, 1968, 22 July, 42-5.
28. Rajendran S, Anand S. Clinical research. design and development of novel bandages for compression therapy. *Br J Nurs* 2003 03/28;12(6):S20.

29. Miao X, Ge M. The compression behaviour of warp knitted spacer fabric. *Fibres & Textiles in Eastern Europe* 2008 Jan;16(1):90-2.
30. Davies A JW. The use of spacer fabrics for absorbent medical applications. *Journal of Fiber Bioengineering and Informatics* 2009;1(4).
31. Ye X, Hu H, Feng X. Development of the warp knitted spacer fabrics for cushion applications. *Journal of Industrial Textiles* 2008 01;37(3):213-23.
32. Lee G, Rajendran S, Anand S. New single-layer compression bandage system for chronic venous leg ulcers. *Br J Nurs* 2009 08/13;18(15):S4-18.
33. ASTM D3887 – 96 (Reapproved 2008) Standard Specification for Tolerances for Knitted Fabrics [Internet] West Conshohocken, PA 19428-2959, United States.: ASTM International; c2008 [cited 2011 Aug,01]
34. ASTM D 1777 – 96 (2007) Standard Test Method for Thickness of Textile Materials. [Internet] West Conshohocken, PA 19428-2959, United States.: ASTM International; c2007.
35. ASTM F2450 – 10(2010) Standard guide for assessing microstructure of polymeric scaffolds for use inTissue-engineered medical products. 2010 April:7. West Conshohocken, PA 19428-2959, United States.: ASTM International; c2008 [cited 2011 Aug,01]
36. Specific gravity of major polymers [Internet]: Eastpoint-Oltean; c2005 [cited 2011. <http://www.plasticsusa.com>.
37. ASTM D6571-01 Standard Test Method for Determination of Compression Resistance and Recovery Properties of Highloft Nonwoven Fabric Using Static Force Loading

- [Internet] West Conshohocken, PA 19428-2959, United States.: ASTM International; c2001 [cited 2011]
38. ASTM D1388-08 Standard Test Method for Stiffness of Fabric [Internet] West Conshohocken, PA 19428-2959, United States.: ASTM International; c2008. [cited 2011]
  39. ASTM D3787 Bursting Strength of Textiles—Constant-Rate-of-Traverse (CRT) Ball Burst Test Method [Internet] West Conshohocken, PA 19428-2959, United States.: ASTM International; c2011. [cited 2011]
  40. ISO 7198:1998(E) cardiovascular implants — tubular vascular prostheses. Aug 1998.
  41. A microtiter plate after an MTT assay. Increasing amounts of cells resulted in increased purple colouring. [Internet]: wikipedia; c2010
  42. McDowell, EM, and Trump BF, Histologic fixatives suitable for diagnostic light and electron microscopy. 1976;100:405-14.
  43. Dykstra, M.J. and L.E. Reuss. Biological Electron Microscopy: Theory, Techniques and Troubleshooting. 2nd Edition, 2003, Raleigh, NC, North Carolina State University.
  44. Dykstra MJ1. A manual of applied techniques for biological electron microscopy, 2011 Raleigh, NC, North Carolina State University.
  45. Dykstra MJ1. A routine schedule for the preparation of cell and tissue samples for scanning electron microscopy, laboratory for advanced electron and light optical methods, 2011 Raleigh, NC, North Carolina State University.

## APPENDICES

Appendix A

ANOVA analysis

Dependent Variable: Thickness

	<b>Df</b>	<b>Sum Sq</b>	<b>Mean Sq</b>	<b>F value</b>	<b>Pr(&gt;F)</b>	
factor(E)	1	0.26	0.26	12.878	0.000517	***
factor(GB)	1	1.98625	1.98625	98.383	< 2.2e-16	***
factor(E):factor(GB)	1	0.59904	0.59904	29.672	3.68E-07	***
Residuals	100	2.0189	0.02019			

Signif. codes: 0 '\*\*\*' 0.001 '\*\*' 0.01 '\*' 0.05 '.' 0.1 ' ' 1

<b>Thickness</b>	<b>(Intercept)</b>	<b>factor(E)2</b>	<b>factor(GB)2</b>	<b>factor(E)2:factor(GB)2</b>
Coefficients:	2.5309	0.22	0.4401	-0.312

Appendix B

ANOVA analysis

Dependent Variable: Total Porosity

	<b>Df</b>	<b>Sum Sq</b>	<b>Mean Sq</b>	<b>F value</b>	<b>Pr(&gt;F)</b>	
factor(E)	1	0.011917	0.011917	49.516	1.89E-10	***
factor(GB)	1	0.0017765	0.001777	7.3813	0.007677	**
factor(E):factor(GB)	1	0.0012237	0.001224	5.0847	0.026154	*
Residuals	108	0.0259923	0.000241			

Signif. codes: 0 '\*\*\*' 0.001 '\*\*' 0.01 '\*' 0.05 '.' 0.1 ' ' 1

<b>Total Porosity</b>	<b>(Intercept)</b>	<b>factor(E)2</b>	<b>factor(GB)2</b>	<b>factor(E)2:factor(GB)2</b>
Coefficients:	0.88399	-0.02501	-0.01646	0.01383

Appendix C

ANOVA analysis

Dependent Variable : Compression Resistance

	Df	Sum Sq	Mean Sq	F value	Pr(>F)	
factor(E)	1	0.0187452	0.0187452	43.84	8.04E-08	***
factor(GB)	1	0.0196451	0.0196451	45.9445	4.92E-08	
factor(E):factor(GB)	1	0.0003962	0.0003962	0.9265	0.3419	
Residuals	38	0.0162481	0.0004276			

Signif. codes: 0 '\*\*\*' 0.001 '\*\*' 0.01 '\*' 0.05 '.' 0.1 ' ' 1

<b>Compression Resistance</b>	<b>(Intercept)</b>	<b>factor(E)2</b>	<b>factor(GB)2</b>	<b>factor(E)2:factor(GB)2</b>
Coefficients:	0.34744	0.04869	0.04945	-0.0123

Appendix D

ANOVA analysis

Dependent Variable: Extent of Recovery

	<b>Df</b>	<b>Sum Sq</b>	<b>Mean Sq</b>	<b>F value</b>	<b>Pr(&gt;F)</b>	
factor(E)	1	0.004442	0.0044419	5.2665	0.02706	*
factor(GB)	1	0.005804	0.0058035	6.8809	0.01227	*
factor(E):factor(GB)	1	0.000097	0.0000965	0.1144	0.73692	
Residuals	40	0.033737	0.0008434			

Signif. codes: 0 '\*\*\*\*' 0.001 '\*\*' 0.01 '\*' 0.05 '.' 0.1 ' ' 1

<b>Extent of Recovery</b>	<b>(Intercept)</b>	<b>factor(E)2</b>	<b>factor(GB)2</b>	<b>factor(E)2:factor(GB)2</b>
Coefficients:	0.762478	0.02334	0.026039	-0.00595

Appendix E

ANOVA analysis

Dependent Variable: Bursting Strength

	<b>Df</b>	<b>Sum Sq</b>	<b>Mean Sq</b>	<b>F value</b>	<b>Pr(&gt;F)</b>	
factor(E)	1	1918	1918	0.9007	0.34634	
factor(GB)	1	120215	120215	56.4519	3.03E-10	***
factor(E):factor(GB)	1	7505	7505	3.5244	0.06525	.
Residuals	61	129900	2130			

Signif. codes: 0 '\*\*\*' 0.001 '\*\*' 0.01 '\*' 0.05 '.' 0.1 ' ' 1

<b>Bursting Strength</b>	<b>(Intercept)</b>	<b>factor(E)2</b>	<b>factor(GB)2</b>	<b>factor(E)2:factor(GB)2</b>
Coefficients:	232.72	31.38	107.85	-43

Appendix F

ANOVA analysis

Dependent Variable: Warp Tensile Strength

	<b>Df</b>	<b>Sum Sq</b>	<b>Mean Sq</b>	<b>F value</b>	<b>Pr(&gt;F)</b>	
factor(E)	1	1659	1659	0.5692	0.4571	
factor(GB)	1	90203	90203	30.9541	6.73E-06	***
Residuals	27	78680	2914			

Signif. codes: 0 '\*\*\*' 0.001 '\*\*' 0.01 '\*' 0.05 '.' 0.1 ' ' 1

<b>Warp Tensile Strength</b>	<b>(Intercept)</b>	<b>factor(E)2</b>	<b>factor(GB)2</b>
Coefficients:	649.3	105.3	130.1